

INFRARED AND MICROWAVE VARIABILITY OF OH/IR STARS  
AND  
A ONE MILLIMETER WAVELENGTH DETECTING SYSTEM FOR THE 200-INCH TELESCOPE

Thesis by  
Paul Michael Harvey

In Partial Fulfillment of the Requirements  
for the Degree of  
Doctor of Philosophy

California Institute of Technology  
Pasadena, California

1974

(Submitted August 3, 1973)

## ACKNOWLEDGEMENTS

Many people made possible the work described in this thesis. I particularly thank my advisor, Gerry Neugebauer, as well as Eric Becklin and Michael Werner, for a great deal of help and advice. Kenneth Bechis and William Wilson generously allowed the use of their microwave observations in this thesis. George (H.) Aumann built the bolometer used in the 1 mm system. Discussions with many people including all of those above and John Kwan, Harry (A. R.) Hyland, M. Litvak, J. Pipher, and P. Goldreich have contributed to the ideas presented here.

For the arduous task of plotting the near infrared and microwave data and drawing the finished figures I am grateful to my mother, Jean Harvey. Many people helped with the near and far infrared observing including Gene Clough, Jay Frogel, Susan Harvey, Alex Law, Steve Loer, Oren Maxwell, Frank Porter, Michael Schroeder, Ed Sutton, Henry Tye, Glenn Veeder, and Steve Willner. I also thank the night assistants, Juan Carrasco, Tom Gregory, and all the staff at Palomar for their help at the telescopes; and the Hale Observatories for providing observing time.

As a graduate student I have been supported by a NASA Traineeship, several GTA's from Caltech, NASA grants NGL 05-002-007 and NGL 05-002-207, and the U. S. Air Force contract F19628-70-C-0127.

Finally, I am grateful to my wife, Susan, for typing this thesis, and especially for her patience and support during the time of this research.

## ABSTRACT

This thesis consists of two distinct parts, an observational section concerned with the variability of OH/IR stars, and an instrumental section describing the development and calibration of a 1 mm detecting system.

In the first part systematic observations are presented for 14 OH/IR stars. Many of the sources show clear periodic variations between 1 and  $10\mu$  and at 1612 MHz with no observable phase difference between the infrared and microwave. The best explanation for this correlation seems to be that the OH masers are radiatively pumped. In at least two sources the 1665/1667-MHz variations are significantly greater and more random than the 1612-MHz variations. The data are not of sufficient quality to determine if the 1665/1667-MHz and infrared variations are correlated. No evidence is seen in the infrared for periodic variations of the color temperatures of the circumstellar dust shells which are believed to surround many of these stars. For the Mira stars observed, a correlation exists between the period of variation, the amplitude of variation at  $2.2\mu$ , the  $[3.5\mu] - [10\mu]$  color index, the separation in velocity of the two OH emission features, and the existence of  $1.35 \text{ cm H}_2\text{O}$  emission.

The 1 mm detecting system described in the second part of this thesis utilizes a germanium bolometer as the detecting element. Various filter materials -- glass fiber impregnated teflon, black polyethylene, a wire mesh in reflection, the atmosphere, and diffraction effects -- combine to limit the bandwidth of the system to the approximate range of 0.8 mm to 2 mm. A dual beam chopper is employed with a beam separation of 2.3 arcminutes and a half-power beamwidth of 1.7 arcminutes. The absolute

and relative calibrations of the system are based on assumed planetary brightness temperatures. The sensitivity of the calibration to changes in atmospheric conditions and to differences in source spectra is investigated, and the sample calibration of several observations is described for illustration.

## TABLE OF CONTENTS

|  |     |
|--|-----|
| PART I - Infrared and Microwave Variability of OH/IR Stars                                     | 1   |
| I. Introduction  | 2   |
| II. Summary of Results   | 11  |
| APPENDICES   |     |
| Appendix A - Time Variations in the OH Microwave<br>and Infrared Emission From Late Type Stars | 19  |
| Appendix B - Instrumentation and Observing Techniques  | 87  |
| Appendix C - Data Analysis   | 97  |
| REFERENCES - Part I  | 108 |
|  |     |
| PART II - A One Millimeter Detecting System for the 200-Inch<br>Telescope                      | 111 |
| I. Introduction  | 112 |
| II. Instrumentation  | 113 |
| III. Observing Techniques  | 132 |
| IV. Calibration Procedures   | 134 |
| V. Sample Observations   | 144 |
| APPENDIX   | 150 |
| REFERENCES - Part II   | 162 |

PART I

INFRARED AND MICROWAVE VARIABILITY OF OH/IR STARS

## I. INTRODUCTION

Microwave emission from OH molecules in astronomical objects was first detected in 1965 from sources associated with H II regions (Gunderman 1965; Weaver, Williams, and Dieter 1965). Measurements of the angular sizes of the emitting regions (Rogers et al. 1967) implied brightness temperatures far in excess of any physical temperature associated with the sources and suggested that some kind of maser mechanism was probably responsible for the radiation. Since that time many other OH microwave emission sources have been found which also appear to be masers. Sources with particular microwave characteristics appear to be associated with particular types of astronomical objects, H II regions, supernova remnants, and infrared stars. In order to understand more about the OH masers associated with infrared stars, and more about the stars themselves, a program was initiated in the fall of 1969 to study the time variations in the microwave and infrared luminosities of these objects. This is the principal subject of part I of this thesis. The program has been a joint effort between the author, who has made most of the infrared measurements, and Kenneth P. Bechis, who has made most of the microwave measurements.

In the remaining part of this chapter the previously known properties and theories of the OH/infrared star sources will be reviewed. The preliminary analysis and interpretation of the microwave and infrared variability have been performed by the author and are described briefly in Chapter II which is a summary of the results of this study of variability. Appendix A of part I of this thesis is a separate paper which

will be submitted for publication and is co-authored by K. Bechis, W. Wilson, and J. Ball. The paper contains brief descriptions of the observational techniques and data analysis and the entire discussion and interpretation of the data. The appendix to the paper contains the observations and the results of statistical analyses of the observations. Appendix B of part I of this thesis is a detailed description of the infrared equipment and observational procedures, and Appendix C describes the computer programs used in the data analysis.

The sources which were observed in this study of variability are listed in Table 1. A typical microwave spectrum is shown in Figure 1. One property which appears to be common to all the OH/IR stellar sources is that the positions of the OH source and the associated infrared star always coincide within the accuracy of the measurements which in some cases is better than  $\pm 5$  arcsec (Hyland et al. 1972). All of these sources emit microwave line radiation at either 1612, 1665, 1667 MHz or some combination of the three. Emission is not observed at 1720 MHz, the fourth possible transition in the hyperfine split, lambda-doubled ground state of the OH molecule. There is also no observable 18 cm wavelength continuum flux from these emitters. The sources which are variable are associated with oxygen rich, Mira type or semi-regular long period variable stars. The two sources, NML Cyg and VY CMa, which may not be periodic variables are associated with oxygen rich late M type supergiant stars (Hyland et al. 1972).

The microwave emission is usually observed at two nearby frequencies which, if taken as a separation in velocity of two emitting regions,

TABLE 1  
SOURCES OBSERVED

| Name    | IRC <sup>1</sup> | $\nu$ - OH Emission (MHz) | References |
|---------|------------------|---------------------------|------------|
| CIT-3   | +10011           | 1612, 1667*               | 2,6        |
|         | +50137           | 1612, 1667*               | 2,6        |
| U Ori   | +20127           | 1665, 1667                | 7          |
| VY CMA  | -30087           | 1612, 1665, 1667          | 2,3,9      |
|         | -20197           | 1612, 1667*               | 2,6        |
| W Hya   | -30207           | 1665, 1667                | 7          |
| S CrB   | +30272           | 1612*, 1665, 1667         | 7          |
| U Her   | +20298           | 1665, 1667                | 7          |
| VX Sgr  | -20431           | 1612, 1665*, 1667*        | 2,4,5      |
| R Aql   | +10406           | 1612, 1667                | 2,6        |
|         | -20540           | 1612, 1667*               | 2,5        |
| RR Aql  | 00458            | 1612, 1665*, 1667*        | 2,5        |
|         | -10529           | 1612, 1665*, 1667*        | 2,5        |
| NML Cyg | +40448           | 1612, 1665, 1667, 6035*   | 2,6,8      |

- (1) Neugebauer and Leighton (1969)
- (2) Hyland et al. (1972)
- (3) Robinson, Caswell, and Goss (1970)
- (4) Robinson, Caswell, and Dickel (1971)
- (5) Wilson (1970)
- (6) Wilson, Barrett, and Moran (1970)
- (7) Wilson et al. (1972)
- (8) Zuckermann et al. (1972)
- (9) Eliasson and Bartlett (1969)

\* No observations

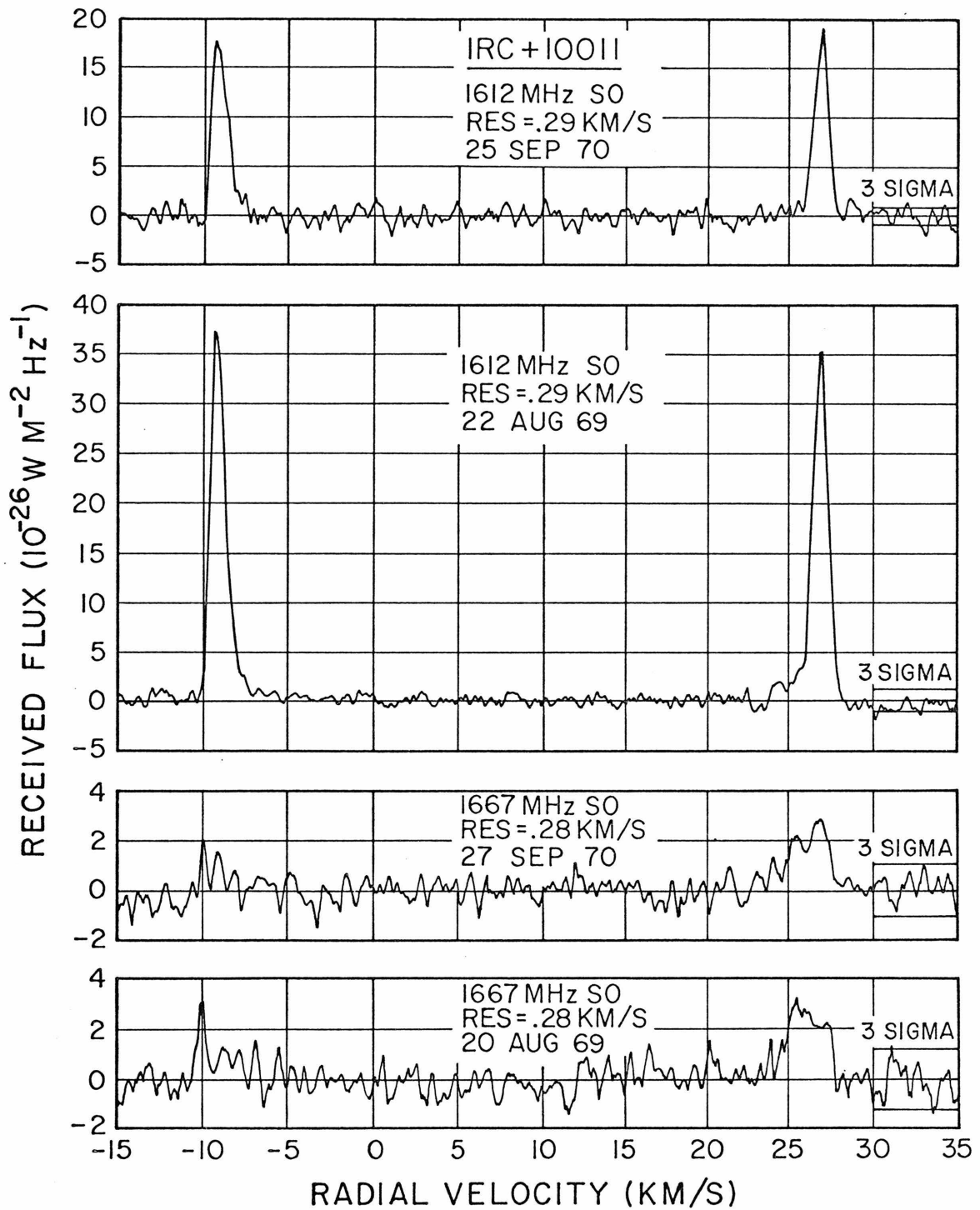


Fig. 1 - Sample OH microwave spectra of IRC+10011 are shown, taken from Wilson (1970).

imply velocity differences of 5 to 60 km s<sup>-1</sup>. When optical absorption lines have been observed, generally the numerically greater OH velocity (receding) coincides closely with the velocity of the optical lines which are believed to indicate the stellar velocity (Wilson, Barrett, and Moran 1970; Wallerstein 1971).

In the infrared between 5 and 20 $\mu$  many of the stars show excess radiation over that which would be expected from their color temperatures at shorter wavelengths. This has generally been taken as implying the existence of a dust shell around the star which absorbs some of the 1 to 3 $\mu$  radiation of the star, is heated to about 600°K, and reradiates the energy between 5 and 20 $\mu$ . There is evidence that many of these stars are relatively old and evolved and therefore are less likely to have circumstellar shells left over from their formation (Hyland et al. 1972). In addition, there is evidence from optical spectra that many late type stars are losing mass (Deutsch 1960; Wallerstein 1971). Therefore, it is likely that the dust shells around these stars form from mass which is lost from the stars (Hyland et al. 1972; Gehrz and Woolf 1971).

There is a definite tendency for the stars with large excess infrared radiation at the longer wavelengths to have the 1612-MHz OH emission stronger than the 1665/1667-MHz emission and to have a greater separation in velocity between the two microwave features. There is also an indication that all the sources may exhibit a considerably narrower range in intrinsic luminosities at 1665/1667 MHz than at 1612 MHz (Wilson et al. 1972).

Only one source, NML Cyg, has been interferometrically mapped and

only in its 1612-MHz emission (Davies, Mashedier, and Booth 1972). The emission at different velocities comes from many distinct points which are typically separated by 0.1 to 1.0 arcsec. This corresponds to a physical separation of about  $10^{15}$  to  $10^{16}$  cm at a distance of 500 pc which has been derived from considerations of interstellar reddening (Johnson 1968). The characteristic size of the emitting regions is about 0.08 arcsec (Wilson, Barrett, and Moran 1970).

In the visual part of the spectrum a vast quantity of data exists on Mira variables but there is still no detailed picture of what causes the variations or even what happens during the variations. The observations are consistent with a model in which the star pulsates in size with the surface temperature varying by 400 to 800°K as an inverse function of the size. In this model maximum visual light (0.4 to 0.7 $\mu$ ), which is highly dependent on molecular absorbers, occurs about the same time as minimum size, while maximum luminosity occurs about 0.1 period later (Pettit and Nicholson 1933). Variations in the radial velocity of optical emission lines of up to about 5 km s<sup>-1</sup> occur during the cycle of variation. Changes in the character of the spectrum are also observed. Basically the absorption spectrum appears cooler as the star becomes fainter, but spectral changes only approximately follow the light variations. Somewhat before maximum light, emission lines are seen which remain until close to minimum light and which appear to have a negative (approaching) radial velocity relative to the absorption lines (Merrill 1960). It has been suggested by Merrill and Deutsch (1959) and Fujita (1970) that these originate in material near a shock wave which starts deep in the star and slowly propagates outward. At

maximum light, when the proposed shock wave reaches the photosphere of the star where the absorption lines originate, the shock may slowly dissipate, although emission lines may still be excited as the shock moves out through optically thin parts of the atmosphere (Frogel 1971).

The physical processes related to the occurrence of and properties of the maser emission from these stars are not well understood. Previous investigators have made suggestions as to the nature of the sources based on the available theory and observations, and these will now be summarized.

Before any of the OH/IR sources were discovered, Litvak (1969) described a theory of near infrared,  $2.8\mu$ , pumping of OH masers which predicted 1612-MHz emission. Wilson, Barrett, and Moran (1970) subsequently observed such emission from several infrared stars and found that, to some extent, they could interpret their observations in terms of Litvak's model with reasonable assumptions of the unknown parameters. More recently, however, Wilson et al. (1972) noted that the existence of sources with 1665/1667-MHz emission stronger than any 1612-MHz emission is not readily predicted by Litvak's model. In addition, Litvak and Dickinson (1972) have found that the near infrared pumping model is quite sensitive to the strengths of the near infrared transitions which are not well known. Therefore, although there is some agreement between the observations and the  $2.8\mu$  pumping model, it is by no means certain that these sources are described completely by that model.

In order to explain the occurrence of 1665/1667-MHz emission along with 1612-MHz emission in terms of Litvak's (1969) model, Wilson, Barrett, and Moran (1970) had to assume kinetic temperatures larger than those

implied by the maser linewidths. They assumed, therefore, that some line-narrowing had probably occurred and concluded from the work of Litvak (1970) that the masers were not completely saturated. Goldreich and Kwan (1973, private communication) have recently shown, however, that in some cases line-narrowing may occur in fully saturated astrophysical masers. Furthermore, Wilson, Barrett, and Moran (1970) found that other characteristics of these masers, principally the polarization properties, suggested that the masers are saturated. In summary, the question of saturation is not well resolved, but it appears more likely that the masers are saturated than unsaturated.

Several models have been suggested to explain the occurrence of emission from these sources in two restricted velocity ranges; none, however, is completely free of problems. Wilson and Barrett (1972) ruled out rotating gas cloud models on the basis of stability and ruled out contracting models on the basis of insufficient path length to explain the observations in terms of Litvak's pumping model. In addition, the infrared and visual observations mentioned previously suggest that these stars are losing mass and may have expanding gas shells surrounding them. Wilson and Barrett (1972), therefore, suggested a shock front model. In this model there is a shock front located far from the star with rapidly expanding gas on the side nearest the star and gas stationary with respect to the star on the other side. Woolf (1972), on the other hand, has proposed an expanding model where the emission arises from material in the line of sight to the star and from material  $90^\circ$  away with respect to the star which has only a tangential component of velocity. He suggests that these two components of the expanding

circumstellar gas cloud would be the only two with both large path length and no significant velocity gradient. This type of model was also invoked by Davies, Masheder, and Booth (1972) to explain their observations of NML Cyg. There is no strong evidence from other observations to support either model in particular and, therefore, the geometry of these sources, as well as the pumping and saturation, are still open to question.

## II. SUMMARY OF RESULTS

The aim of the joint study of variability described here has been to obtain monthly measurements of the microwave spectra and infrared fluxes of ten 1612-MHz sources and more recently of several 1665/1667-MHz sources. The microwave data have been characterized by the following five quantities: the peak flux densities of both the low and high velocity emission features, the integrated flux in both features, and the total integrated flux. The infrared fluxes have been measured in six wavelength bands centered around 1.2, 1.6, 2.2, 3.5, 4.8, and 10 $\mu$  and are plotted in magnitudes ( $-2.5 \log F_{\lambda} + C_{\lambda}$ ) in Appendix A of part I of this thesis along with the microwave data.

It is clear from Appendix A that the microwave and infrared variations of many of these sources are roughly periodic. Sine waves have been fit to the 1612-MHz and infrared variations with all parameters of the sine wave determined by the fitting and also with the period fixed to that of the 2.2 $\mu$  variations. In all of the 1612-MHz sources both the period and phase of the microwave variations are identical to those of the infrared variations within the error limits of the data. These limits generally imply an upper limit to the phase differences of about 60 days. Correlation coefficients between the microwave and infrared variations were also computed and these confirm the apparent correlation between the 1612-MHz and infrared variations. The correlations are less clear in the weakest microwave sources, but within the errors the data are consistent with the microwave and infrared variations being correlated as for the other sources.

Two sources have not shown obvious periodic variations in either their 1612-MHz or infrared fluxes. VY CMa has remained constant in both wavelength regions while NML Cyg has shown only small but significant long term correlated variations in its 1612-MHz and infrared fluxes. Both sources, therefore, also exhibit correlations similar to those of the periodic variables.

The behavior of the 1665/1667-MHz emitters is not clear because the sources associated with periodic variable stars are weak; the only strong sources are associated with VY CMa and NML Cyg. Sine wave fits and correlation coefficients indicate a possible, but not definite, correlation between the microwave and infrared variations of most of the sources. Because of the short time coverage, however, and larger relative errors for these weak microwave sources, it is impossible to draw definite conclusions. It is certain, however, that the 1665/1667-MHz variations of VY CMa and NML Cyg are significantly larger and more random than either the infrared or 1612-MHz variations.

A by-product of this study has been the determination of the periods of several optically faint Mira type variable stars with large  $10\mu/3.5\mu$  flux ratios and therefore probably with relatively thick circumstellar dust shells. In Figure 2 the periods of variation of all the periodic variable stars observed in this study are plotted along with: (1) the amplitudes of variation at  $2.2\mu$ , (2) the  $[3.5\mu] - [10\mu]$  color indices, and (3) the separations in velocity between the two OH microwave emission features. Hyland et al. (1972) noted a tendency for longer period stars to have larger amplitudes and larger  $[0.8\mu] - [2.2\mu]$  color indices, and Wilson et al. (1972) found that the stars with larger  $[3.5\mu] - [10\mu]$

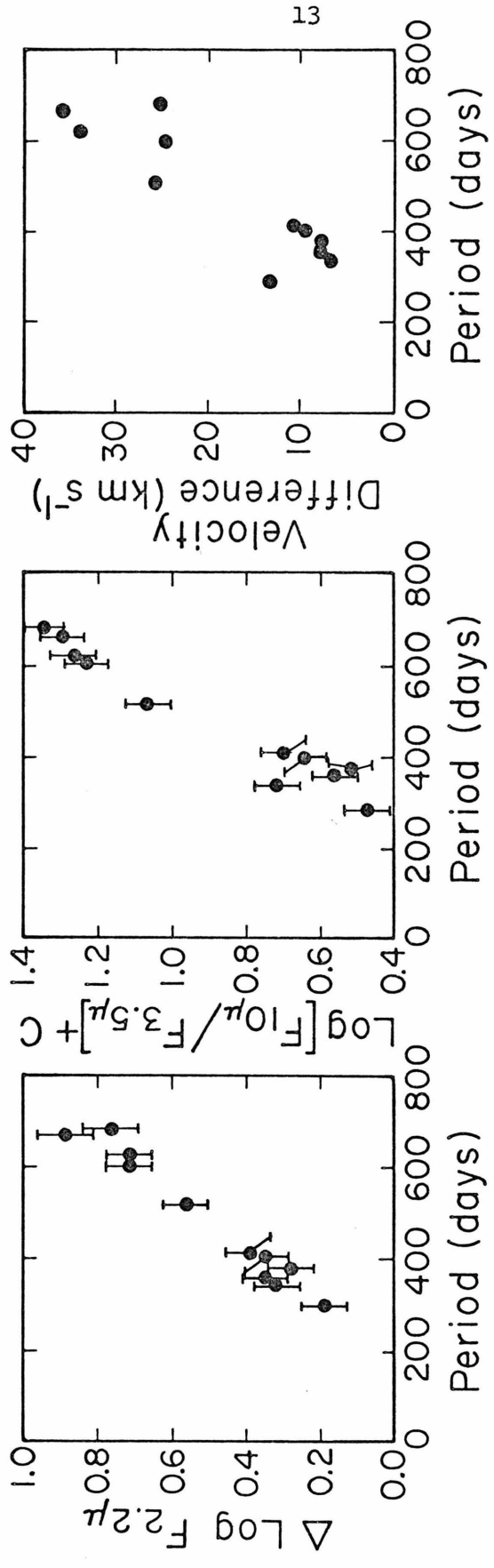


Fig. 2 - The log of the amplitude of variation at 2.2 $\mu$ , the [3.5 $\mu$ ] - [10 $\mu$ ] color index, and the separation in velocity between the two OH emission features are shown as functions of the period of variation for the 11 Mira type variables observed, including both 1612- and 1665/1667-MHz sources. Velocities were taken at the maximum of OH emission. Uncertainties in the periods and velocities are on the order of the size of the points plotted.

color indices had larger separations in velocity between the microwave emission features. In fact, it is clear from Figure 2 that all four quantities are correlated with each other. The interpretation of these relationships in terms of cause and effect is not clear, but it is certain that the longer period stars have larger amplitudes of variation. The larger amplitudes may be accompanied by greater mechanical activity leading to more mass loss and higher velocities of expulsion of the gas, or the longer period stars may have intrinsically greater luminosities driving more mass loss and greater velocities of expulsion.

The two most important results of this study are the findings of a correlation between the 1612-MHz and the infrared variations, and the lack of a phase lag between the two for all the sources observed. Other results which bear on the conclusions are: (1) there are no periodic or monotonic variations in velocity of the microwave emission features greater than  $0.4 \text{ km s}^{-1}$ , (2) there are no systematic or periodic variations in the shape of the 1612-MHz spectra, although there are occasional random changes, (3) the 1612-MHz flux of one source, VY Cma, has remained constant for over three years, and (4) the 1612-MHz fluxes of the periodic variable stars are roughly repeatable.

The conclusions of this study are based on the premise that in all the sources the physical separation between the OH maser and the star is too large for any mass motion or pressure wave to travel from the star to the OH cloud without an observable phase lag. With this premise the 1612-MHz/infrared correlation must be due to some radiative coupling mechanism between the stars and the masering OH clouds. Three points suggest that the OH is at least  $3 \times 10^{14}$  cm away from the stars. First,

assuming a distance to NML Cyg of 500 pc, which is probably accurate to within a factor of 3, Davies, Mashedier, and Booth (1972) have shown from VLBI measurements that the typical separation of OH maser emitting points in NML Cyg is about  $10^{16}$  cm. Therefore, the masering OH clouds are on the order of  $10^{16}$  cm from the star. Secondly, as Wilson (1970) noted, because no variation is seen in the velocity of the OH maser lines, although variations are seen in the velocity of optical spectral lines, the OH is probably mechanically decoupled from the star. Therefore, the OH is probably at least several stellar radii or a few  $\times 10^{14}$  cm distant from the stars. Thirdly, Litvak (1969) has noted that far infrared resonance fluorescence, which is probably necessary in the maser pump to select particular hyperfine states, is quenched at densities greater than about  $10^8 \text{ cm}^{-3}$ . These densities are at least  $10^3$  lower than typical stellar photospheric densities also suggesting that the OH must be at least several stellar radii away from the stars. An upper limit to the velocity of mass motion seems to be about  $50 \text{ km s}^{-1}$  which is the separation in velocity of the microwave or optical spectral lines; the velocity of sound in the circumstellar medium is probably even smaller, only a few  $\text{km s}^{-1}$  (Wilson 1970). Therefore, the minimum phase lag for mass motion or pressure waves to travel from the star to the OH cloud is  $(3 \times 10^9 \text{ km}) / (50 \text{ km s}^{-1})$  or two years.

Possible radiative coupling mechanisms which might cause the correlated variations are: (1) the stellar light may be able to affect the creation or destruction of OH molecules in the maser region, or (2) the maser may be amplifying the variable 1612-MHz continuum radiation directly from the star, or (3) the varying stellar radiation may be able

to affect the collision rate populating or de-populating the inversion by changing the temperature in the masering region, or (4) the masers may be radiatively pumped by the infrared radiation from the star and/or dust shell. The first suggestion can be ruled out because the minimum energy necessary to affect the electronic configuration of OH corresponds to radiation of wavelength  $0.4\mu$  where these infrared stars emit very little energy. The second suggestion is also unlikely for two reasons. If the maser were amplifying the background stellar radiation, emission would only be seen in the line of sight to the star, contrary to the findings of Davies, Mashedier, and Booth (1972) for NML Cyg. Secondly, if the masers are saturated, as seems likely, the maser output would not depend on the input intensity unless the maser beaming were variable. It is also unlikely that the microwave variations are due to a varying temperature in the maser medium although this possibility cannot definitely be ruled out. In a few  $\times 10^6$  seconds, the upper limit to the phase lag between the infrared and 1612-MHz variations, the circumstellar gas temperature can probably vary only about 0.1 to 1 percent. If the masers were sensitive to such small temperature variations, then random variations in the kinetic temperature of the maser medium would lead to large random variations in the maser output which are not seen.

The explanation for the 1612-MHz/infrared correlations which is most consistent with the observations is that the masers are pumped by the stellar infrared radiation. Hyland et al. (1972) showed that, assuming isotropic microwave and infrared emission and equal fractional line widths, the number of photons emitted from most of the OH/IR stars at 2.8 and  $35\mu$  is comparable to or exceeds the number of 1612-MHz photons,

and therefore infrared radiative pumping is at least energetically possible. This conclusion is not significantly changed by the present observations; the ratios of infrared to 1612-MHz photons do not vary by more than a factor of 2 to 3 during the cycles of variation. The most likely infrared pump transitions are at those wavelengths where the ratio of infrared to 1612-MHz photons is greater than 1. Assuming a reasonable extrapolation of the energy distributions, this occurs for most of the sources between about 2 and  $40\mu$ . Since the only allowed transitions from the ground state of the OH molecule in this range involve 2.8 or  $35\mu$  radiation, these are probably the most likely pump wavelengths.

As was noted earlier, it seems probable that these masers are saturated. Small random changes in the population inversion in the maser are likely because of turbulence and, if the masers were unsaturated, these changes in the population inversion would exponentially affect the output. This would lead to large random changes in the maser emission which are not observed.

If the masers are saturated, then the microwave output should be linearly proportional to the pump rate. In many cases, however, the infrared variations are significantly larger than the microwave variations, and in one case, R Aq1, the infrared variations are smaller than the microwave. Therefore, the pump rate is probably not strictly proportional to the infrared photon rate, possibly because of collisional pumping, non-linearities in the radiative processes due to stimulated emission, or a color dependence of the pumping mechanism because of the existence of more than one pump wavelength.

It was noted in Chapter I that only one theory exists at present

for the pumping of these masers, that of Litvak (1969) and Litvak and Dickinson (1972). The existence of a correlation between the infrared and microwave variations is consistent with virtually any radiative pumping model and is therefore consistent with Litvak and Dickinson's model as they have stated. Except for the possible wavelength limits on the pumping transitions of 2 to  $40\mu$  suggested earlier, however, there is no clear evidence for any particular radiative pumping scheme.

In summary, the main observational results of this study are:

- (1) A good correlation exists between the period of variation, amplitude of variation in the infrared,  $[3.5\mu] - [10\mu]$  color index, and velocity separation of the two microwave emission features for the Mira type variable stars observed.
- (2) The 1612-MHz and infrared flux variations in the sources observed are correlated and in phase within the errors.

The most important conclusions of this study are:

- (1) The best explanation for the correlated microwave and infrared variations is that the masers are radiatively pumped.
- (2) The masers are probably saturated.

## APPENDIX A

TIME VARIATIONS IN THE OH MICROWAVE AND  
INFRARED EMISSION FROM LATE TYPE STARS

Paul M. Harvey<sup>\*</sup>, Kenneth P. Bechis<sup>†</sup>, William J. Wilson<sup>x</sup>, and John A. Ball<sup>§</sup>

<sup>\*</sup>George W. Downs Laboratory of Physics, California Institute of  
Technology, Pasadena, California

<sup>†</sup>Department of Physics and Research Laboratory of Electronics,  
Massachusetts Institute of Technology, Cambridge, Massachusetts

<sup>x</sup>Electronics Research Laboratory, The Aerospace Corporation,  
El Segundo, California

<sup>§</sup>Harvard College Observatory, Cambridge, Massachusetts

## ABSTRACT

The OH microwave and infrared variability of 14 OH/IR stars have been studied. Many of the sources show clear periodic flux variations between 1 and  $10\mu$  and in the 1612-MHz OH lines with no observable phase difference between the infrared and microwave. The best explanation for this correlation seems to be that the OH masers are radiatively pumped. In at least two sources the 1665- and 1667-MHz variations are significantly greater and more random than in the 1612-MHz sources. The data are not of sufficient quality to determine if the 1665/1667-MHz and infrared variations are significantly correlated. A correlation exists between the period of variation, the amplitude of variation at  $2.2\mu$ , the  $[3.5\mu] - [10\mu]$  color index, the separation in velocity of the two OH emission features, and the existence of 1.35 cm  $H_2O$  emission in the Mira type stars observed. No evidence is seen in the infrared for periodic variations of the color temperatures of the circumstellar dust shells which are believed to surround many of these stars.

## I. INTRODUCTION

The class of OH microwave emission sources associated with infrared stars was first studied in detail by Wilson, Barrett, and Moran (1970). Since then there have been several microwave and infrared studies of these and other similar objects (Hyland et al. 1972; Wilson and Barrett 1972; and Wilson et al. 1972). The properties of these sources delineated in the previous studies can be summarized as follows. The stars with which the OH sources are associated are irregular supergiant variables or are Mira type long period variables with regular variations of periods of one to two years. All appear to be oxygen rich stars with surface temperatures of 1800 to 2800°K. Most are believed to be evolved stars undergoing mass loss and surrounded by 600 to 800°K dust shells. These shells presumably absorb near infrared stellar radiation and emit strongly between 3 and 20 $\mu$ . The OH emission typically occurs in two velocity ranges separated by 5 to 50 km s<sup>-1</sup>. There is a tendency for those sources with the thickest dust shells to have 1612-MHz emission stronger than any 1665- or 1667-MHz emission, and conversely. The OH emission is typically weakly polarized if at all, and there is no detectable radio continuum or 1720-MHz emission.

The above studies have included some mention of the variability of the sources, and on the basis of four OH microwave measurements Wilson (1970) suggested a possible correlation between the 1612-MHz OH and infrared flux variations of IRC+10011. No detailed investigation of the variability has been reported, however. Such a study is especially important for the stellar OH/IR sources because the OH masers are apparently

coincident with known variable stars which are probably the best understood of any type of object with which OH masers are associated.

In this paper we report results of a study initiated in the fall of 1969. The aim of this program was to measure monthly the microwave spectra at 1612 MHz and the broadband infrared fluxes at six wavelengths for ten OH/IR sources. These observations represent the first conclusive evidence for well-defined, periodic variations in the flux from any type of OH microwave emitter. Following the discovery of OH/IR stars that emit mainly at 1665 and/or 1667 MHz (see e.g. Wilson et al. 1972), the program was expanded to include four of these sources, as well as the 1665/1667-MHz emission of three of the 1612-MHz sources. These data are not nearly as extensive as those on the 1612-MHz sources, but they are interesting enough to warrant inclusion in this study.

## II. INSTRUMENTATION

### A. Microwave Equipment and Techniques

Nearly all the OH spectral line measurements were made by KPB with the Harvard College Observatory--Smithsonian Astrophysical Observatory 84-foot radio telescope at Agassiz Station, in Harvard, Massachusetts. In a Cassegrainian configuration the half-power beamwidth of the antenna at 18 cm wavelength is approximately 30', and the pointing accuracy is approximately  $\pm 3'$ . The receiver contained an uncooled non-degenerate parametric amplifier. Signal processing was done with a 50-filter spectral line radiometer, and the resolution was usually 1.5 or 5 KHz (0.3 or 1.0 km s<sup>-1</sup>). Over the three years of the observations, the total system noise temperature of the receiver varied from about 150°K

to about 250°K. This slow change has been taken into account in all the measurements and calibrations. The two senses of circular polarization were observed separately and later summed to give Stokes parameter  $S_0$ , the total unpolarized flux.

Flux calibrations were done mainly using 3C274 (Virgo A) and occasionally Cas A. It was assumed that the calibration sources and the OH emission sources are all small compared to the beamwidth. The flux density of 3C274 was taken to be  $S_0 = 180.5$  f.u. at 1612 MHz (1 f.u. =  $10^{-26} \text{ Wm}^{-2}\text{Hz}^{-1}$ ). The Cas A flux density was calculated from the formula suggested by Allen (1967):  $S_0 = 6500(\nu/0.4)^{-0.785}$  f.u. for  $\nu$  in GHz for the epoch 1964.4, and a secular decrease of 1.1 percent per year. This gives, for example, 2015 f.u. at 1612 MHz for the epoch 1971.4, which is approximately halfway through the observing program. The ratio of flux to antenna temperature (both  $S_0$ ) for a small diameter source is approximately 6.5 f.u. °K<sup>-1</sup>.

Five times during the monitoring program additional OH observations were made with the 140-foot telescope of the National Radio Astronomy Observatory (NRAO)\*. These observations were made during 1969 August/

---

\*The National Radio Astronomy Observatory, Green Bank, West Virginia, is operated by Associated Universities, Inc., under contract with the National Science Foundation.

---

September, 1970 February, 1970 September/October, 1971 October/November and 1972 April by WJW, KPB, and JAB. This antenna was illuminated at the prime focus with a scalar feed that gave a half-power beamwidth of 18' at a wavelength of 18 cm. The feed provided two orthogonally polarized

ports, and a cooled parametric amplifier receiver was connected to each port. The system noise temperature of each receiver was about 75°K. Spectral line processing was done with the NRAO 384-channel autocorrelation system, which was used either as one 384-channel autocorrelator or as two 192-channel autocorrelators. For all observations at least two orthogonal senses of linear polarization were observed and later summed to give  $S_{\circ}$ . In some cases left and right circular polarizations were measured and summed to provide an independent measurement of  $S_{\circ}$ .

Flux calibrations at the NRAO were made using the unpolarized continuum source 3C218 which was assumed to have a flux density of 37.5 f.u. at 1612 MHz, 36.4 f.u. at 1666 MHz, and a spectral index of -0.91 (Kellermann, Pauliny-Toth, and Williams 1969). The ratio of flux to antenna temperature (both  $S_{\circ}$ ) for a small diameter source was typically about 1.98 f.u. °K<sup>-1</sup>.

#### B. Infrared Equipment and Techniques

The broad-band infrared fluxes between 1 and 10 $\mu$  were measured primarily by PMH with the 60-inch telescope of the Hale Observatories on Mt. Wilson, using the photometer described by Becklin and Neugebauer (1968). Measurements were made relative to five or six standard stars on each night. These were used to determine a sensitivity for the night at each wavelength, and, for all but the faintest stars, the relative agreement of the standards determined the errors assigned to the measurements. Nominal air mass corrections were applied to all the data, and, whenever possible, measurements were made at zenith angles less than 60°. The wavelengths observed were 1.25 $\mu$  (1.15 - 1.35 $\mu$ ), 1.65 $\mu$

(1.50 - 1.75 $\mu$ ), 2.2 $\mu$  (2.0 - 2.4 $\mu$ ), 3.5 $\mu$  (3.2 - 4.1 $\mu$ ), 4.8 $\mu$  (4.6 - 5.1 $\mu$ ), and 10 $\mu$  (8 - 13 $\mu$ ). The absolute calibration has been described by Wilson et al. (1972).

### III. OBSERVATIONS AND DATA ANALYSIS

#### A. The Data

The microwave and infrared observations of all the observed stars are displayed as light curves in the Appendix. The following five parameters of the 1612-MHz data have been graphed: the peak flux densities within the low- and high-velocity features, the integrated flux in each group of features, and the total integrated flux. These five parameters generally specify all the 1612-MHz variations because the velocities and shapes of the OH features have not varied significantly in most cases. Except for some of the spectra of R Aql, VY CMa, and NML Cyg, the 1665- and 1667-MHz data were parametrized only by the peak and integrated flux densities of all the features in each spectrum.

Errors in the microwave and infrared observations arise from both random noise in the detectors and from systematic changes in the calibration of the detecting system. For many of the microwave data and for almost all of the infrared data, the principal contribution to the errors is from the calibration changes.

The error limits on the microwave observations were estimated from observed changes in system gain and from the agreement of measurements made less than a few days apart. These limits appear to be about  $\pm 15$  percent. On the 84-foot telescope the integration times on the weaker sources were usually chosen to give a statistical error of about

$\pm 2$  f.u. ( $2\sigma$ ), and this was added in quadrature to the 15 percent stability error for all measurements. These error estimates are believed to represent 90 to 95 percent confidence limits. One confirmation of the estimated size of the errors is that the 1612-MHz flux of VY CMa has remained constant within the errors for the entire period of the observations. This would be unlikely unless the source had remained nearly constant and the errors had been determined correctly.

The error limits on the infrared observations were determined from the agreement of the standard sources measured along with the OH/IR stars. The agreement is usually either on the order of, or significantly better than,  $\pm 10$  percent; the corresponding error limits on the magnitudes were set to either  $\pm 0.15$  or  $\pm 0.10$  magnitude.

A  $\chi^2$  test for the degree of variability, several sine wave fits, and a correlation coefficient test were performed on the infrared and microwave data. These are described in detail in the Appendix. In the following sections we discuss the observed infrared and microwave variability and the results of these statistical tests.

### B. Infrared Variations

Except in NML Cyg and VY CMa, the values of  $\chi^2$  given in Table 1 of the Appendix indicate significant variation of all the stars at all infrared wavelengths. Both the appearance of the light curves and the values of  $\chi^2$  suggest that NML Cyg has probably shown small long-term variations while VY CMa has probably remained constant within the errors.

For the stars for which both visual and infrared periods have been determined, the periods agree well (Appendix, Table 2). In addition,

the phases of the infrared variations are equal at all wavelengths except that the long wavelength flux may peak slightly ahead of the shorter wavelength fluxes (Appendix, Table 3). Where available, the times of visual maxima and minima obtained from light curves of the AAVSO (Mayall, private communication) are indicated on the infrared light curves in the Appendix. The infrared light maximum lags the visual typically by 0.1 to 0.2 period, in agreement with the previous observations of Pettit and Nicholson (1933), Mendoza (1967), Lockwood and Wing (1971), and Frogel (1971). The amplitudes of variation of the broad-band  $2.2\mu$  fluxes are somewhat smaller than the  $1.04\mu$  amplitudes of Lockwood and Wing, and marginally larger than the narrow-band  $2.25\mu$  amplitudes of Frogel.

For the Mira variables observed, a definite correlation has been found between the four quantities plotted in Figure 1 -- the period, the  $2.2\mu$  amplitude, the  $[3.5\mu] - [10\mu]$  color index, and the separation in velocity between the two groups of OH emission features. Several aspects of this correlation were seen previously. In particular, Merrill (1960) has noted a possible correlation between the periods of variation and the visual amplitudes of Mira stars, and Lockwood and Wing (1971) found a clear period-amplitude relationship at  $1.04\mu$ , especially for a sample restricted to pure M stars. Furthermore, Hyland et al. (1972) noted a tendency for longer period stars to have larger amplitudes and larger  $[0.8\mu] - [2.2\mu]$  color indices, and Wilson et al. (1972) found that the stars with larger  $[3.5\mu] - [10\mu]$  color indices have larger separations in velocity between the OH microwave emission features. It may also be

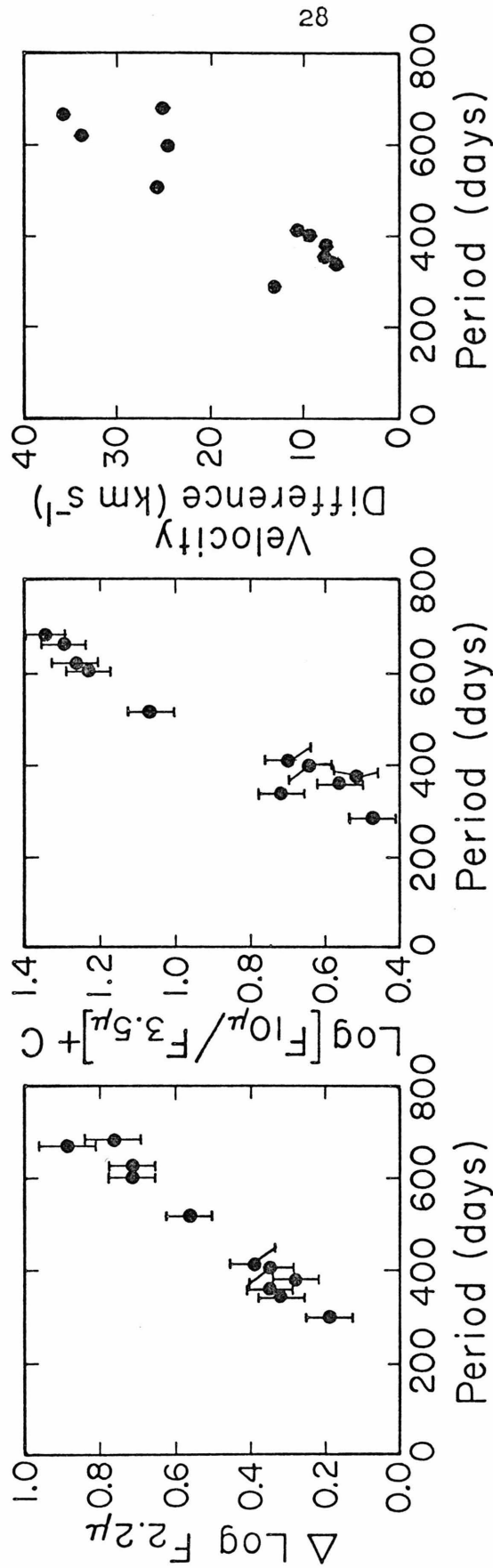


Fig. 1 (Appendix A) - The log of the amplitude of variation at  $2.2\mu$ , the  $[3.5\mu] - [10\mu]$  color index, and the separation in velocity between the two OH emission features are shown as functions of the period of variation for the 11 Mira type variables observed, including both 1612- and 1665/1667-MHz sources. Velocities were taken at the maximum of OH emission. Uncertainties in the periods and velocities are on the order of the size of the points plotted. The constant, C, equals 0.88 (Wilson et al. 1972).

significant that the six shorter-period stars in Figure 1 all show 1.35 cm  $H_2O$  emission while none of the five longer-period stars are known to have such emission.

Most of the stars observed show variations in color during their cycles of light variation. The amplitudes of variation at each wavelength shown in Figure 2 for four of the stars observed in this study are illustrative of the general behavior of all the sources (Appendix, Table 6). The amplitudes generally decrease from 1.2 to  $3.5\mu$  and are roughly constant between  $3.5$  and  $10\mu$ . The phase of the color variations is the same as that of the flux variations, that is, the stars appear reddest at minimum light. This is consistent with Frogel's (1971) broad-band observations between 1.2 and  $3.5\mu$ . The stars with the least color variation are those with the shortest periods and smallest  $[3.5\mu] - [10\mu]$  color indices; these stars also tend to have 1665/1667-MHz emission stronger than any 1612-MHz emission that may be present.

### C. Microwave Variations

The significance of the observed microwave variability was established by performing a  $\chi^2$  test on all the data (Appendix, Table 1). Except for NML Cyg and VY CMa, the value of  $\chi^2$  is greater than about 2 for the variations of virtually all the peak and integrated 1612-MHz flux densities of all the sources. In the three cases where the value of  $\chi^2$  is less than 2 at 1612 MHz, the average value of the peak flux density is only about 5 f.u. In these cases the errors are apparently masking the variations which have been observed in the data taken on the 140-foot antenna with a higher signal-to-noise ratio. The values of  $\chi^2$

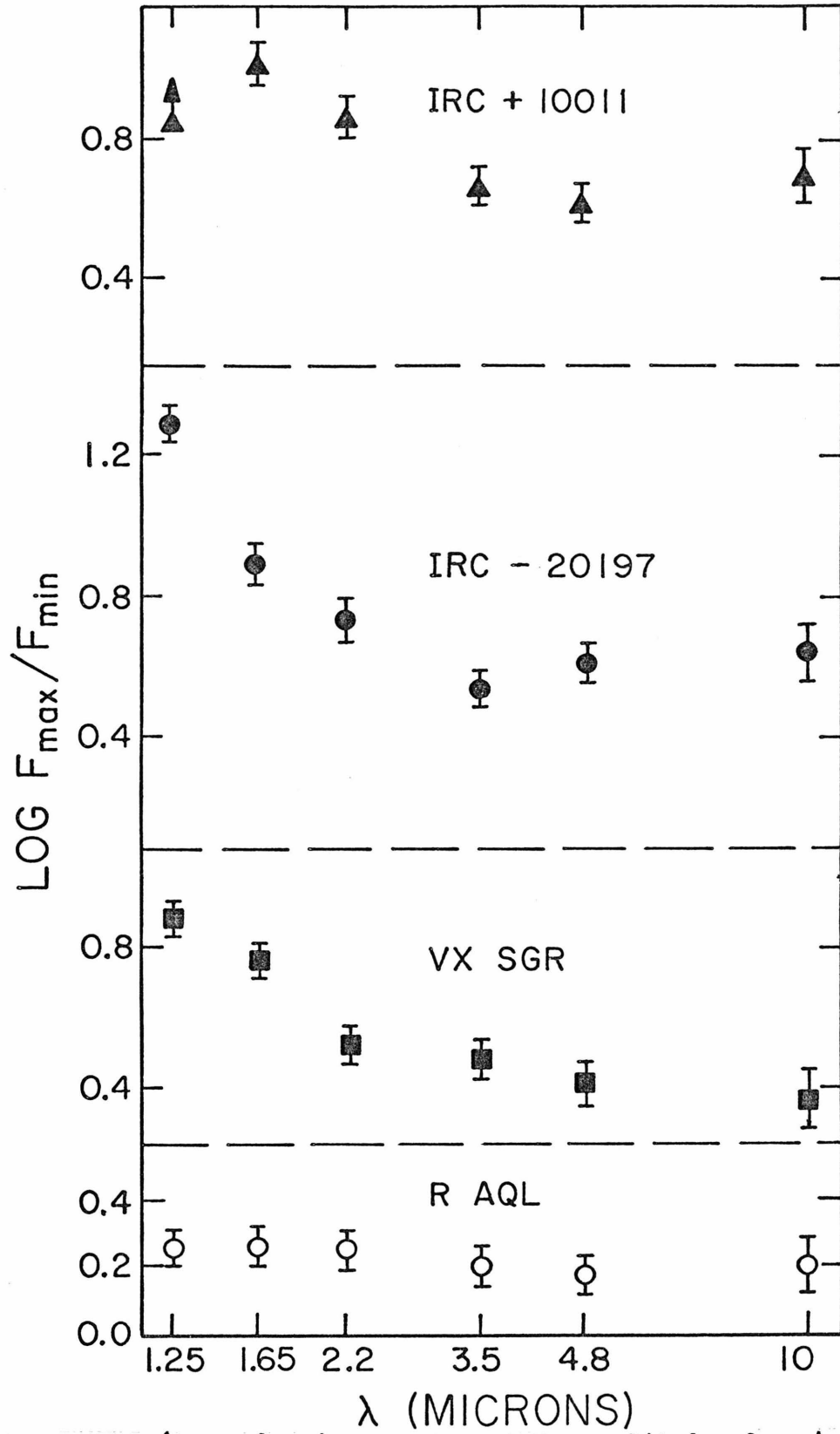


Fig. 2 (Appendix A) - The log of the amplitude of variation at 1.2, 1.6, 2.2, 3.5, 4.8, and  $10\mu$  is shown for four representative stars.

for the 1612-MHz fluxes of VY Cma and NML Cyg indicate that VY Cma has remained constant within the errors but that the integrated flux of NML Cyg is probably variable and with a larger amplitude than that of the peak flux density.

Except for some of the parameters of the 1665/1667-MHz fluxes of VY Cma, the only cases where the values of  $\chi^2$  indicate no significant variability at 1665 and 1667 MHz are those where the peak flux densities average less than 5 f.u. Therefore, all the sources are probably variable. Several of the parameters of the 1665/1667-MHz fluxes of VY Cma appear to be relatively constant while others show large variations. Since Robinson, Caswell, and Goss (1970) have found large changes in the intensity and polarization of the 1665/1667-MHz spectra of VY Cma, and since we have not measured all the Stokes parameters of the emission, it is difficult to conclude more from our data than the fact that the 1665/1667-MHz spectra of VY Cma vary considerably more than the 1612-MHz spectra. The variations in the 1667-MHz and perhaps the 1665-MHz flux of NML Cyg are also larger than the 1612-MHz variations, and in general, the variations of the 1665/1667-MHz fluxes of all the sources seem to be greater than the typical 1612-MHz variations.

The periods of the 1612-MHz variations determined by sine wave fitting are given in Table 2 of the Appendix. The 1665/1667-MHz data are not of sufficient quality or quantity to obtain meaningful determinations of the periods, if periods exist.

#### D. Correlations Between Microwave and Infrared Variations

The most important aspect of this study is the indication of a

correlation between the infrared and 1612-MHz OH variability of the sources observed. This is illustrated in Figure 3 for four of the stronger sources and has been confirmed for all the sources in several ways.

It is clear from Table 2 of the Appendix that for virtually all the sources the periods determined by the sine-wave fitting for the 1612-MHz and infrared fluxes are roughly equal. The only exceptions are IRC-20540 which is a relatively weak microwave source and VX Sgr which has large differences in amplitude from cycle to cycle. The phases of the infrared and microwave variations in Table 3 of the Appendix for the 1612-MHz sources are also equal within the confidence limits for virtually all the sources. Finally, correlation coefficients between the microwave and infrared variations were computed as described in the Appendix and listed there in Table 4 for the 1612-MHz sources. These coefficients show that the microwave and infrared variations are clearly correlated in the stronger sources, although less obviously correlated in several of the weaker sources. In the weaker microwave sources, however, the error limits are comparable to the probable size of the variations and a smaller correlation would be expected. Correlation coefficients were also computed for NML Cyg because it has probably shown small but significant variations. The variations in the integrated flux of NML Cyg are well correlated with the infrared, but the variations in the peak flux densities do not show any definite correlation. It should be noted that the variations of NML Cyg may be periodic but of such a long period and small amplitude that the time scale of these observations is too short to establish the periodicity.

The uncertainties in the OH microwave amplitudes are too large to

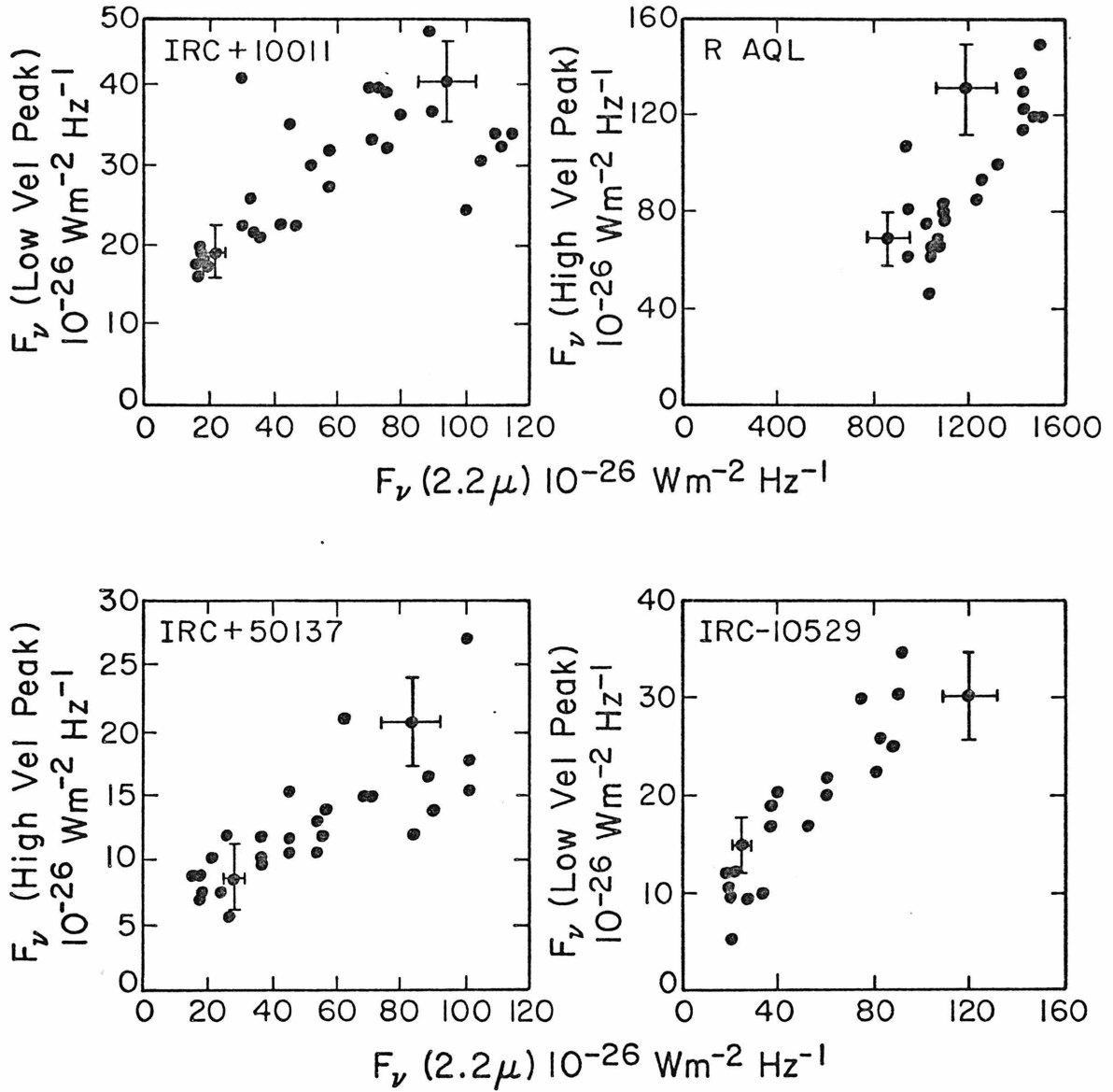


Fig. 3 (Appendix A) - The flux density of the stronger of the two OH emission features is shown as a function of the flux density at  $2.2\mu$  at various times in the light cycles for four of the stronger 1612-MHz sources. The fluxes at  $2.2\mu$  were interpolated between nearby observations. Typical error limits are shown.

determine if a correlation exists between the infrared and 1612-MHz OH amplitudes. The data in Table 6 of the Appendix, however, suggest that, except for R Aql, the amplitudes of the 1612-MHz variations are significantly less than, or at most equal to, the infrared amplitudes.

The phases derived by sine wave fitting with the period fixed to that of the visual variations and the correlation coefficients for the variations of the 1665/1667-MHz sources are given in Table 5 of the Appendix. The short time coverage and weaker fluxes of the 1665/1667-MHz sources make the detection of a correlation with the infrared difficult, if such exists. The results in Table 5 are not conclusive; within the errors they may be consistent with the existence of a correlation between the infrared and 1665/1667-MHz variability of most sources.

#### E. Summary of Observational Results

The most important observational results of this study are:

- (1) The infrared and 1612-MHz variations of VX Sgr and of all the observed Mira type OH/IR stars are roughly periodic. The periods in both the infrared and microwave are equal and range from about 300 to 700 days (Appendix, Table 2). The maxima and minima of both the infrared and 1612-MHz fluxes of the periodic sources are roughly repeatable. The infrared and 1612-MHz fluxes of VY CMa have remained constant while NML Cyg has probably shown small long-term variations at both wavelengths.
- (2) The amplitudes of variation in the infrared generally decrease with increasing wavelength from 1.2 to  $3.5\mu$  and are

- roughly constant between 3.5 and 10 $\mu$  (Figure 2; Appendix, Table 6). The ratios of maximum to minimum flux range from less than 2 to greater than 10 for different stars at different wavelengths.
- (3) The amplitude of variation in the OH microwave flux is usually on the order of or significantly smaller than the amplitude at all observed infrared wavelengths (Appendix, Table 6). The ratio of maximum to minimum 1612-MHz flux density is typically between 2 and 4.
  - (4) The phases of the variations at all infrared wavelengths and at 1612 MHz for the periodic variables are equal within the computed confidence limits of the observations, generally about 60 days, or 0.1 to 0.2 period (Appendix, Table 3). The 1612-MHz and infrared variations of the periodic variables are well correlated (Figure 3; Appendix, Table 4) as are the small long-term variations of NML Cyg.
  - (5) There are no velocity variations of the 1612-MHz OH lines within the observational uncertainty -- about 0.3 km s<sup>-1</sup> for strong features.
  - (6) There are no systematic or periodic changes in the 1612-MHz feature widths, separations, or the number of features of the spectra as the total flux varies, but there are occasional random variations in feature strength.
  - (7) The 1665/1667-MHz flux variations are not definitely correlated with the infrared variations, and in at least two sources, NML Cyg and VY CMa, they are significantly greater

and more random than the 1612-MHz variations.

- (8) A close correlation exists between the period of variation, the amplitude of variation, the  $[3.5\mu] - [10\mu]$  color index, and the separation in velocity between the OH emission features for the Mira type stars as shown in Figure 1. Some correlation between these four quantities and the occurrence of 1.35 cm  $H_2O$  emission is also present.

#### IV. INTERPRETATION AND SPECULATION

##### A. Radiative Coupling

The main conclusion of this study is that the correlation between the infrared and 1612-MHz OH variations is due to some radiative coupling mechanism between the stars and the masering OH clouds. This conclusion is based on the premise that in all the 1612-MHz sources the distance between the OH maser and the star is too large for any mass motion or pressure wave of reasonable velocity to travel from the star to the maser without an observable phase lag. This premise will now be substantiated.

Three considerations suggest that the OH is at least  $3 \times 10^{14}$  cm away from the stars. Assuming a distance to NML Cyg of 500 pc, which is probably accurate to within a factor of 3, Davies, Masheder, and Booth (1972) have shown from VLBI measurements that the typical separation of OH maser emitting points in NML Cyg is about  $10^{16}$  cm. Therefore, the masering OH clouds must be located at least  $10^{16}$  cm away from the star. Secondly, as Wilson (1970) noted, because no variation is seen in the velocity of the OH maser lines, although variations are seen in the velocity of optical spectral lines, the OH is probably mechanically

decoupled from the star. Therefore, the OH is probably at least several stellar radii or a few  $\times 10^{14}$  cm distant from the stars. Thirdly, Litvak (1969) has noted that far infrared resonance fluorescence, which is probably necessary in the maser pump to select particular hyperfine states, is quenched at densities greater than about  $10^8 \text{ cm}^{-3}$ . These densities are at least  $10^3$  lower than typical stellar photospheric densities, also suggesting that the OH must be at least several stellar radii away from the stars.

An upper limit to the velocity of mass motion is about  $50 \text{ km s}^{-1}$ . This is the separation in velocity of the microwave or optical spectral lines, and the velocity of sound in the circumstellar medium is even smaller, probably only a few  $\text{km s}^{-1}$ . Therefore, the minimum phase lag for mass motion or pressure waves to travel from the star to the OH cloud is  $(3 \times 10^9 \text{ km}) / (50 \text{ km s}^{-1})$ , two years.

Several radiative coupling mechanisms can be imagined which might cause the maser output to follow the stellar variations: (1) the masers may be radiatively pumped by the infrared radiation from the star and/or dust shell; (2) the stellar light may be able to affect the creation or destruction of OH molecules in the maser region; (3) the maser may be amplifying variable 1612-MHz continuum radiation directly from the star; (4) the varying stellar radiation may be able to affect the collision rate populating or de-populating the inversion by changing the temperature in the masering region.

The first suggestion, radiative pumping of the maser, seems to be the most likely and will be discussed in detail below. The second suggestion seems unlikely since the minimum energy necessary to affect the

electronic configuration of OH corresponds to  $0.4\mu$  radiation. Assuming equal fractional linewidths in the visual and microwave, the photon emission rate at  $0.4\mu$  for the late type stars studied by the OAO (Doherty 1972) is typically less than  $10^{-2}$  times the 1612-MHz photon emission rate of the OH sources. There is no reason to believe that the OH sources would have a UV excess relative to the late type stars studied by Doherty. Amplification of the stellar 1612-MHz continuum background is also unlikely for two reasons. If the maser were amplifying the stellar background, emission would only be seen in the line of sight to the star and, at least in the case of NML Cyg, this is contrary to the findings of Davies, Masheder, and Booth (1972). Secondly if the masers are saturated, as seems likely, the maser output is almost independent of the brightness of the source being amplified unless the beaming of the maser were variable. It is also unlikely that the microwave variations are due to a varying temperature in the maser medium, although this possibility cannot definitely be ruled out. Between 1 and  $10\mu$ , where most of the stellar energy is emitted, the principal sources of opacity are the fundamental vibrational bands of  $H_2O$ , CO, and OH. Using some typically assumed values for the parameters of the circumstellar cloud (see e.g. Litvak and Dickinson (1972) --  $r = 10^{15}$  cm,  $n(H) = 10^6$   $cm^{-3}$ ,  $n(H_2O) \sim n(CO) \sim n(OH) \sim 10^{-4} n(H)$ ,  $L_* = 10^4 L_\odot$  -- the energy absorbed by the circumstellar gas in a few  $\times 10^6$  seconds (the upper limit to the phase difference between the microwave and infrared) can only change the gas temperature by 0.1 to 1 percent. Furthermore, if the masers were sensitive to such small changes in the kinetic temperature of the gas, then random variations in the gas flow and turbulence would

probably lead to large random variations in the maser emission which are not seen. The Reynolds number for the probable outward flow of the gas in which the maser is situated is on the order of  $10^6$  for the observed flow velocities and reasonable densities and temperatures. Therefore, the flow may be highly turbulent. In fact, it should be noted that such turbulence could be the prime factor determining the temperature in the maser medium.

#### B. Radiative Pumping

Radiative pumping of the maser population inversion seems to be the most likely coupling mechanism because it is the mechanism most consistent with all the observations to date including our measurements of the variability.

Hyland et al. (1972) have shown that, if one assumes isotropic microwave and infrared emission and equal fractional line widths, the number of photons emitted from most of the OH/IR stars at 2.8 and  $35\mu$  is comparable to or exceeds the number of 1612-MHz photons. This conclusion is not significantly changed by the present observations; the ratios of infrared to 1612-MHz photons do not vary by more than a factor of 2 to 3 during the cycles of variation. Since a radiative pumping mechanism that yields more maser photons than pump photons is possible but unlikely, the most likely infrared pump transitions are at those wavelengths where the ratio of infrared to 1612-MHz photons is greater than 1. Assuming a reasonable extrapolation of the energy distributions, this occurs for most of the sources between about 2 and  $40\mu$ . Since the only allowed transitions from the ground state of the OH molecule in this range are

at 2.8 or  $35\mu$ , these seem to be the most likely pump wavelengths.

The functional relationship between the 1612-MHz and infrared fluxes is not inconsistent with the conclusion that the masers are radiatively pumped, despite the fact that the infrared and microwave amplitudes are not equal. Regardless of the degree of saturation, almost any radiative pumping model would predict an increase in the maser output with an increase in the pump flux, and this is observed in all the 1612-MHz sources. Without a detailed theory for the pumping, however, it is impossible to predict the exact dependence of the maser flux on the pump flux. In fact, one might expect different relationships under the different physical conditions in different sources. For example, in a model proposed by Litvak (1969) wherein collisions are considered negligible, the unsaturated population inversion depends only on the density of OH and to a small extent on the spectral distribution of the incident radiation, but not on the intensity of the infrared radiation. In that case, if the maser were not fully saturated, the periodic microwave variations would be smaller than the infrared variations, although random variations would probably be larger.

As will be discussed later, however, it seems more likely that the masers are saturated. In a saturated maser the output should be proportional to the pump rate, but in the OH/IR stars there are at least three ways in which the pump rate may not be exactly proportional to the infrared photon rate. Some other inverting or anti-inverting mechanism may exist such as the collisional pumping suggested by Litvak and Dickinson (1972). Alternatively, non-linearities in the pumping may result from stimulated emission in some of the far infrared transitions; or the

maser intensity may depend not only on the intensity of the infrared radiation but on its spectral distribution. In summary, because of the many ways in which the maser and infrared amplitudes can differ, one cannot determine any details of the pumping process from the relationships between the pump and maser fluxes.

Our observation of a correlation between the infrared and microwave variability is not only consistent with general considerations of radiative pumping, but also with the particular model of Litvak and Dickinson (1972) as they have noted. This fact does not necessarily confirm their model, but it does support the conclusion that the masers are radiatively pumped.

### C. Saturation

The output of a fully saturated maser is linearly proportional to the pump rate and independent of the input signal, whereas in an unsaturated maser the output is linearly proportional to the input signal being amplified and exponentially dependent on the population inversion. Therefore, in an unsaturated maser relatively large random variations are likely because of random variations in the population inversion caused by changes in the collision rate, density, etc. The relatively small and periodic variations of most of the sources and the constancy of one source, VY CMa, thus suggest that the masers associated with infrared stars are saturated. This is in agreement with the conclusions of Wilson, Barrett, and Moran (1970) based on polarization measurements.

### D. Circumstellar Dust Shells and Stellar Properties

The interpretation generally given to the low color temperatures at

long wavelengths of many late type stars is that these stars are surrounded by dust envelopes which absorb the visible and near infrared radiation of the star, are heated to about  $600^{\circ}\text{K}$ , and re-radiate the energy between  $3$  and  $20\mu$ . In this section we first consider the luminosity variations of the dust shells of the three stars -- IRC+10011, IRC+50137, and IRC-10529 -- that have the largest radiation excesses at  $10\mu$  and thus presumably the densest shells. We then discuss possible interpretations of the period-amplitude-color-velocity separation relationship for all the Mira sources.

Frogel (1971) established a relationship between the variation of the  $[1.2\mu] - [3.5\mu]$  color index and the amplitude of variation at  $2.25\mu$  for stars with little excess  $10\mu$  radiation. The color variations of the three OH/IR stars with large excess  $10\mu$  radiation are consistent with the variations predicted from their  $2.2\mu$  amplitudes and Frogel's relationship. Therefore, the difference in amplitude of variability between the short and long wavelengths in the OH/IR stars is probably related to the central star rather than to the nature of the shell. The amplitude difference can probably be explained by variations of both the effective temperature of the stars and of the molecular band strengths at the shorter wavelengths.

Table 6 of the Appendix shows that the color temperatures of the above three stars, as well as all the OH/IR stars studied here, do not vary within the observational limits at wavelengths longer than  $3\mu$ . An upper limit to the variability of the  $[4.8\mu] - [10\mu]$  color for all the stars in Table 6 is  $\pm 0.2$  mag. For a dust-shell temperature of  $600^{\circ}\text{K}$  this implies a maximum color temperature variation of  $\pm 40^{\circ}\text{K}$ . For the three stars -- IRC+10011, IRC+50137, and IRC-10529 -- the  $4.8$  and  $10\mu$

emission arises almost entirely from the dust shells and, therefore, the physical temperature of the dust shell particles which are emitting probably does not vary much more than  $\pm 40^\circ\text{K}$ . With no change in size or optical depth, this range of temperature variation implies a variation in luminosity by no more than a factor of 1.7, not 2.5 to 3 as observed. Therefore, the effective radiating size of the dust cloud is probably smaller at minimum luminosity than at maximum for the above three stars. This does not imply that the cloud pulsates in size, but only that we tend to see particles farther from the star at maximum light.

The correlation between the four quantities -- period, amplitude, color, and velocity -- implies an interdependence between all of them. Clearly, the longer-period stars have larger amplitudes of variation, but the interpretation of the other relationships in terms of cause and effect is unclear. Larger amplitudes may be accompanied by greater mechanical activity leading to more mass loss and higher velocities of expulsion of the gas, or the longer-period stars may have intrinsically greater luminosities driving more mass loss and greater velocities of expulsion by means of radiation pressure acting on the dust grains (Gilman 1972).

The existence of  $1.35 \text{ cm H}_2\text{O}$  emission from the six shorter-period stars in Figure 1, but not from the longer-period stars, may be due to an additional correlation with one or more of the other quantities above. It may also be due to a correlation with the temperature of the stars which in turn may be correlated with one of the above quantities, or it could be a distance or luminosity effect. For instance, with the assumption that all these stars have equal luminosities of  $10^4 L_\odot$ , Hyland et al.

(1972) and Wilson et al. (1972) found that the distances of the six shorter-period stars are less than about 500 pc while the distances of the five longer-period stars are greater than about 500 pc. If all the sources had comparable  $\text{H}_2\text{O}$  luminosities, this would lead to the observed absence of 1.35 cm emission from the more distant stars.

#### V. SUMMARY

The principal conclusions of this study are:

- (1) The observed correlation between the infrared and 1612-MHz variability of the OH/IR stars is probably due to a radiative coupling mechanism between the stars and the OH clouds.
- (2) The coupling mechanism most consistent with these and other observations is that the masers are radiatively pumped, possibly at 2.8 or 35 $\mu$ .
- (3) The masers are probably saturated.

## ACKNOWLEDGEMENTS

We wish to thank the staffs of the Hale Observatories, the Harvard College Observatory--Smithsonian Astrophysical Observatory Radio Telescope at the G. R. Agassiz Station, and the National Radio Astronomy Observatory for the use of their facilities and their excellent technical support. PMH especially thanks A. R. Hyland, H. R. Butcher, and E. E. Becklin for making many of the early infrared observations and G. Clough, S. Harvey, S. K. Law, S. Loer, O. Maxwell, F. Porter, M. Schroeder, E. Sutton, H. Tye, and G. Veeder for helping with much of the observing along with the night assistants, J. Ditmar and T. Gregory. KPB, WJW, and JAB thank J. Wenners, J. O'Malley, R. N. Martin, P. R. Schwartz, P. Ho, and D. C. Papa for their help with the OH observations. KPB would also like to thank A. E. Lilley and the Harvard Radio Astronomy Project for their support during the first half of this program. Discussions with A. H. Barrett, M. M. Litvak, D. F. Dickinson, E. E. Becklin, P. Goldreich, G. Neugebauer, and M. W. Werner have been most helpful. PMH gratefully acknowledges support from the National Aeronautics and Space Administration (grants NGL 05-002-007 and NGL 05-002-207) and from the U. S. Air Force (contract G19628-70-C-0127). KPB was supported in part by the National Science Foundation (grant GP-20769). WJW was supported by the U. S. Air Force (contract F04701-72-C-0073).

## APPENDIX

On the following pages we show the infrared and OH microwave observations of the variability of all the sources considered in this study. The infrared data are plotted in magnitudes,  $-2.5 \log F_{\nu} + C_{\nu}$ . The absolute calibration is described by Wilson et al. (1972). The microwave observations are plotted linearly in terms of flux density and integrated flux.

Several tables containing the statistical parameters of the microwave and infrared variability follow the observations. Table 1 lists the reduced  $\chi^2$  of the variations, that is, the ratio of the root-mean-square deviation from the mean to the root-mean-square error. Table 2 lists the periods for the microwave and infrared variations of the 1612-MHz sources. These periods were determined by fitting the data with sine waves which were characterized by four parameters -- average level above zero, amplitude, period, and phase -- all of which were determined from the fit. When known, the visual period is also listed for comparison. Table 3 lists the phases of the 1612-MHz and infrared variations for the 1612-MHz sources. These phases were determined by fitting sine waves to the variations with the period fixed to either the visual or 2.2 $\mu$  period, whichever was best determined. The sign of the phase is defined such that a numerically smaller value of the phase implies a time lag. Table 4 lists the values of the correlation coefficients between the 2.2 $\mu$  and 1612-MHz variations and between the 10 $\mu$  and 1612-MHz variations for the nine variable 1612-MHz sources. These correlation coefficients were computed by interpolating the values of the infrared fluxes on the dates

of the microwave observations and correlating these interpolated values with the microwave fluxes. Table 5 contains the phases and correlation coefficients for the infrared and microwave variations of the 1665/1667-MHz sources, determined as for the 1612-MHz sources. Table 6 lists the amplitudes of variation of all the sources in the microwave and infrared. The amplitudes of the 1612-MHz sources are those determined by the sine wave fitting program. Since the microwave variations of the 1665/1667-MHz sources are not clearly periodic, their amplitudes were estimated directly from the observations.

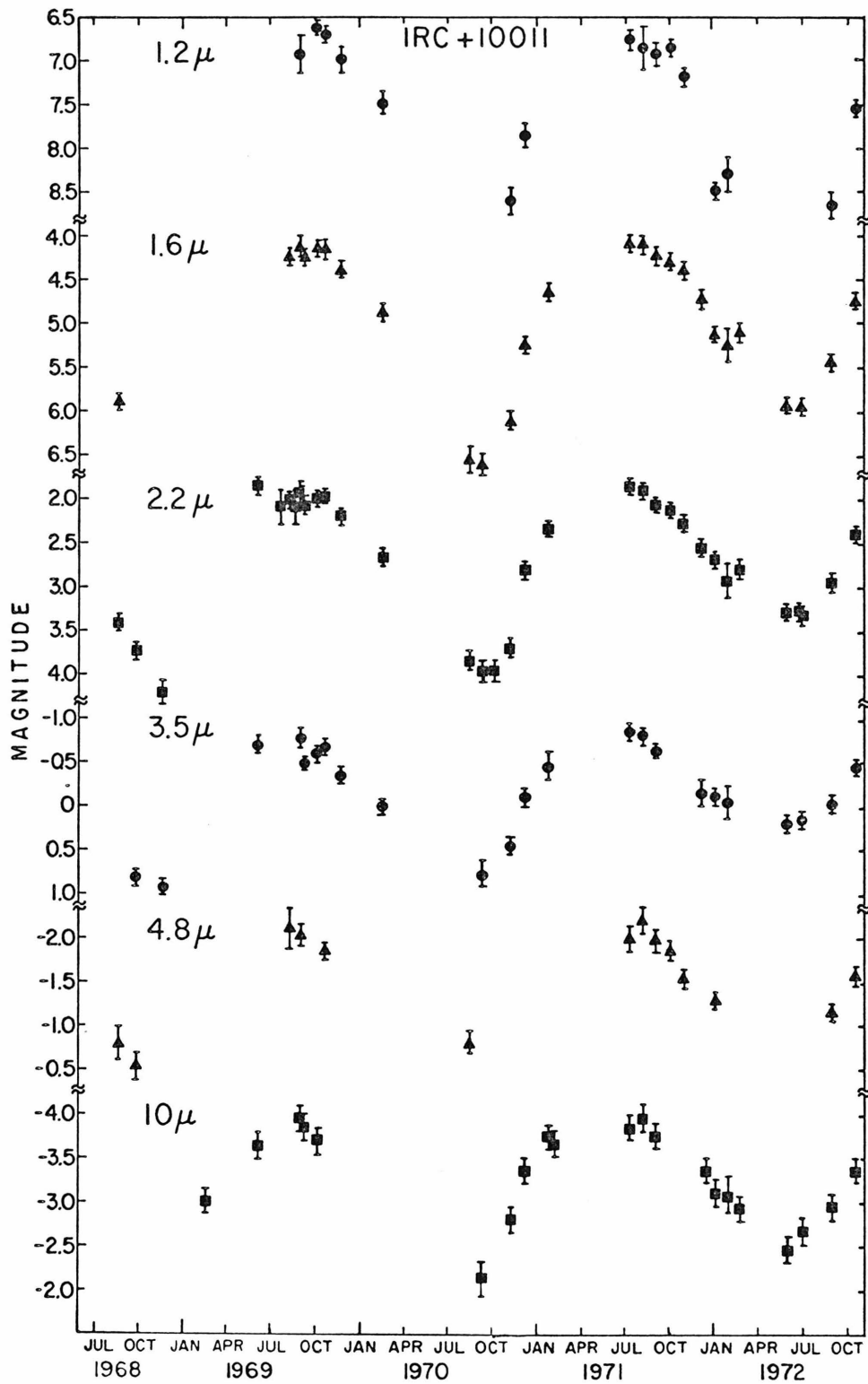


Fig. 4 (Appendix A)- The infrared observations of IRC+10011

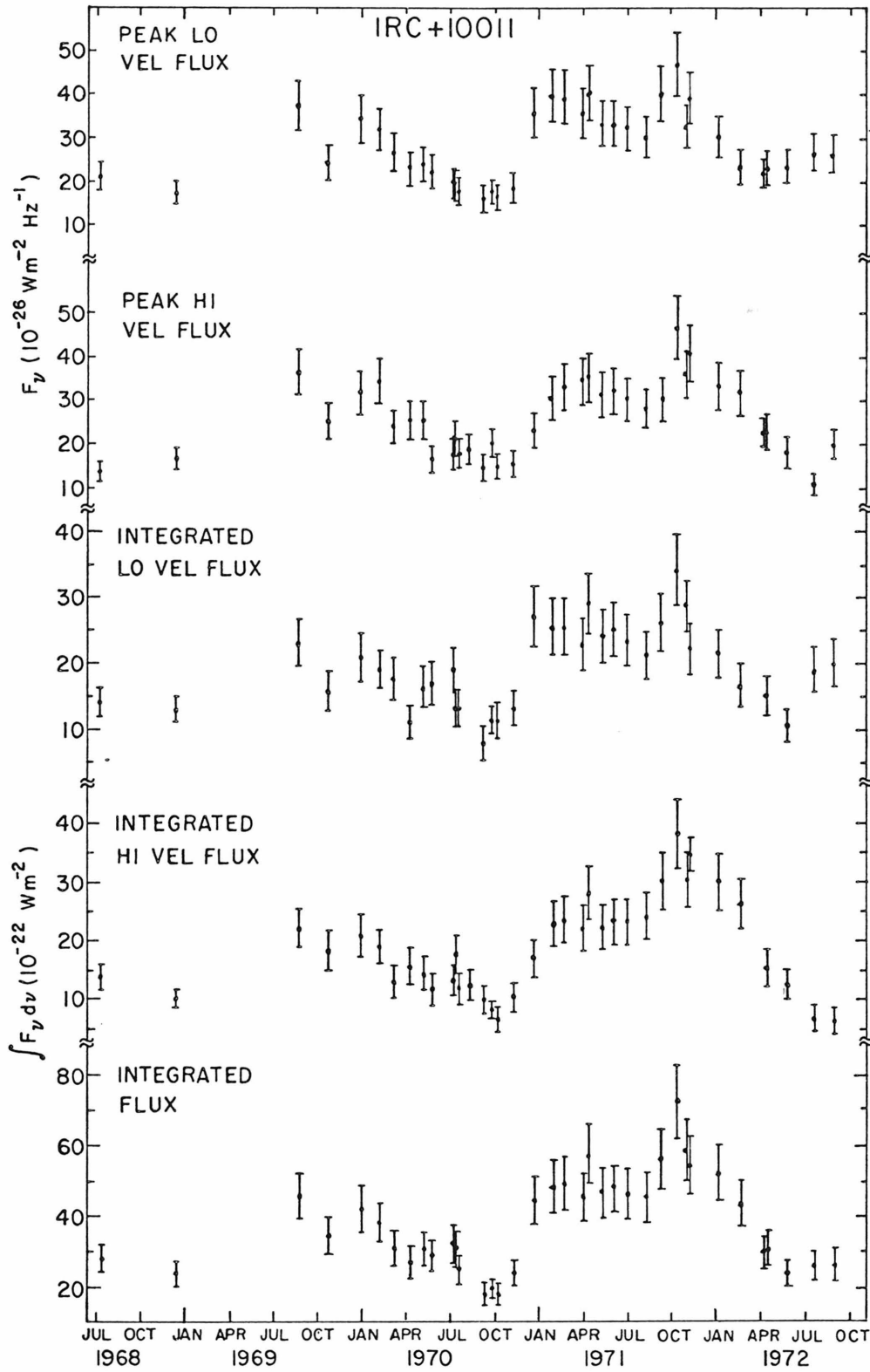


Fig. 5 (Appendix A)- The 1612-MHz observations of IRC+10011

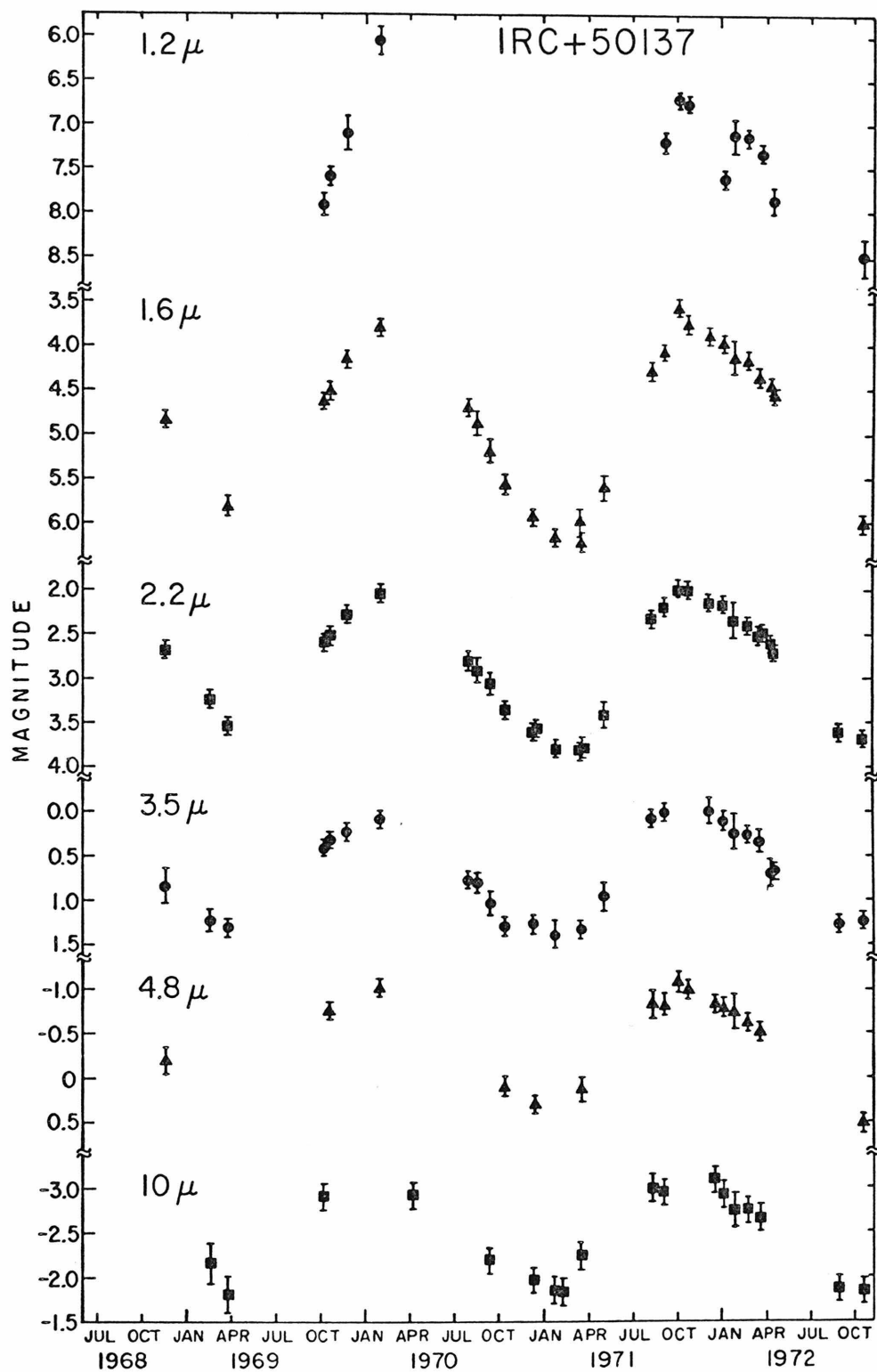


Fig. 6 (Appendix A)- The infrared observations of IRC+50137

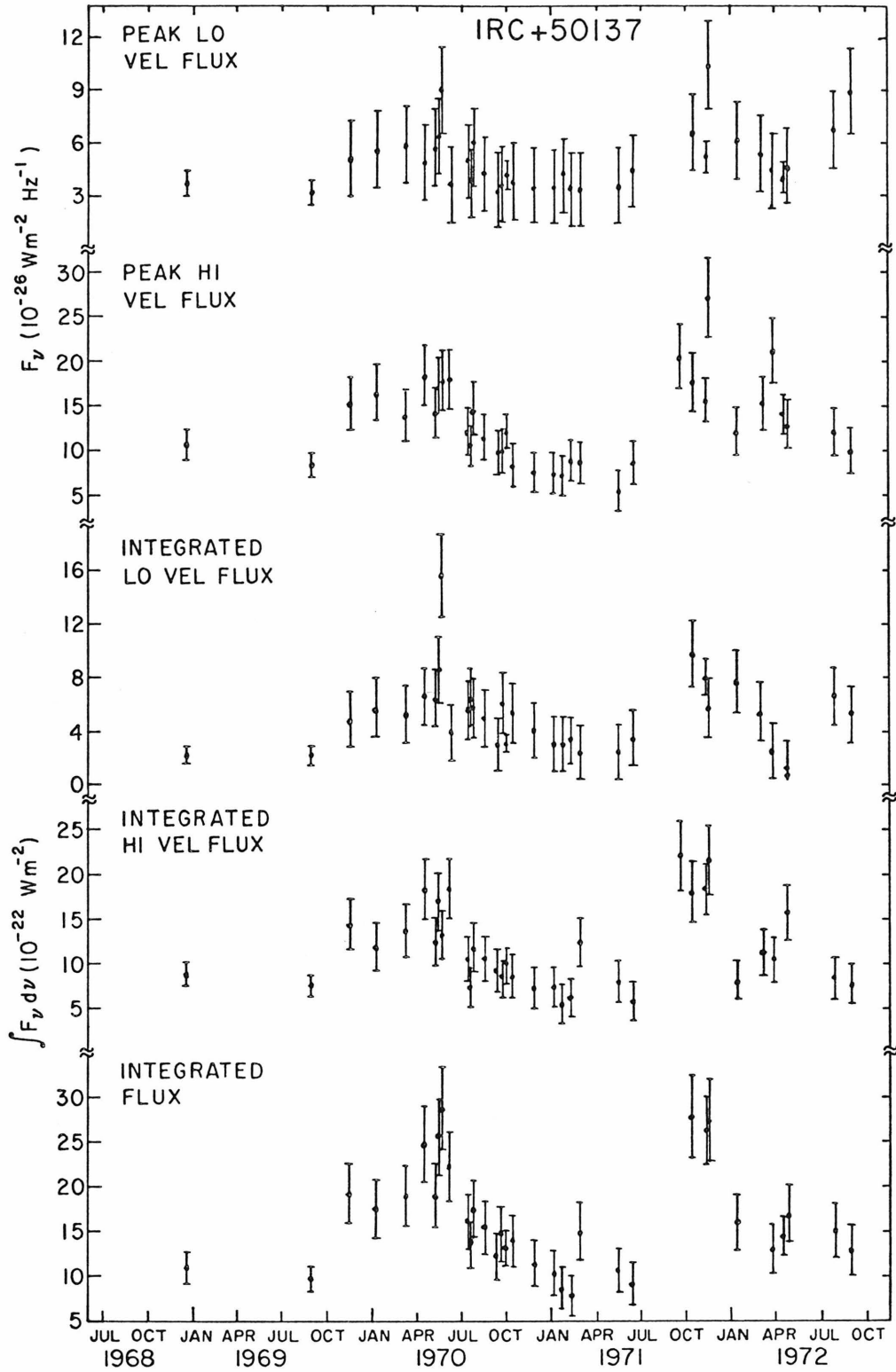


Fig. 7 (Appendix A)- The 1612-MHz observations of IRC+50137

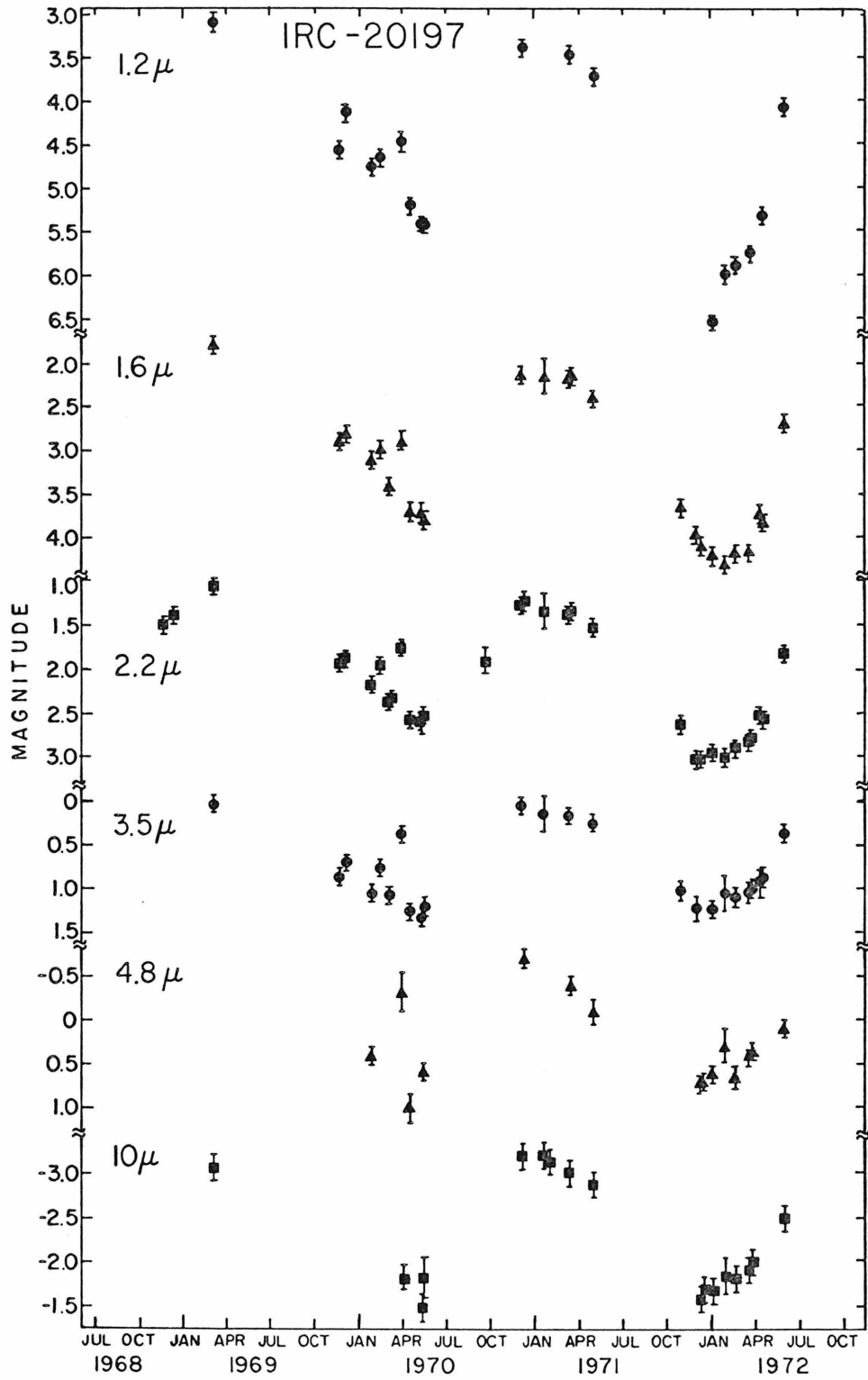


Fig. 8 (Appendix A)- The infrared observations of IRC-20197

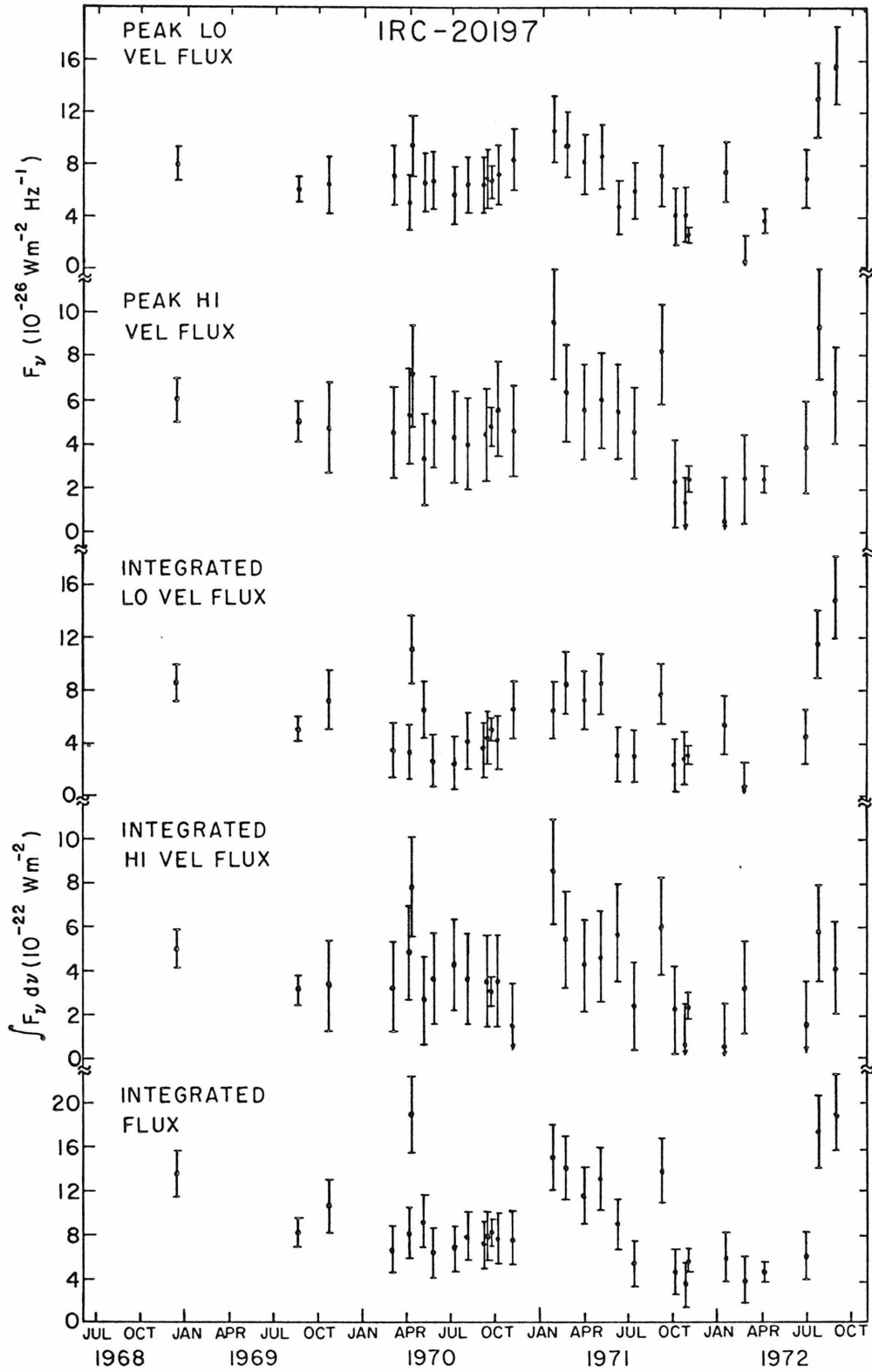


Fig. 9 (Appendix A)- The 1612-MHz observations of IRC-20197

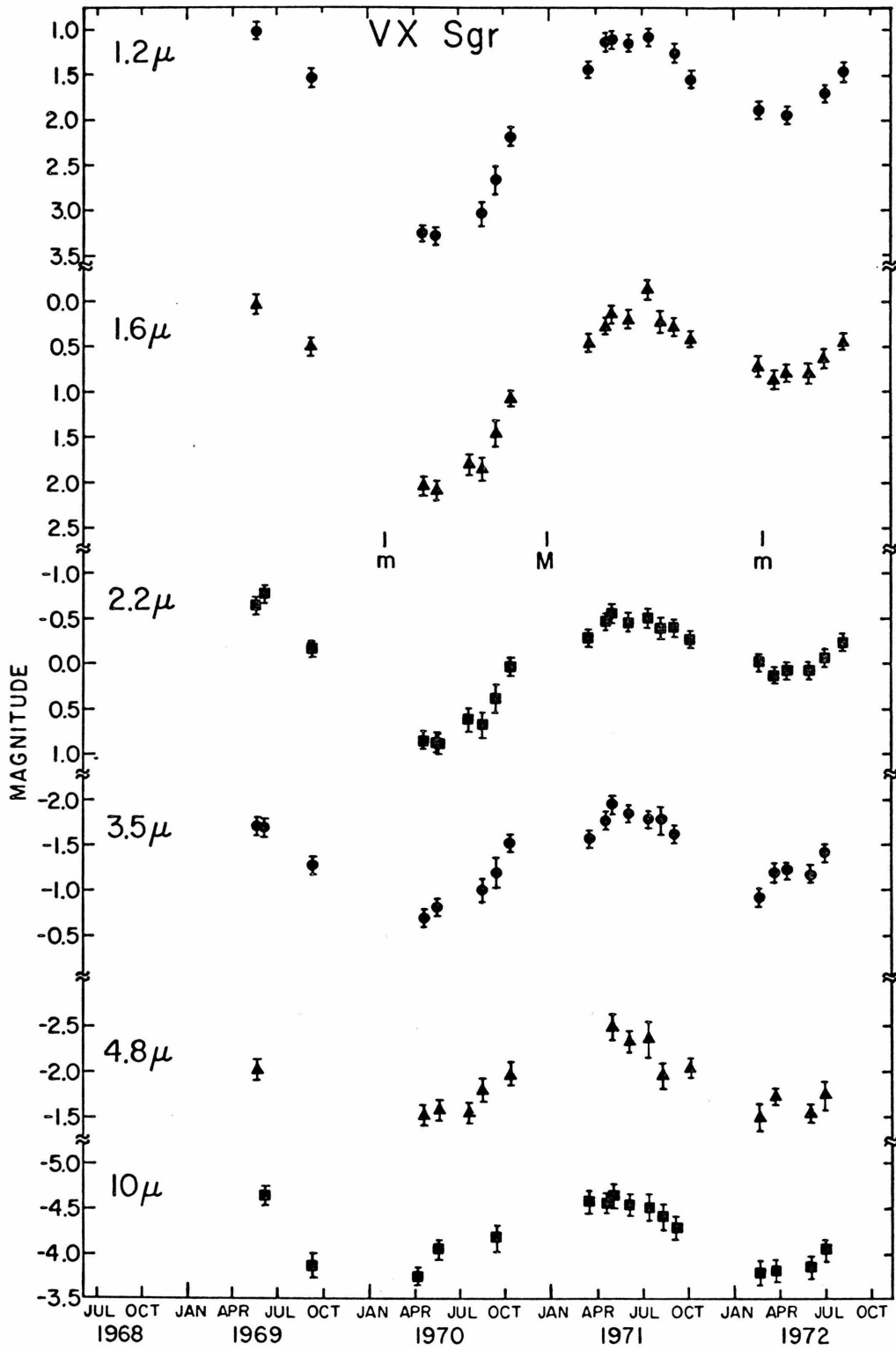


Fig. 10 (Appendix A) - The infrared observations of VX Sgr

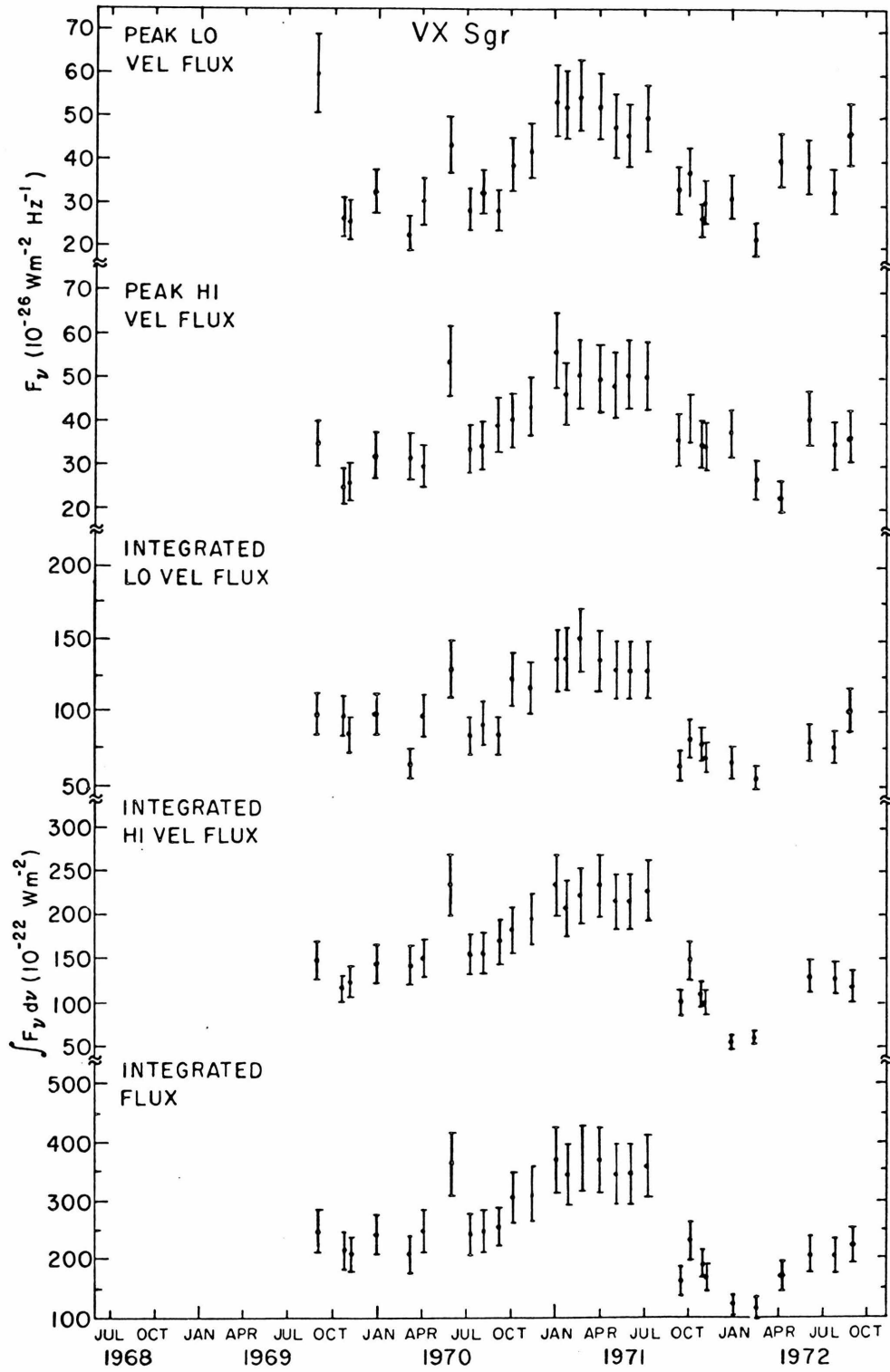


Fig. 11 (Appendix A) - The 1612-MHz observations of VX Sgr

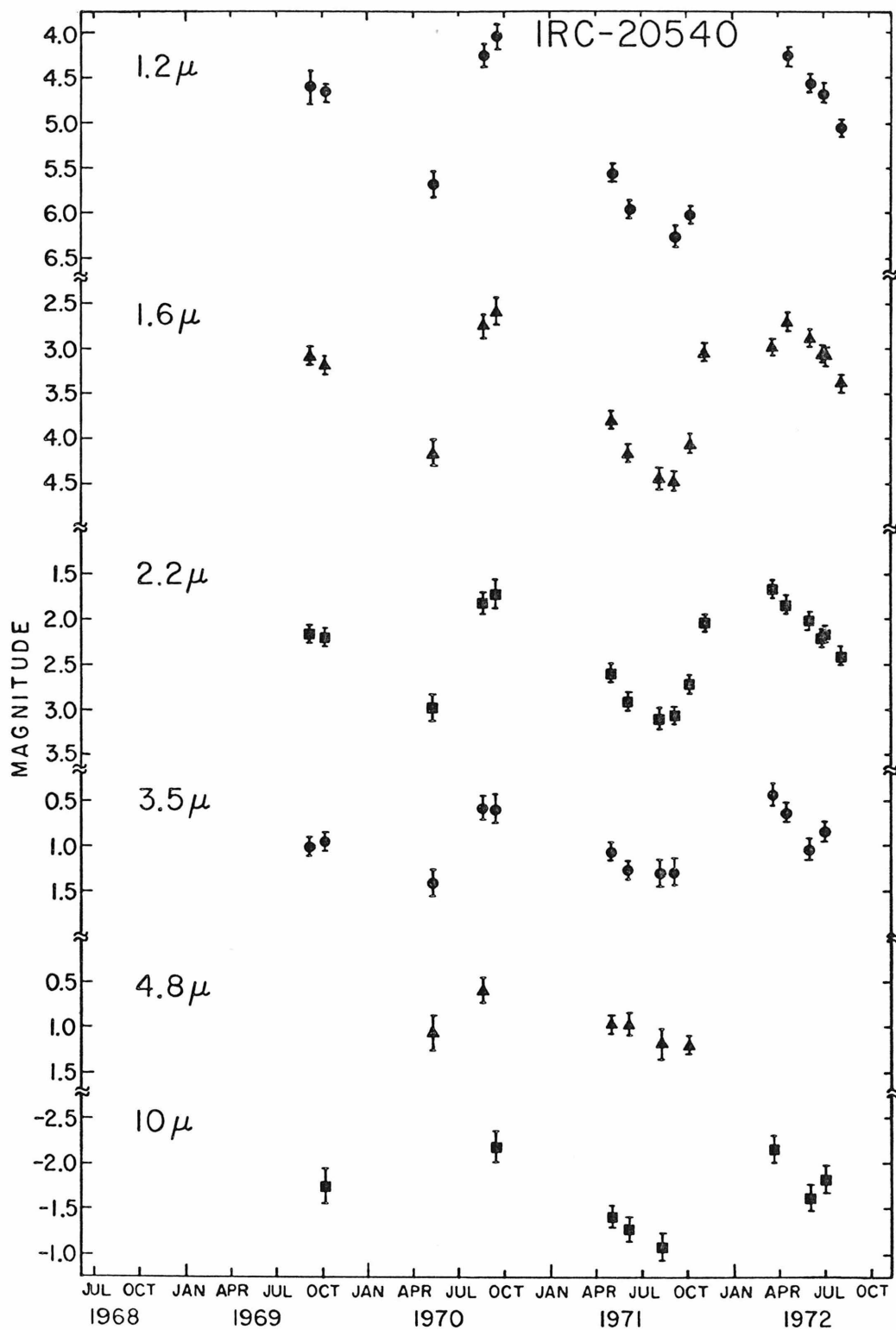


Fig. 12 (Appendix A)-The infrared observations of IRC-20540

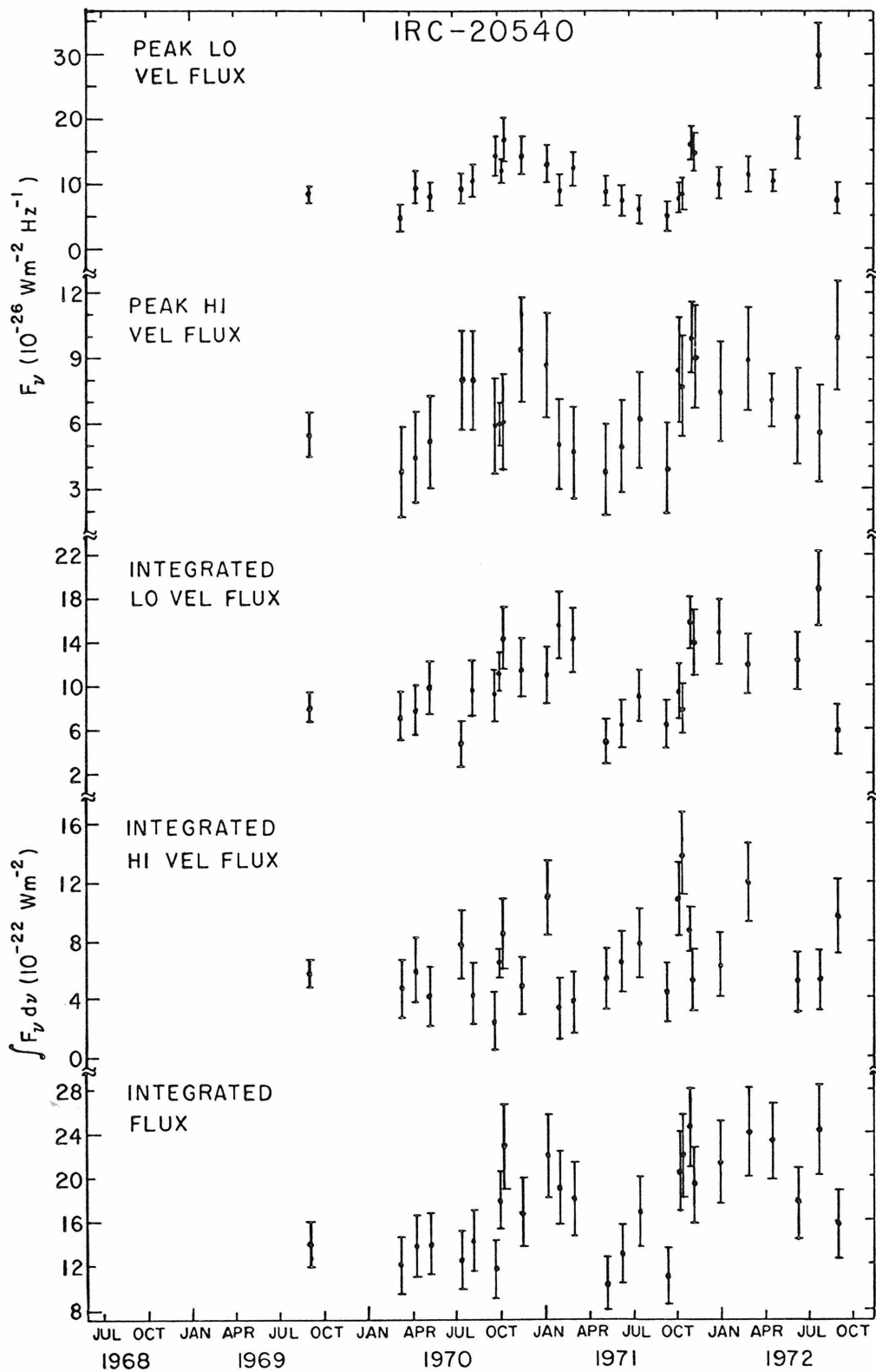


Fig. 13 (Appendix A)-The 1612-MHz observations of IRC-20540

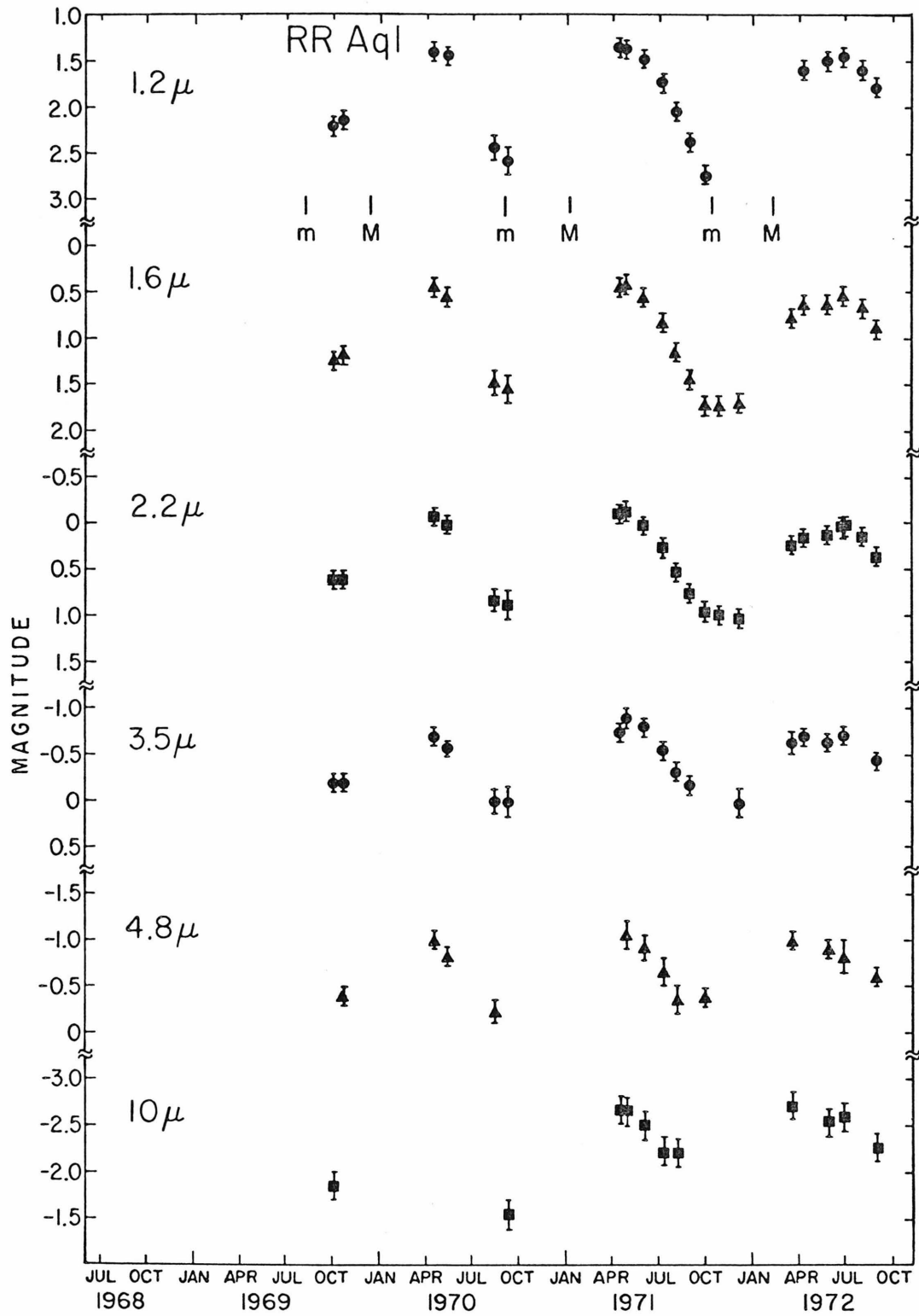


Fig. 14 (Appendix A)-The infrared observations of RR Aql

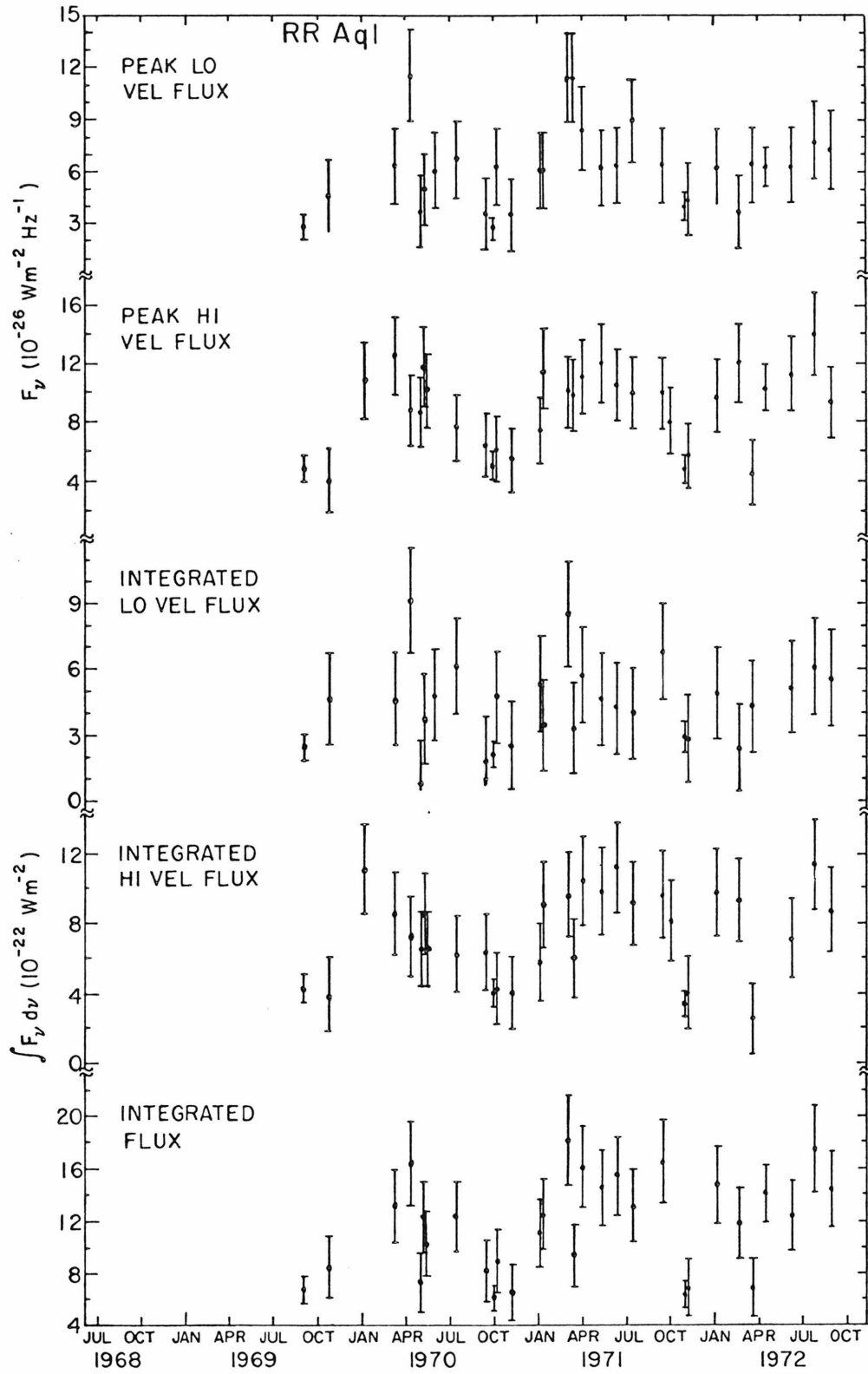
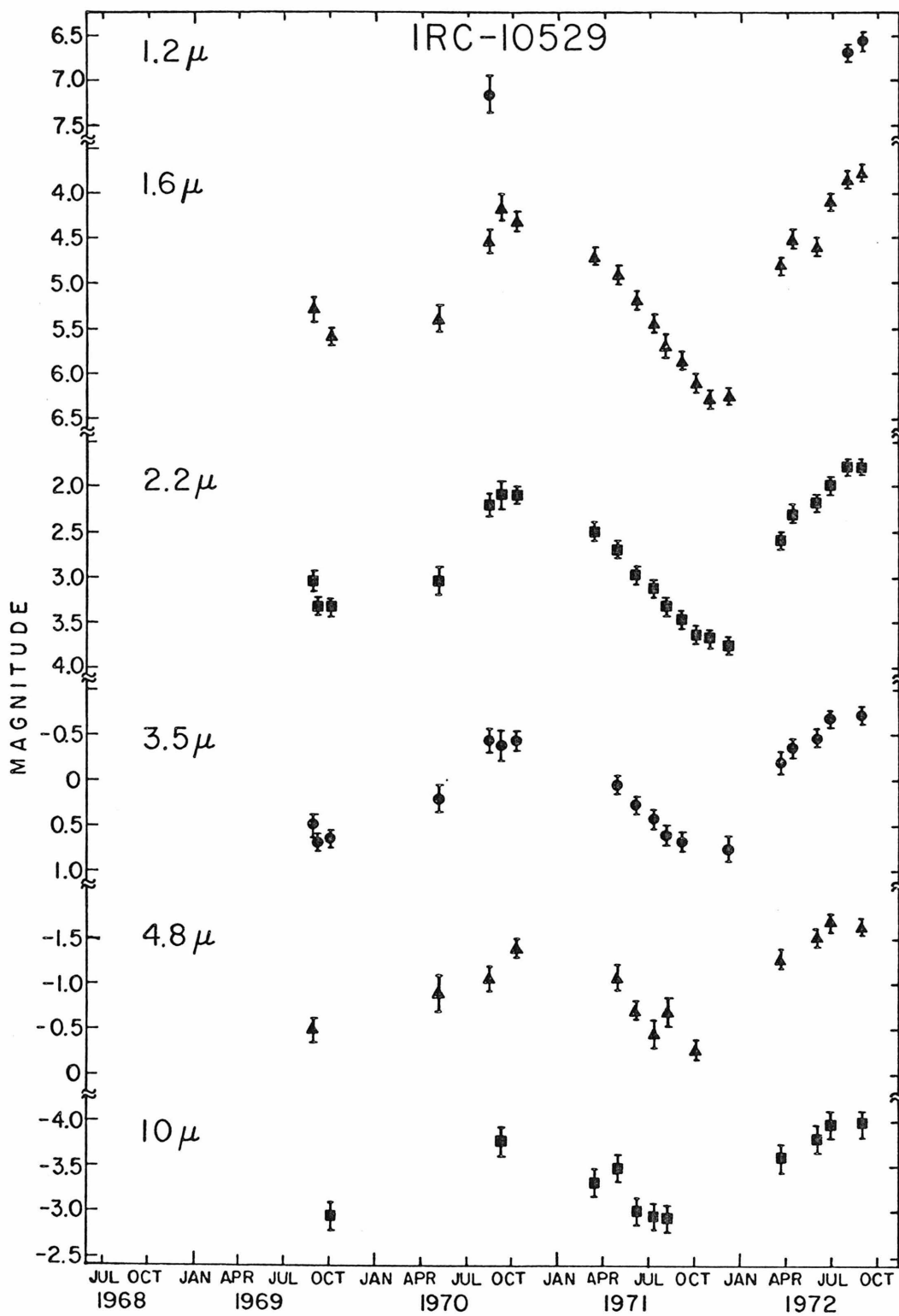


Fig. 15 (Appendix A)-The 1612-MHz observations of RR Aql



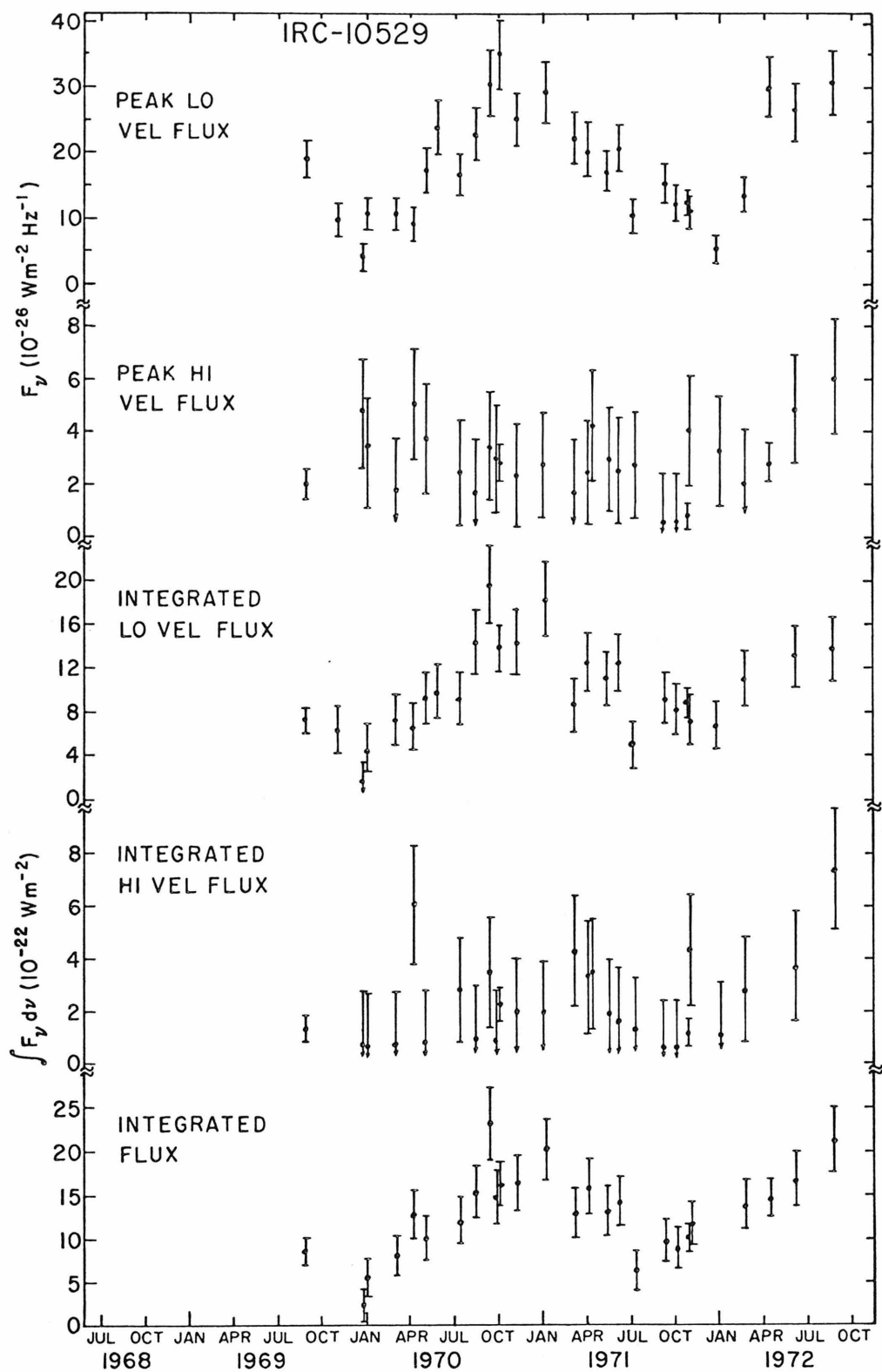


Fig. 17 (Appendix A)-The 1612-MHz observations of IRC-10529

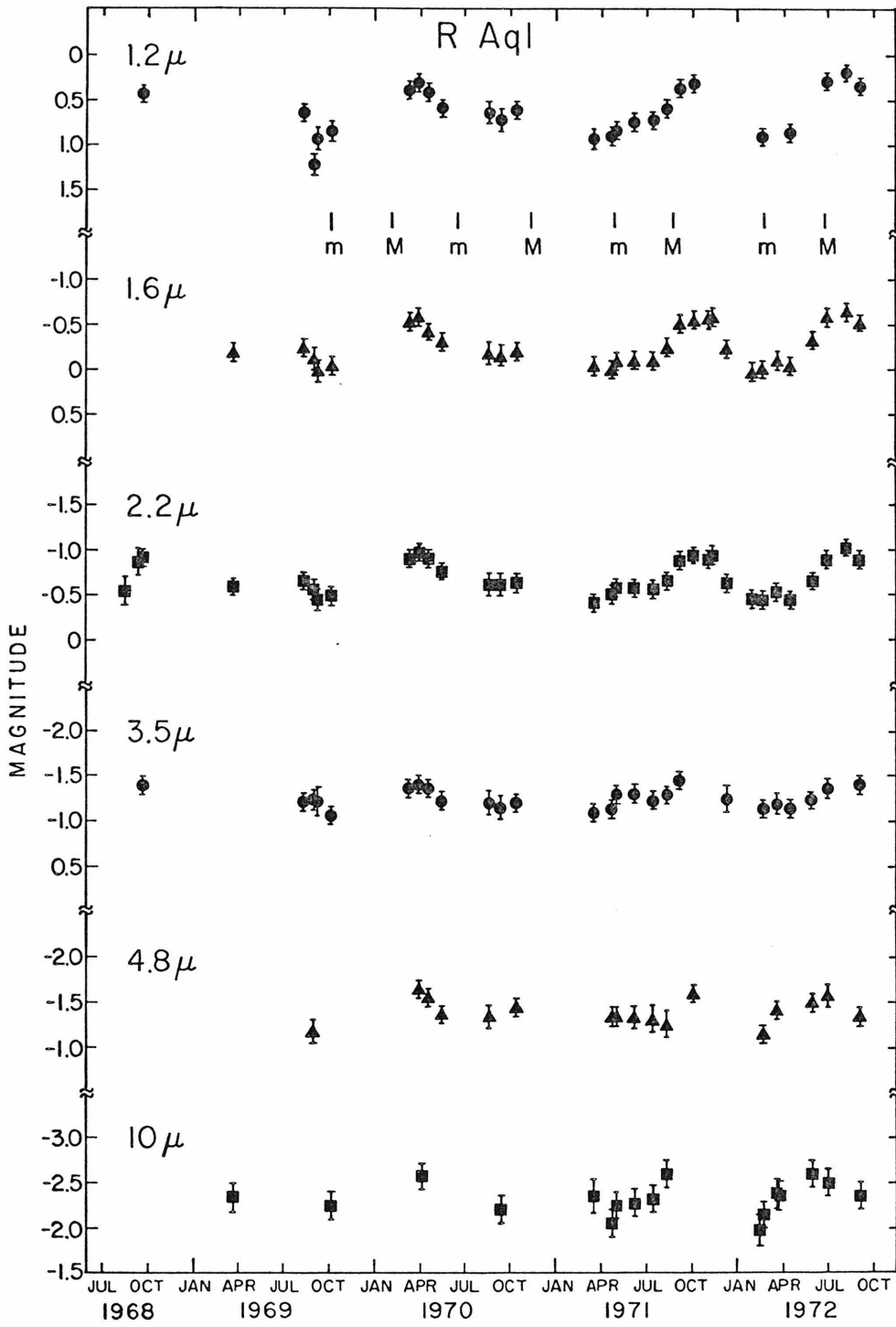


Fig. 18 (Appendix A)-The infrared observations of R Aql

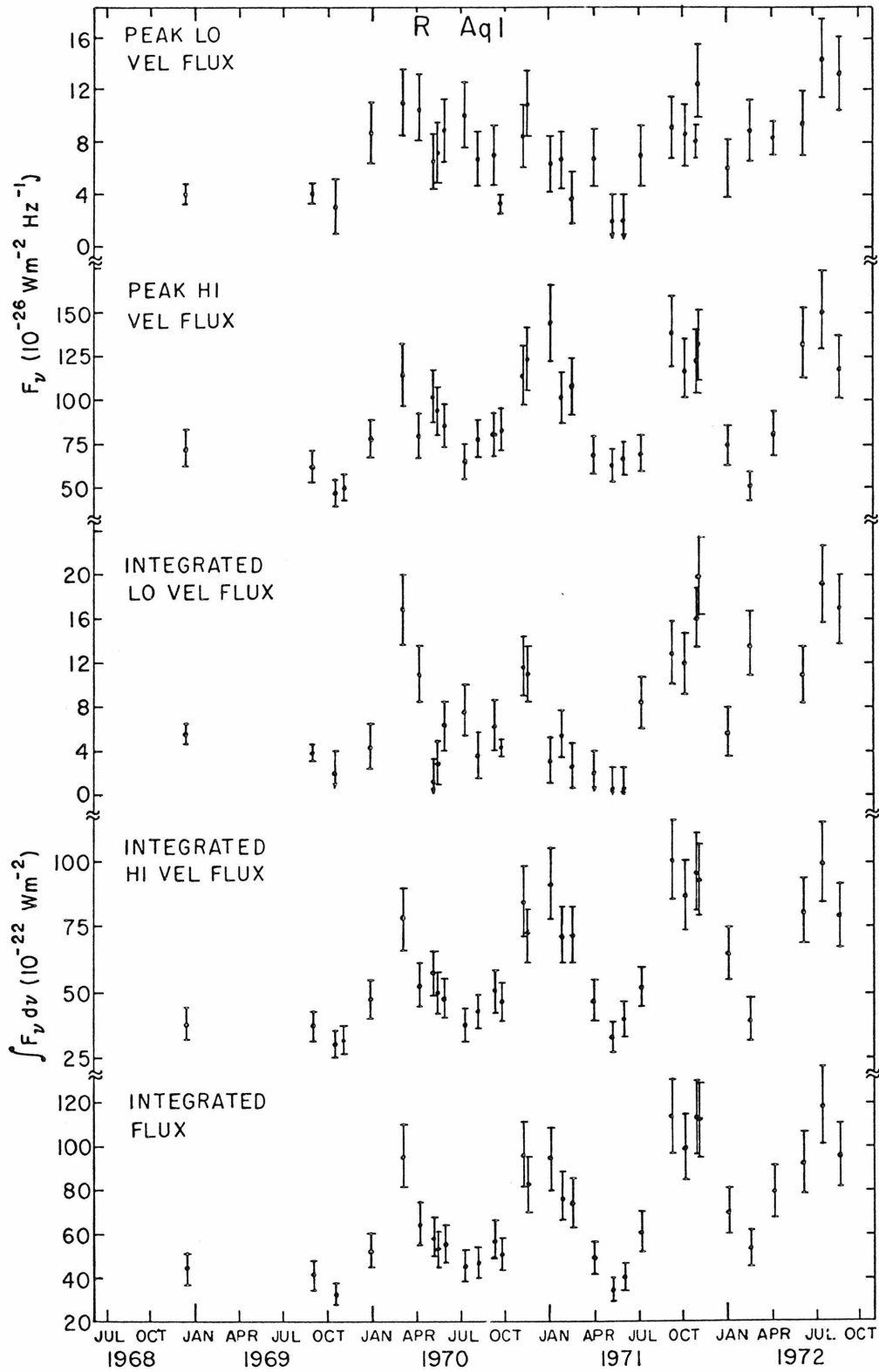


Fig. 19 (Appendix A)-The 1612-MHz observations of R Aql

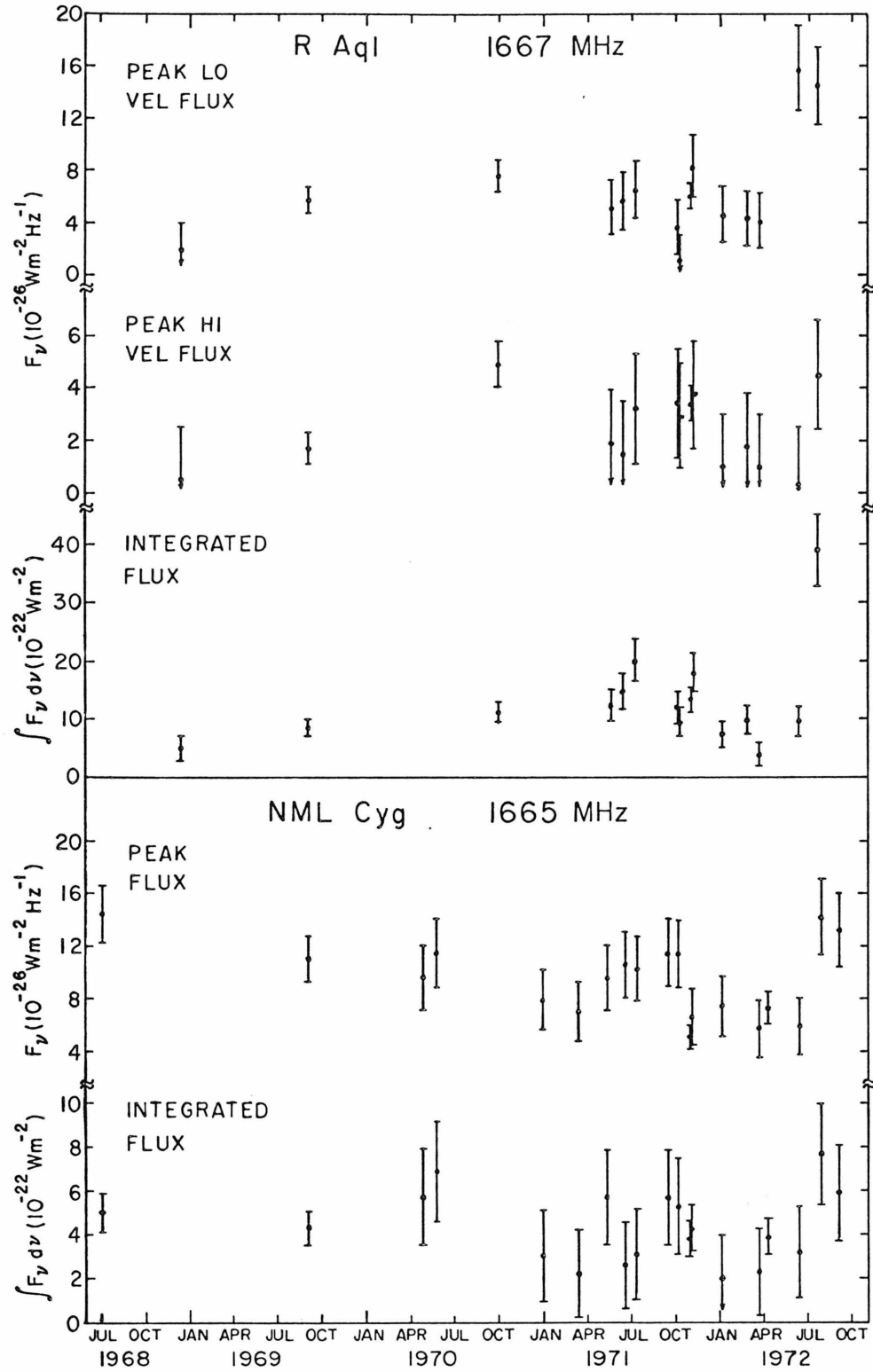


Fig. 20 (Appendix A) - The 1667-MHz observations of R Aql and the 1665-MHz observations of NML Cyg.

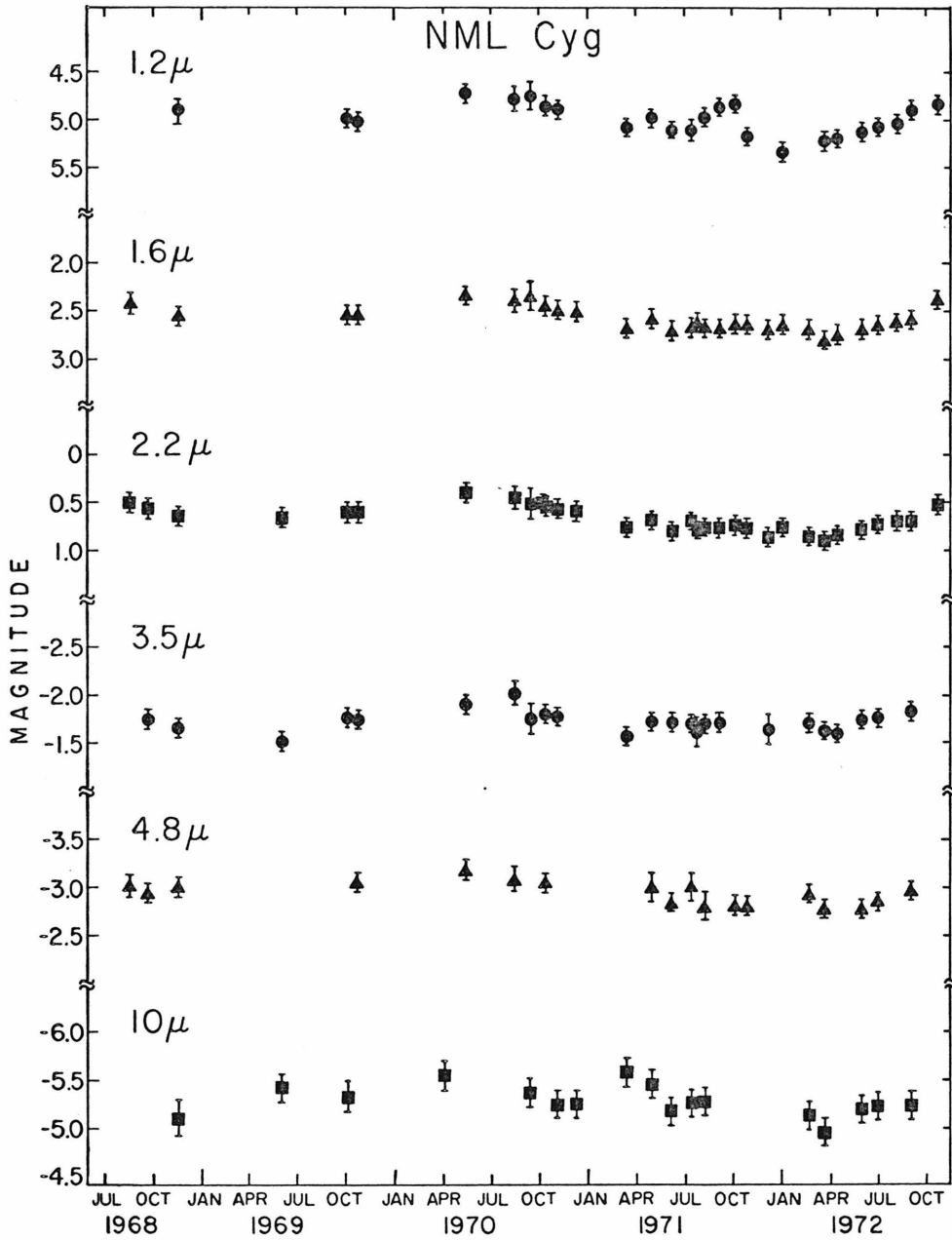


Fig. 21 (Appendix A) - The infrared observations of NML Cyg

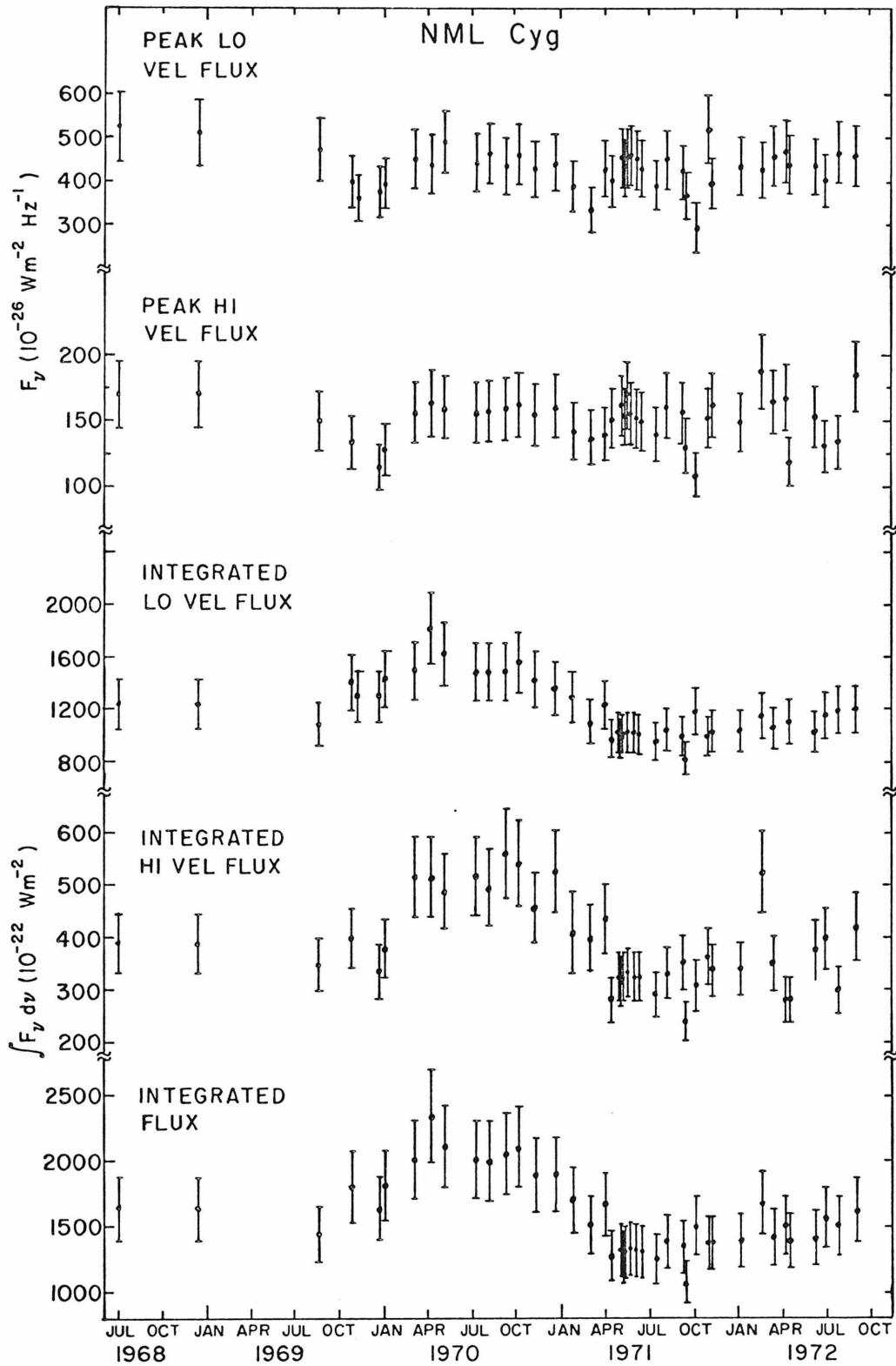


Fig. 22 (Appendix A) - The 1612-MHz observations of NML Cyg

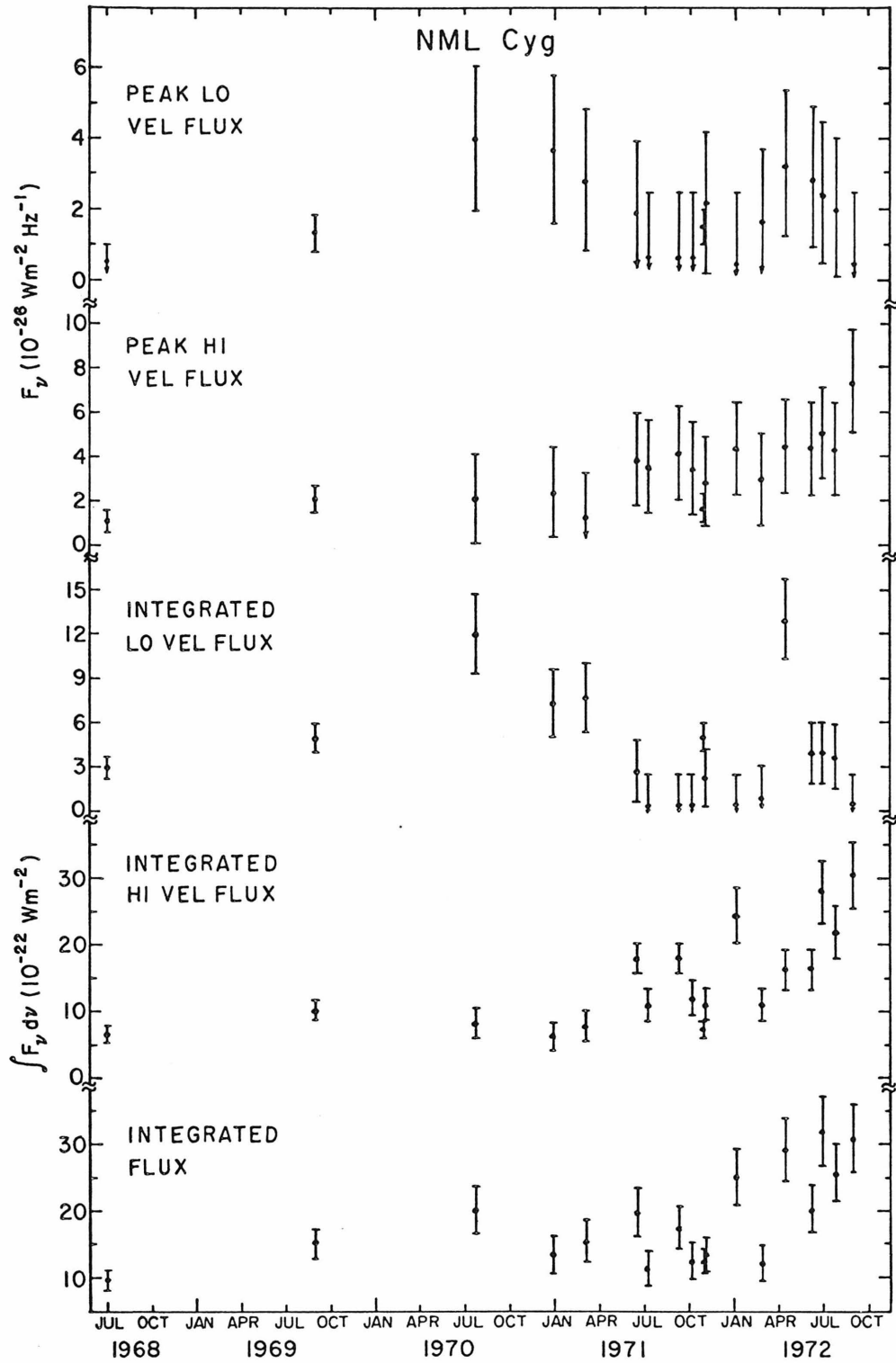


Fig. 23 (Appendix A) - The 1667-MHz observations of NML Cyg

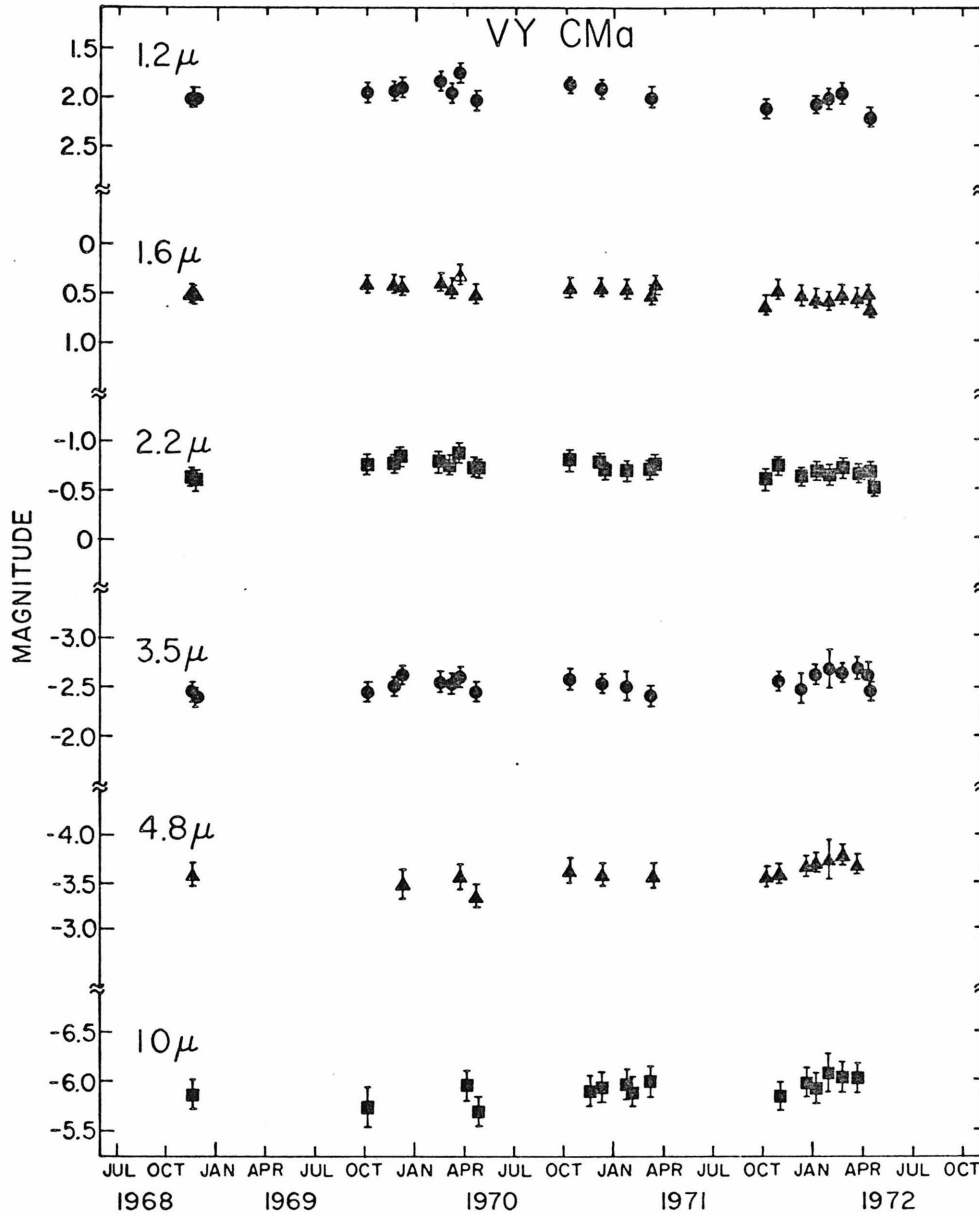


Fig. 24 (Appendix A) - The infrared observations of VY CMa

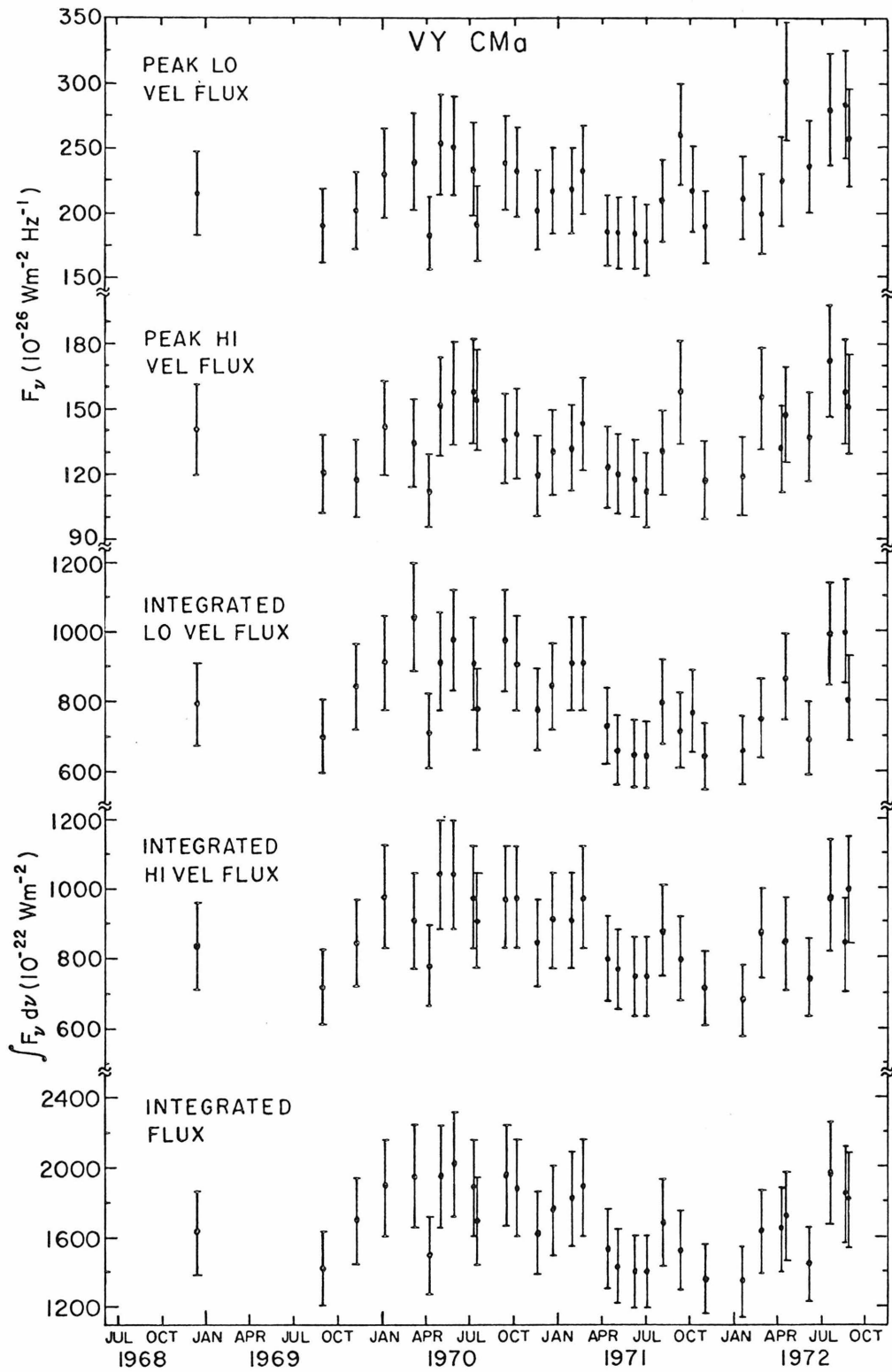


Fig. 25 (Appendix A) - The 1612-MHz observations of VY CMa

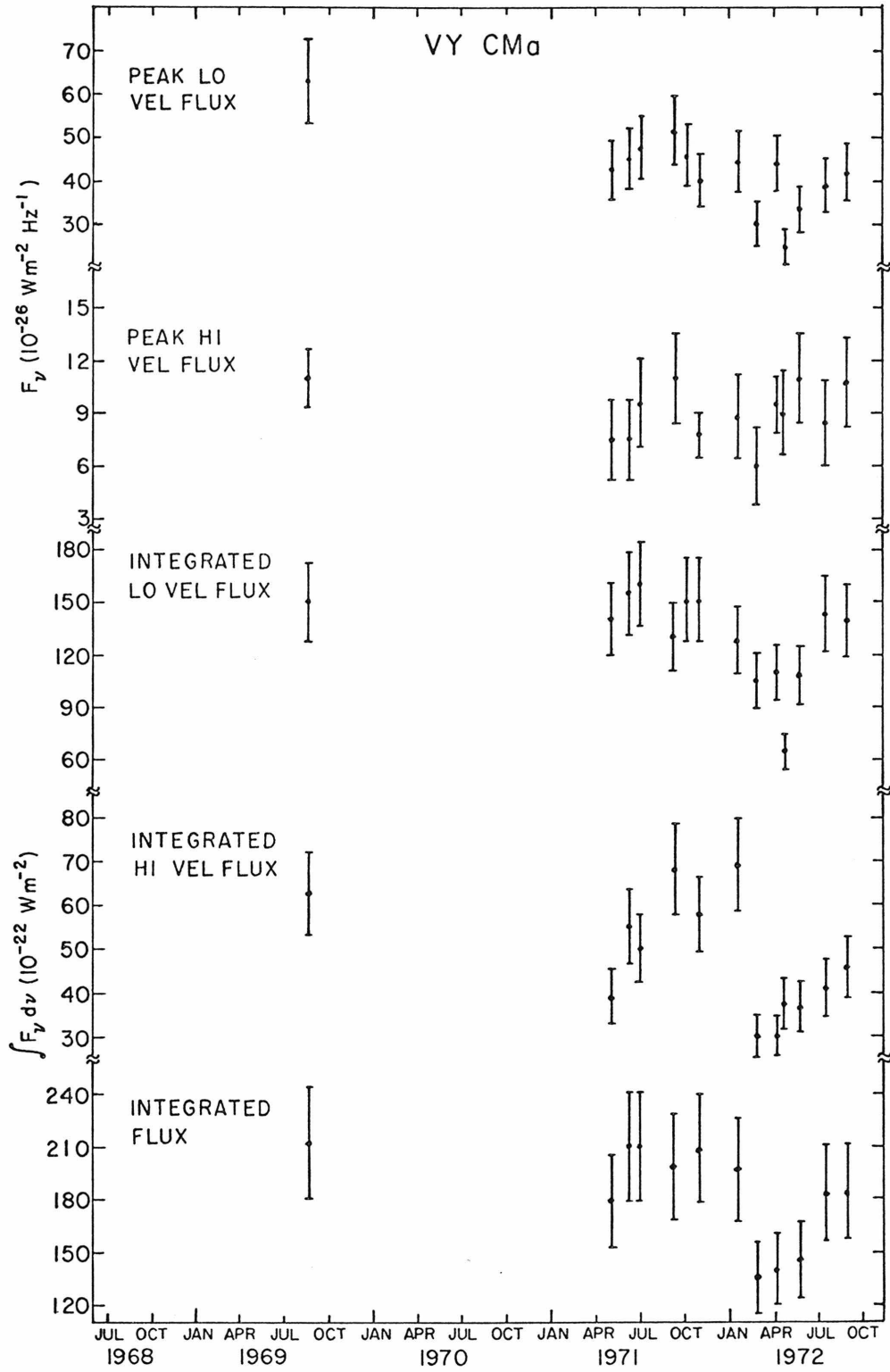


Fig. 26 (Appendix A) - The 1665-MHz observations of VY CMa

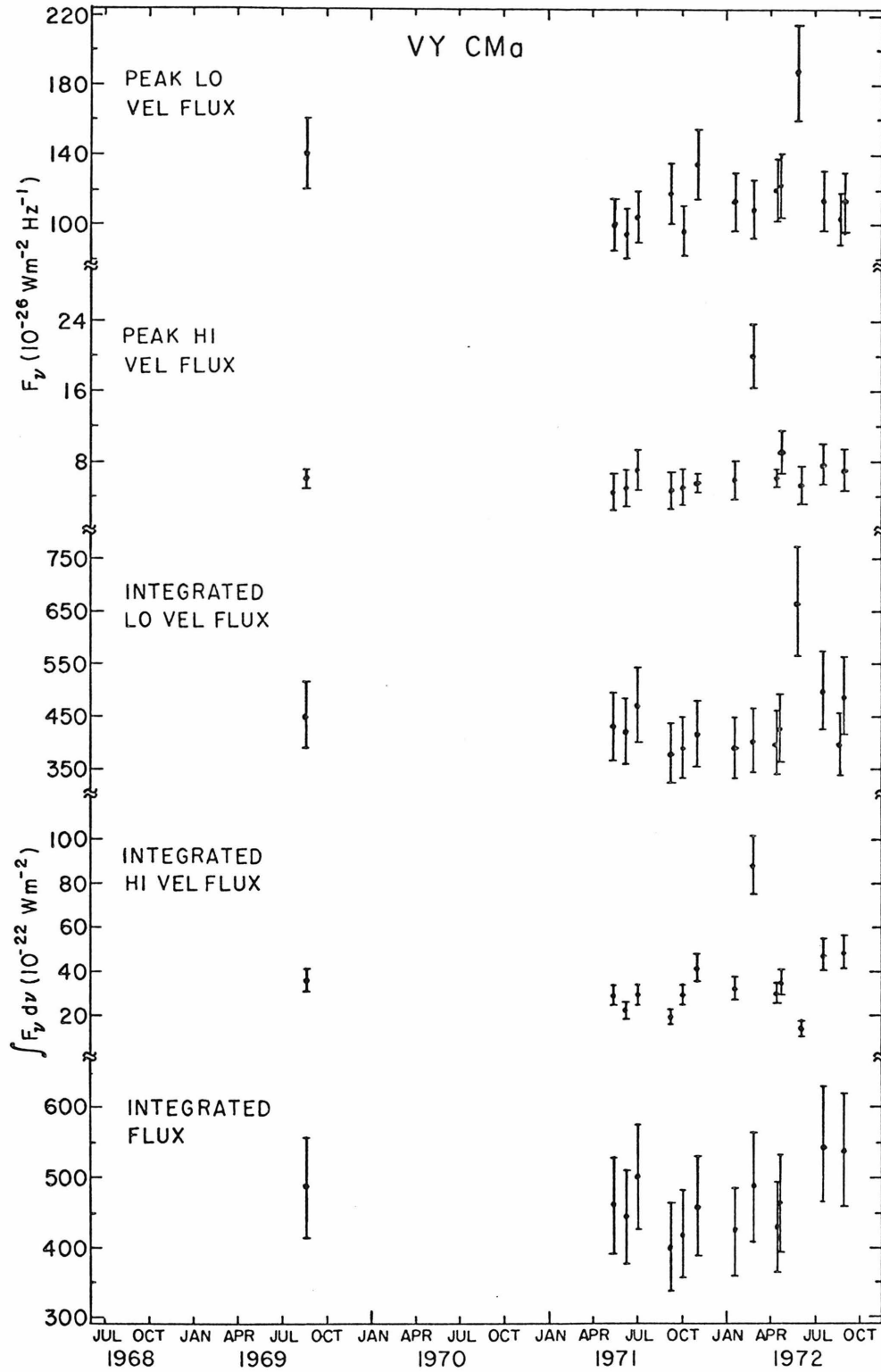


Fig. 27 (Appendix A) - The 1667-MHz observations of VY CM $\alpha$

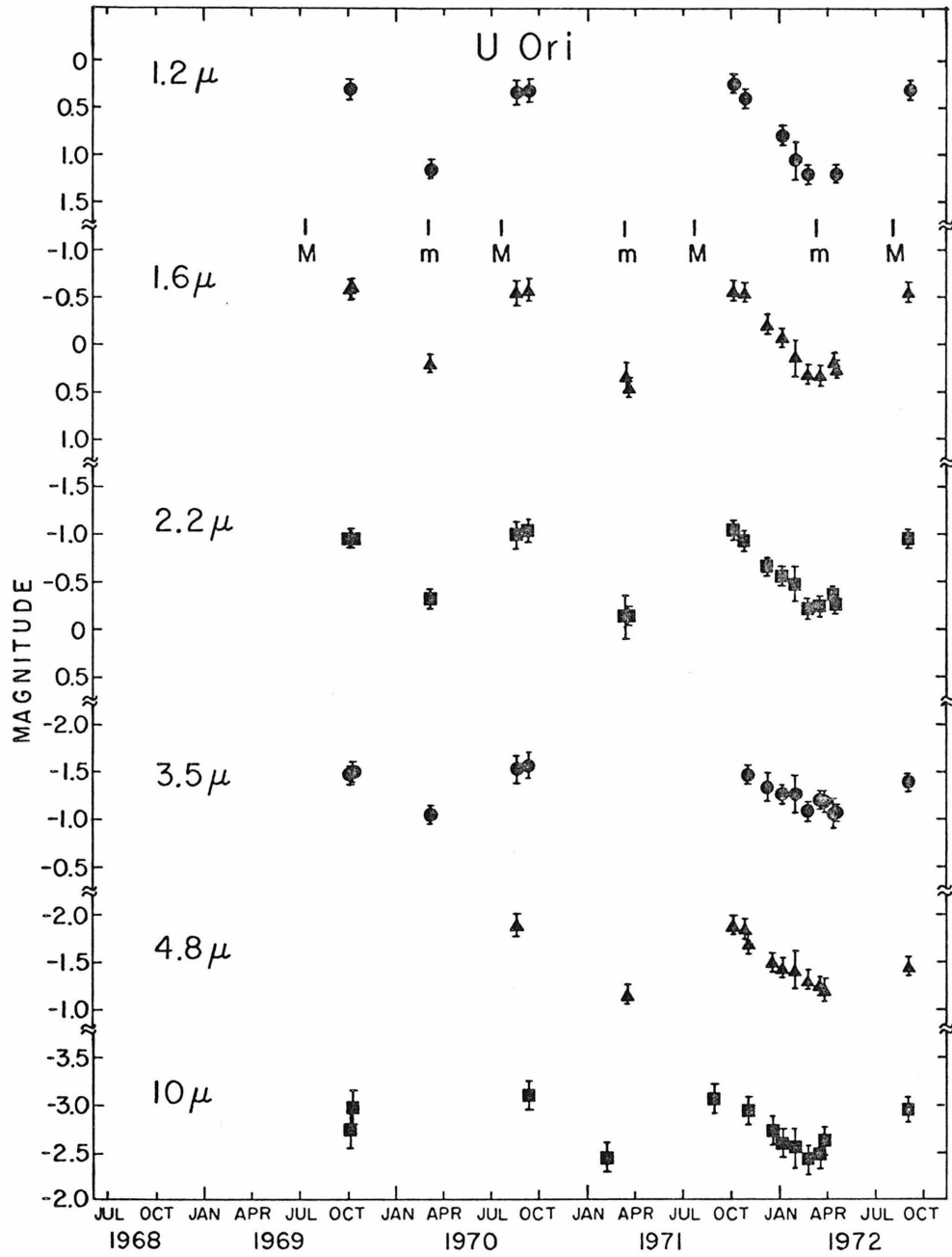


Fig. 28 (Appendix A) - The infrared observations of U Ori

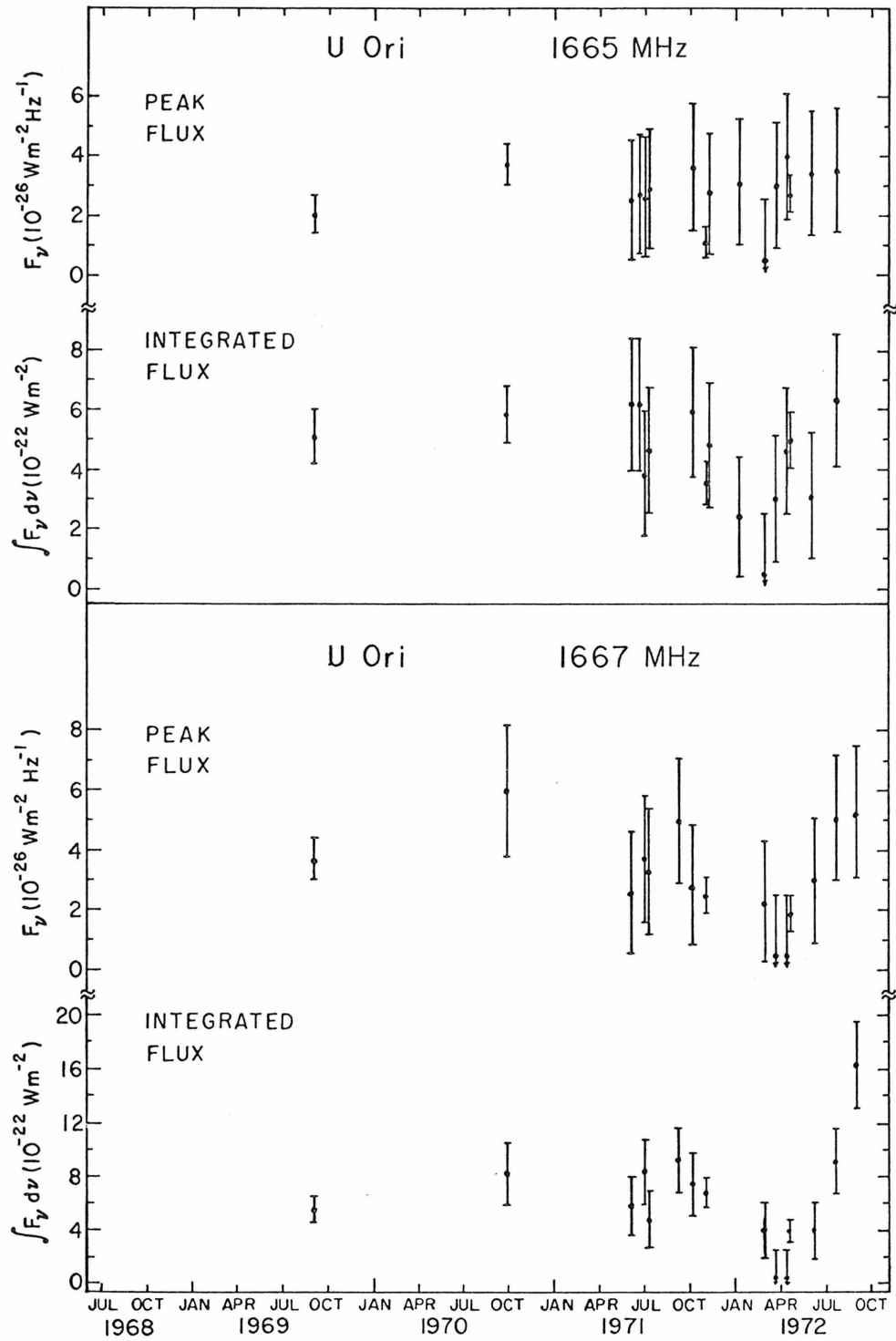


Fig. 29 (Appendix A) - The 1665- and 1667-MHz observations of U Ori

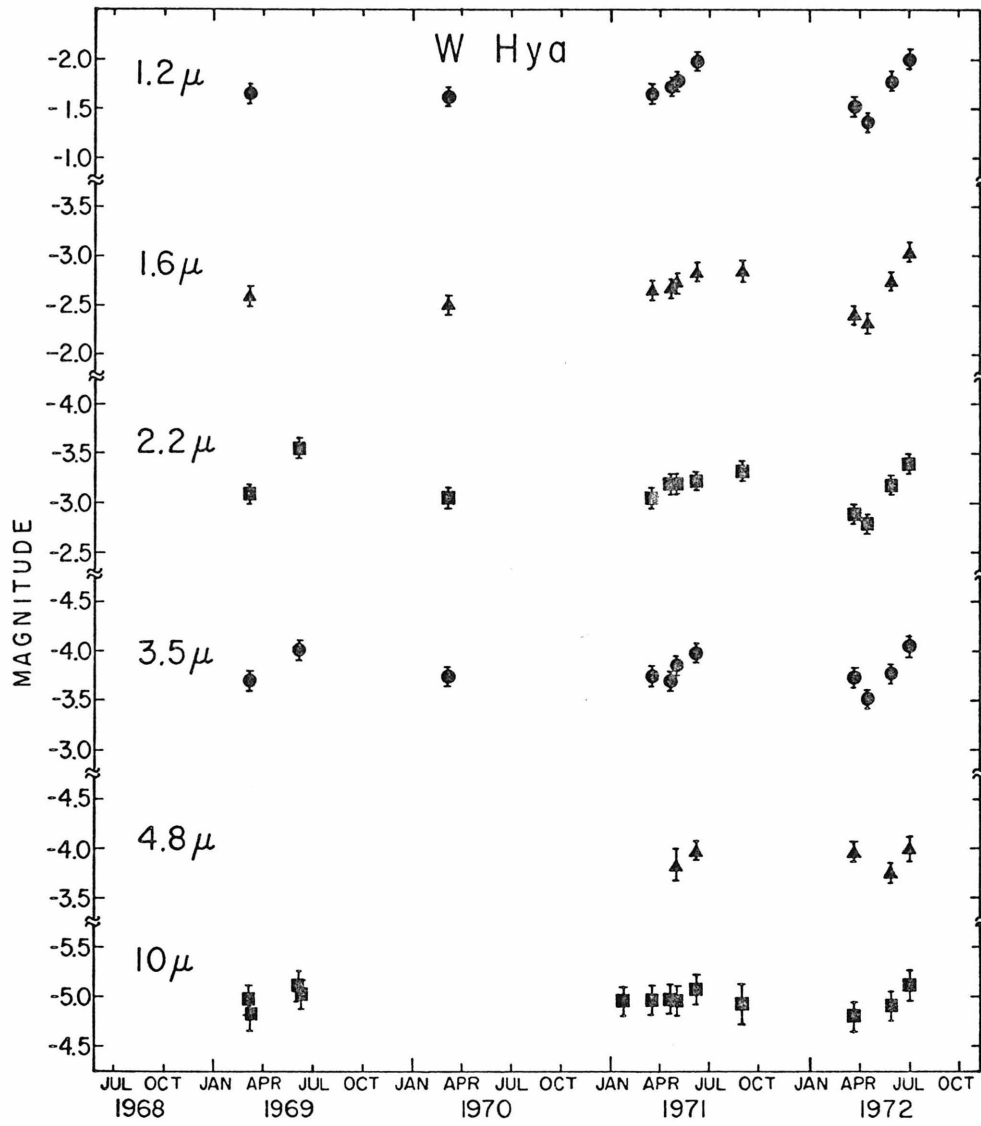


Fig. 30 (Appendix A) - The infrared observations of W Hya

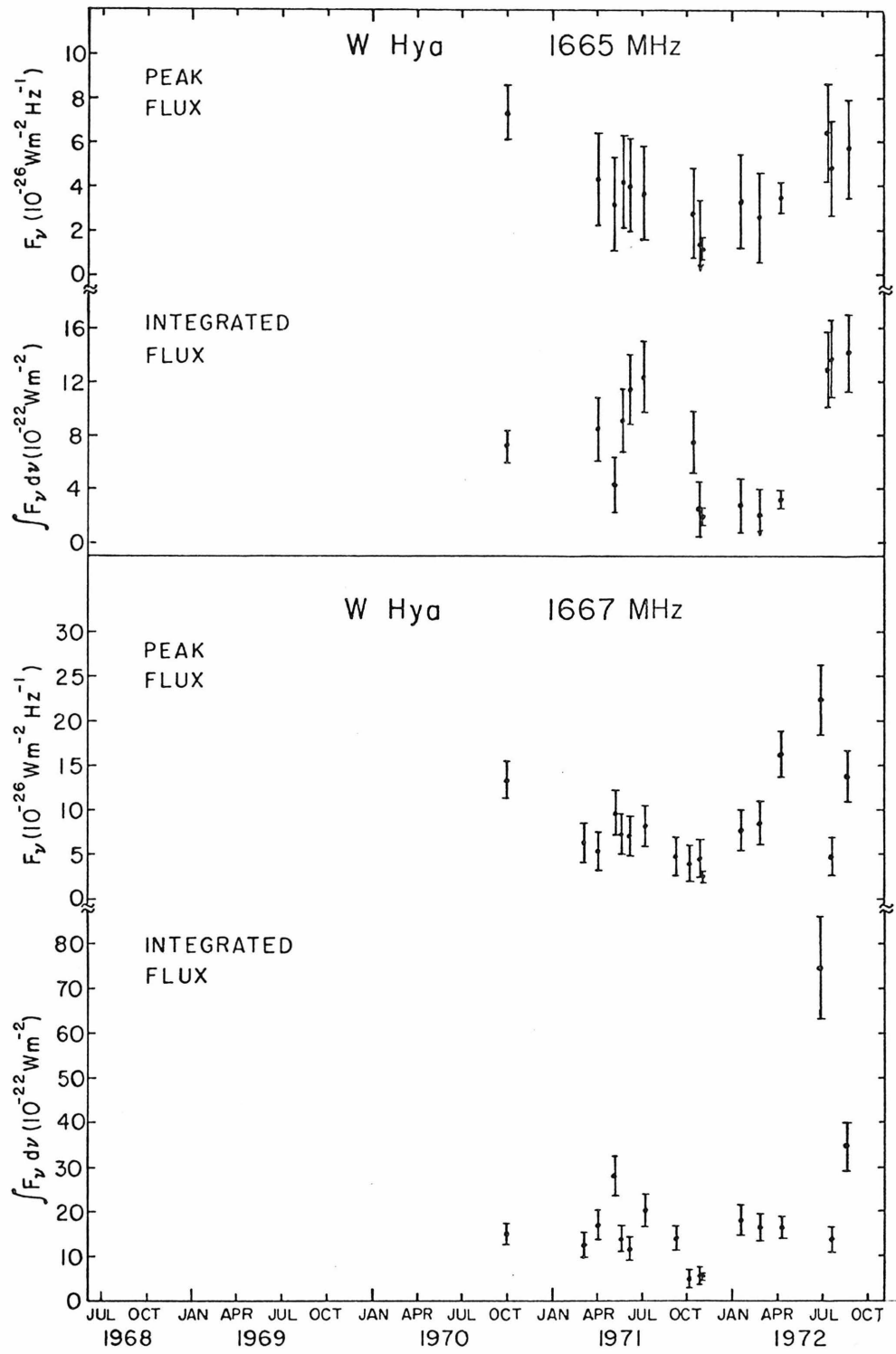


Fig. 31 (Appendix A) - The 1665- and 1667-MHz observations of W Hya

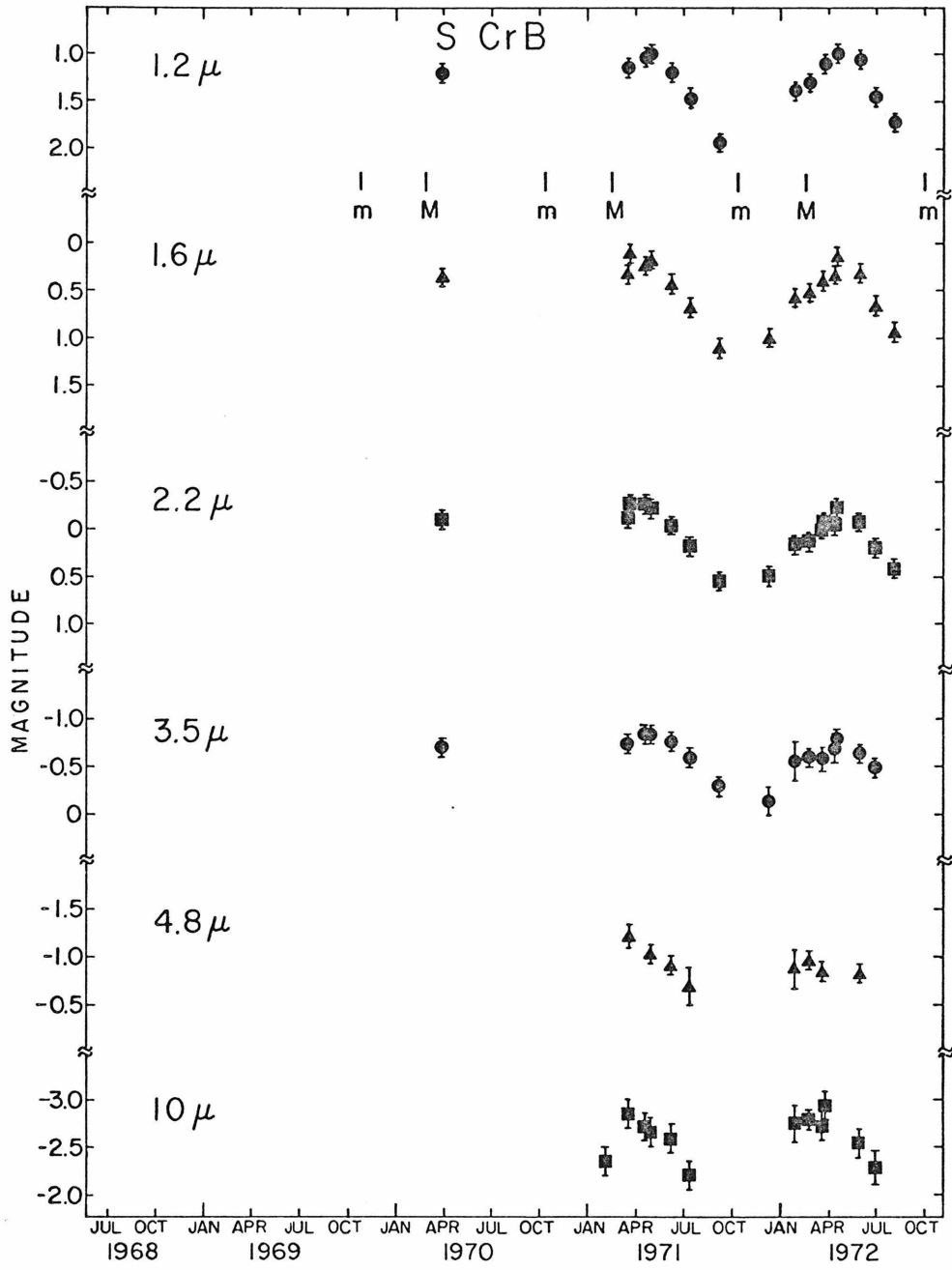


Fig. 32 (Appendix A) - The infrared observations of S CrB

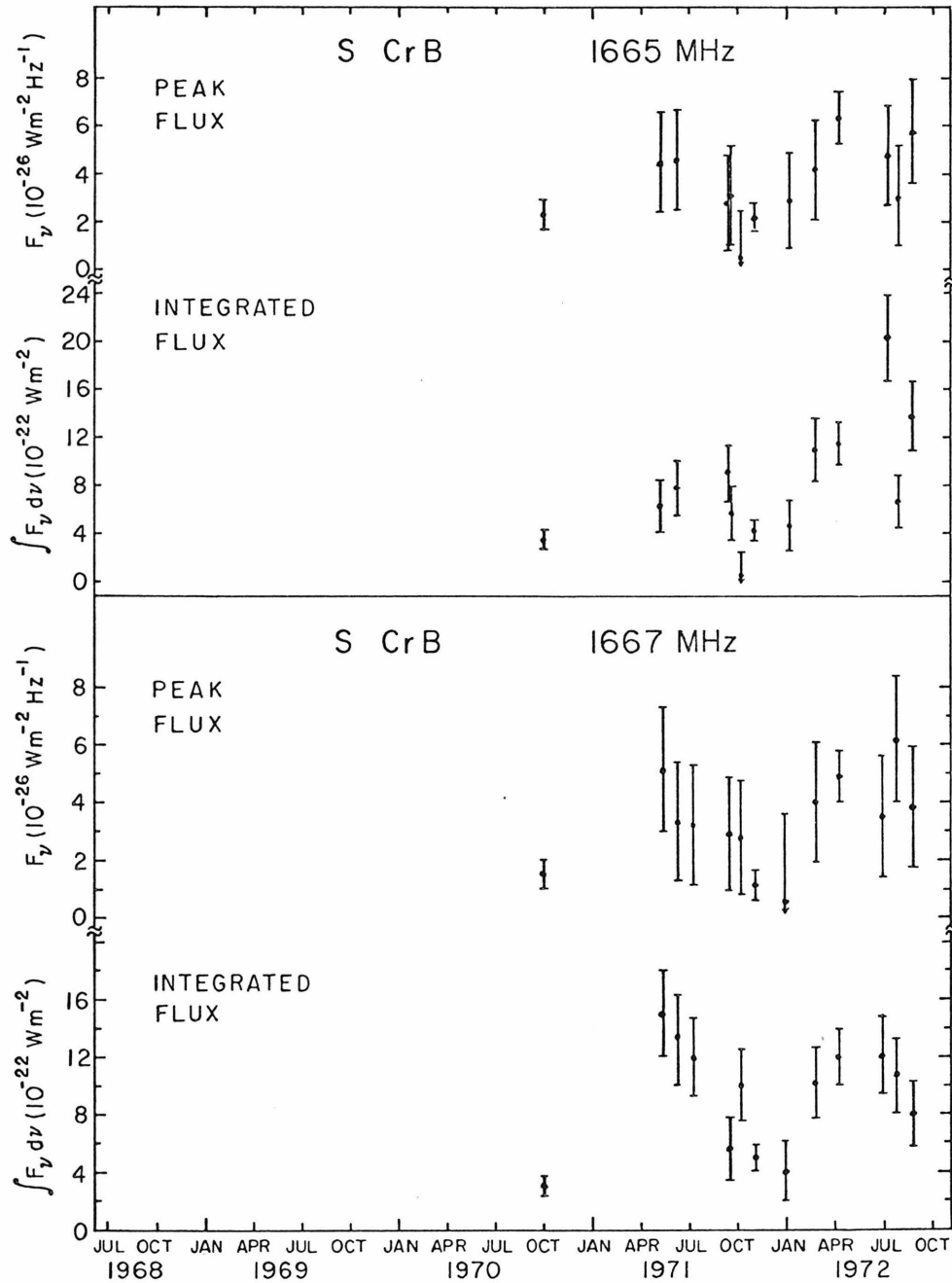


Fig. 33 (Appendix A) - The 1665- and 1667-MHz observations of S CrB

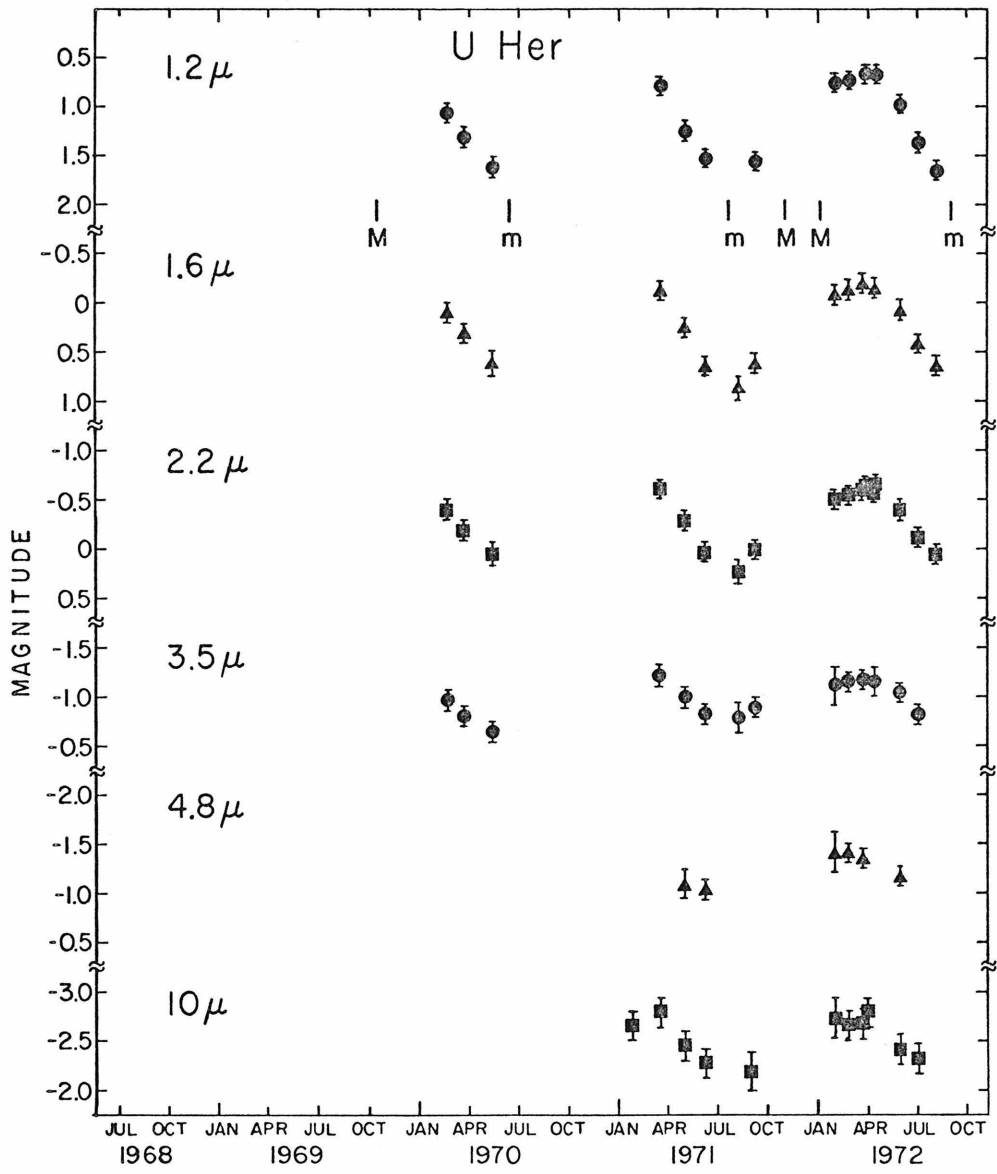


Fig. 34 (Appendix A) - The infrared observations of U Her

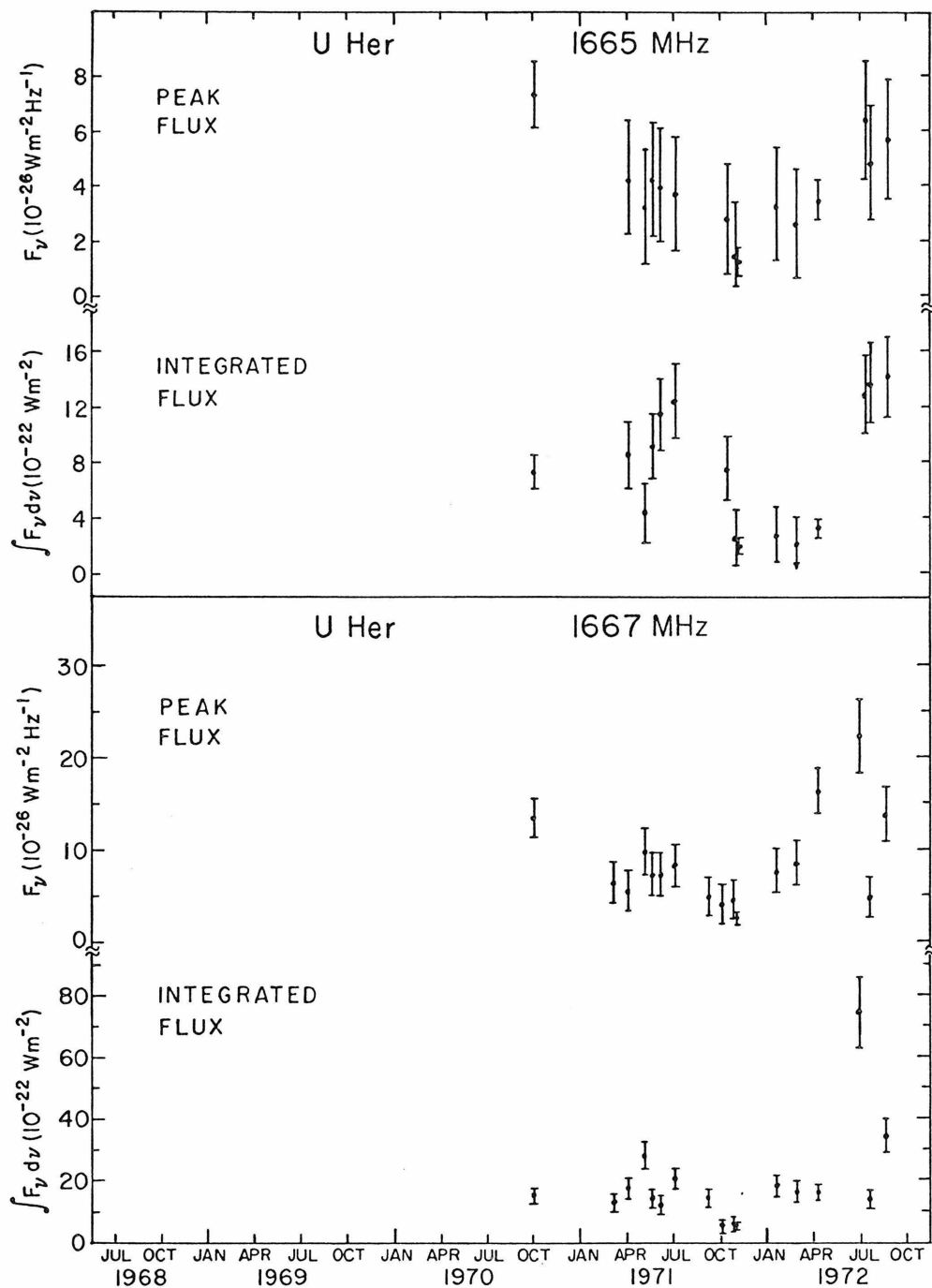


Fig. 35 (Appendix A) - The 1665- and 1667-MHz observations of U Her

TABLE 1 - VALUES OF  $\chi^2$ 

| Star    | $\nu$ - OH<br>(MHz) | OH MICROWAVE       |                     |                    |                     |                     | INFRARED  |           |           |           |           |          |
|---------|---------------------|--------------------|---------------------|--------------------|---------------------|---------------------|-----------|-----------|-----------|-----------|-----------|----------|
|         |                     | Peak<br>Low<br>Vel | Peak<br>High<br>Vel | Intg<br>Low<br>Vel | Intg<br>High<br>Vel | Intg<br>Both<br>Vel | 1.2 $\mu$ | 1.6 $\mu$ | 2.2 $\mu$ | 3.5 $\mu$ | 4.8 $\mu$ | 10 $\mu$ |
| +10011  | 1612                | 4.4                | 6.3                 | 4.8                | 10                  | 7.6                 | 94        | 189       | 136       | 53        | 25        | 22       |
| +50137  | 1612                | 1.1                | 3.7                 | 6.0                | 4.0                 | 5.0                 | 27        | 232       | 74        | 29        | 48        | 20       |
| VY CMa  | 1612                | 0.9                | 0.7                 | 1.0                | 0.7                 | 0.8                 | 1.0       | 0.5       | 0.6       | 0.5       | 0.8       | 0.5      |
| VY CMa  | 1665                | 2.1                | 0.5                 | 4.5                | 4.1                 | 1.5                 |           |           |           |           |           |          |
| VY CMa  | 1667                | 1.1                | 3.8                 | 0.8                | 12                  | 0.4                 |           |           |           |           |           |          |
| -20197  | 1612                | 4.7                | 2.8                 | 5.3                | 1.8                 | 5.7                 | 512       | 132       | 58        | 15        | 18        | 50       |
| VX Sgr  | 1612                | 3.6                | 2.7                 | 4.0                | 14                  | 7.0                 | 216       | 116       | 42        | 16        | 5.7       | 9.1      |
| R Aql   | 1612                | 5.6                | 6.2                 | 16                 | 7.9                 | 8.6                 | 6.4       | 4.2       | 3.2       | 1.0       | 1.6       | 1.8      |
| R Aql   | 1667                | 6.3                | 0.7                 |                    |                     | 10.5                |           |           |           |           |           |          |
| -20540  | 1612                | 4.1                | 1.1                 | 3.1                | 2.5                 | 2.5                 | 107       | 79        | 28        | 6.8       | 2.1       | 9.6      |
| RR Aql  | 1612                | 3.9                | 3.5                 | 2.4                | 3.8                 | 4.8                 | 30        | 32        | 19        | 7.6       | 6.5       | 10       |
| -10529  | 1612                | 12                 | 1.5                 | 4.0                | 2.6                 | 4.5                 | 4.0       | 160       | 73        | 33        | 32        | 13       |
| NML Cyg | 1612                | 0.4                | 0.7                 | 1.4                | 2.1                 | 1.5                 | 2.0       | 1.2       | 1.4       | 0.8       | 1.2       | 1.3      |
| NML Cyg | 1665                |                    | 2.6                 |                    |                     | 1.0                 |           |           |           |           |           |          |
| NML Cyg | 1667                | 0.7                | 1.9                 | 8.8                | 12                  | 5.9                 |           |           |           |           |           |          |
| U Ori   | 1665                |                    | 1.0                 |                    |                     | 1.0                 | 20        | 18        | 11        | 2.5       | 5.8       | 2.9      |
| U Ori   | 1667                |                    | 1.2                 |                    |                     | 6.7                 |           |           |           |           |           |          |
| W Hya   | 1665                |                    | 2.6                 |                    |                     | 26                  | 3.6       | 4.1       | 4.2       | 2.2       | 0.9       | 0.5      |
| W Hya   | 1667                |                    | 20                  |                    |                     | 44                  |           |           |           |           |           |          |
| S CrB   | 1665                |                    | 2.8                 |                    |                     | 11                  | 10        | 11        | 7.2       | 3.1       | 1.1       | 2.5      |
| S CrB   | 1667                |                    | 4.0                 |                    |                     | 5.5                 |           |           |           |           |           |          |
| U Her   | 1665                |                    | 1.1                 |                    |                     | 2.1                 | 16        | 14        | 8.7       | 2.6       | 2.0       | 2.0      |
| U Her   | 1667                |                    | 1.5                 |                    |                     | 2.1                 |           |           |           |           |           |          |

TABLE 2  
PERIODS OF 1612-MHz OH SOURCES

| Star   | Microwave Period <sup>*</sup> | Infrared Period <sup>*</sup> | Visual Period <sup>†</sup> |
|--------|-------------------------------|------------------------------|----------------------------|
| +10011 | 700 ± 30                      | 660 ± 15                     |                            |
| +50137 | 635 ± 30                      | 635 ± 10                     |                            |
| -20197 | 680 ± 40                      | 650 ± 20                     |                            |
| VX Sgr | 740 ± 40                      | 770 ± 150                    | 732                        |
| R Aql  | 285 ± 10                      | 285 ± 10                     | 293                        |
| -20540 | 520 ± 80                      | 510 ± 15                     |                            |
| RR Aql | 425 ± 20                      | 410 ± 10                     | 394                        |
| -10529 | 650 ± 50                      | 670 ± 30                     |                            |

\* Confidence limits determined from statistics of fit and agreement of fits to different microwave parameters and infrared wavelengths.

† Kukarkin et al. (1969)

TABLE 3  
 PHASE OF VARIATIONS OF 1612-MHz OH SOURCES<sup>†</sup>

| Star   | Assmd<br>Period<br>(days) | RELATIVE PHASE - 1612 MHz (days) |                |                    |                    |                    |  | RELATIVE PHASE - INFRARED (days) |              |              |              |              |              |
|--------|---------------------------|----------------------------------|----------------|--------------------|--------------------|--------------------|--|----------------------------------|--------------|--------------|--------------|--------------|--------------|
|        |                           | Peak<br>Low Vel                  | Peak<br>Hi Vel | Intg<br>Low Vel    | Intg<br>Hi Vel     | Intg<br>Flux       |  | 1.2 $\mu$                        | 1.6 $\mu$    | 2.2 $\mu$    | 3.5 $\mu$    | 4.8 $\mu$    | 10 $\mu$     |
| +10011 | 650                       | 128 $\pm$ 50                     | 115 $\pm$ 50   | 136 $\pm$ 50       | 88 $\pm$ 50        | 108 $\pm$ 50       |  | 143 $\pm$ 10                     | 135 $\pm$ 20 | 104 $\pm$ 20 | 148 $\pm$ 30 | 144 $\pm$ 20 | 180 $\pm$ 30 |
| +50137 | 630                       | 578 $\pm$ 75                     | 567 $\pm$ 40   | 586 $\pm$ 50       | 585 $\pm$ 50       | 572 $\pm$ 40       |  | 585 $\pm$ 80                     | 572 $\pm$ 15 | 574 $\pm$ 15 | 601 $\pm$ 20 | 601 $\pm$ 20 | 604 $\pm$ 20 |
| -20197 | 640                       | 282 $\pm$ 50                     | 260 $\pm$ 50   | 256 $\pm$ 65       | 259 $\pm$ 100      | 252 $\pm$ 65       |  | 217 $\pm$ 25                     | 205 $\pm$ 25 | 222 $\pm$ 20 | 249 $\pm$ 25 | 240 $\pm$ 35 | 229 $\pm$ 25 |
| VX Sgr | 730                       | 345 $\pm$ 55                     | 357 $\pm$ 50   | 370 $\pm$ 50       | 370 $\pm$ 45       | 373 $\pm$ 45       |  | 235 $\pm$ 60                     | 233 $\pm$ 70 | 251 $\pm$ 65 | 284 $\pm$ 70 | 254 $\pm$ 70 | 315 $\pm$ 60 |
| R Aql  | 290                       | 155 $\pm$ 35                     | 163 $\pm$ 15   | 170 $\pm$ 45       | 164 $\pm$ 20       | 166 $\pm$ 20       |  | 169 $\pm$ 20                     | 159 $\pm$ 15 | 157 $\pm$ 15 | 163 $\pm$ 25 | 172 $\pm$ 40 | 180 $\pm$ 30 |
| -20540 | 510                       | 212 $\pm$ $\infty$               | 272 $\pm$ 100  | 213 $\pm$ $\infty$ | 292 $\pm$ $\infty$ | 207 $\pm$ $\infty$ |  | 183 $\pm$ 15                     | 189 $\pm$ 15 | 196 $\pm$ 20 | 203 $\pm$ 45 | 169 $\pm$ 40 | 204 $\pm$ 60 |
| RR Aql | 410                       | 303 $\pm$ 50                     | 297 $\pm$ 35   | 304 $\pm$ 60       | 299 $\pm$ 45       | 298 $\pm$ 50       |  | 318 $\pm$ 10                     | 317 $\pm$ 10 | 314 $\pm$ 10 | 315 $\pm$ 10 | 319 $\pm$ 25 | 324 $\pm$ 20 |
| -10529 | 670                       | 364 $\pm$ 45                     | 390 $\pm$ 120  | 386 $\pm$ 60       | 392 $\pm$ 140      | 388 $\pm$ 60       |  | *                                | 374 $\pm$ 20 | 383 $\pm$ 20 | 398 $\pm$ 20 | 408 $\pm$ 50 | 437 $\pm$ 45 |

\* Insufficient data

<sup>†</sup>Phase is defined as the time of maximum emission measured from August 15, 1969.

TABLE 4

## CORRELATION COEFFICIENTS\* BETWEEN 1612 MHz AND INFRARED VARIATIONS

| Star    | 1612 MHz - 2.2 $\mu$ |                |                 |                |              |              | 1612 MHz - 10 $\mu$ |                |                 |                |              |              |
|---------|----------------------|----------------|-----------------|----------------|--------------|--------------|---------------------|----------------|-----------------|----------------|--------------|--------------|
|         | Peak<br>Low Vel      | Peak<br>Hi Vel | Intg<br>Low Vel | Intg<br>Hi Vel | Intg<br>Flux | Intg<br>Flux | Peak<br>Low Vel     | Peak<br>Hi Vel | Intg<br>Low Vel | Intg<br>Hi Vel | Intg<br>Flux | Intg<br>Flux |
| +10011  | 0.73                 | 0.71           | 0.69            | 0.68           | 0.74         | 0.74         | 0.79                | 0.72           | 0.70            | 0.61           | 0.61         | 0.71         |
| +50137  | 0.37                 | 0.75           | 0.69            | 0.77           | 0.85         | 0.85         | 0.31                | 0.72           | 0.44            | 0.75           | 0.75         | 0.79         |
| -20197  | 0.75                 | 0.78           | 0.82            | 0.74           | 0.87         | 0.87         | 0.79                | 0.78           | 0.74            | 0.80           | 0.80         | 0.80         |
| VX Sgr  | 0.53                 | 0.44           | 0.30            | 0.18           | 0.22         | 0.22         | 0.67                | 0.80           | 0.74            | 0.73           | 0.73         | 0.76         |
| R Aql   | 0.68                 | 0.77           | 0.71            | 0.69           | 0.72         | 0.72         | 0.37                | 0.66           | 0.04            | 0.65           | 0.65         | 0.62         |
| -20540  | 0.17                 | 0.20           | 0.34            | 0.01           | 0.37         | 0.37         | 0.05                | 0.74           | 0.30            | 0.75           | 0.75         | 0.55         |
| RR Aql  | 0.67                 | 0.64           | 0.52            | 0.45           | 0.46         | 0.46         | 0.17                | 0.31           | -0.32           | 0.13           | 0.13         | 0.00         |
| -10529  | 0.87                 | 0.36           | 0.79            | 0.35           | 0.79         | 0.79         | 0.81                | 0.57           | 0.65            | 0.53           | 0.53         | 0.60         |
| NML Cyg | 0.11                 | 0.12           | 0.85            | 0.68           | 0.84         | 0.84         | -0.20               | -0.02          | 0.42            | 0.32           | 0.32         | 0.40         |

\* Correlation coefficients greater than 0.4 to 0.5 imply greater than 95% probability that the data are correlated.

TABLE 5

## PHASES AND CORRELATION COEFFICIENTS FOR VARIATIONS OF 1665/1667 MHz SOURCES

| Star    | v - OH<br>(MHz) | Velocity<br>Feature | Assmd<br>Period <sup>†</sup><br>(days) | Relative<br>2.2 $\mu$ Phase<br>(days) | Peak Microwave Flux      |                             | Intg. Microwave Flux     |                             |
|---------|-----------------|---------------------|--|---------------------------------------|--------------------------|-----------------------------|--------------------------|-----------------------------|
|         |                 |                     |  |                                       | Relative<br>Phase (days) | Correlation<br>Coefficient* | Relative<br>Phase (days) | Correlation<br>Coefficient* |
| U Ori   | 1665            | Both                | 370                                    | 75 $\pm$ 15                           | 180 $\pm$ $\infty$       | -0.28                       | 140 $\pm$ $\infty$       | -0.20                       |
| U Ori   | 1667            | Both                | 370                                    | 75 $\pm$ 15                           | 115 $\pm$ 30             | 0.64                        | 90 $\pm$ 50              | 0.59                        |
| W Hya   | 1665            | Both                | 380                                    | 140 $\pm$ 30                          | 200 $\pm$ 35             | 0.78                        | 165 $\pm$ 20             | 0.94                        |
| W Hya   | 1667            | Both                | 380                                    | 140 $\pm$ 30                          | 235 $\pm$ 40             | 0.05                        | 225 $\pm$ 45             | 0.45                        |
| S CrB   | 1665            | Both                | 360                                    | 200 $\pm$ 15                          | 185 $\pm$ 50             | 0.48                        | 165 $\pm$ 90             | -0.07                       |
| S CrB   | 1667            | Both                | 360                                    | 200 $\pm$ 15                          | 165 $\pm$ 40             | 0.33                        | 165 $\pm$ 30             | 0.79                        |
| U Her   | 1665            | Both                | 405                                    | 395 $\pm$ 15                          | 355 $\pm$ $\infty$       | 0.57                        | 385 $\pm$ $\infty$       | 0.43                        |
| U Her   | 1667            | Both                | 405                                    | 395 $\pm$ 15                          | 240 $\pm$ $\infty$       | -0.46                       | 130 $\pm$ $\infty$       | 0.22                        |
| NML Cyg | 1665            | Both                |  |                                       |                          | 0.36                        |                          | 0.56                        |
| NML Cyg | 1667            | Low                 |  |                                       |                          | 0.69                        |                          | 0.31                        |
| NML Cyg | 1667            | High                |  |                                       |                          | 0.22                        |                          | 0.02                        |
| R Aql   | 1667            | Low                 | 290                                    | 155 $\pm$ 15                          | 210 $\pm$ $\infty$       | 0.37                        | 180 $\pm$ $\infty$       | 0.40                        |
| R Aql   | 1667            | High                | 290                                    | 155 $\pm$ 15                          | 150 $\pm$ 70             | 0.70                        |                          |                             |

\* Greater than 0.6 to 0.7 implies greater than 95% probability that data are correlated.

<sup>†</sup> Kukarkin et al. (1969)

TABLE 6

AMPLITUDES OF VARIATION -  $F_{\max}/F_{\min}$ 

| Star   | v-OH<br>(MHz) | MICROWAVE      |                |                     |                |                |              | INFRARED  |           |           |           |           |          |
|--------|---------------|----------------|----------------|---------------------|----------------|----------------|--------------|-----------|-----------|-----------|-----------|-----------|----------|
|        |               | Peak<br>Lo Vel | Peak<br>Hi Vel | Peak<br>*<br>Lo Vel | Intg<br>Lo Vel | Intg<br>Hi Vel | Intg<br>Flux | 1.2 $\mu$ | 1.6 $\mu$ | 2.2 $\mu$ | 3.5 $\mu$ | 4.8 $\mu$ | 10 $\mu$ |
| +10011 | 1612          | 2.0            | 2.7            | 2.1                 | 2.1            | 3.0            | 2.8          | >7.0      | 10.0      | 7.0       | 4.4       | 4.0       | 4.8      |
| +50137 | 1612          | 2.3            | 2.6            | 2.5                 | 2.5            | 2.4            | 2.7          | >9.0      | 9.1       | 5.2       | 3.3       | 3.3       | 3.0      |
| VY CMa | 1612          | <1.3           | <1.3           | <1.3                | <1.3           | <1.3           | <1.3         | <1.3      | <1.3      | <1.3      | <1.3      | <1.3      | <1.3     |
| VY CMa | 1665          | 1.5            | <1.5           | 1.5                 | 1.5            | 2.0            | 1.5          |           |           |           |           |           |          |
| VY CMa | 1667          | <1.3           | <1.5           | <1.3                | <1.3           | 2.5            | 1.4          |           |           |           |           |           |          |
| -20197 | 1612          | 2.4            | 1.8            | 2.5                 | 2.5            | 2.0            | 2.3          | 19.0      | 7.6       | 5.2       | 3.3       | 4.0       | 4.4      |
| VX Sgr | 1612          | 1.8            | 1.8            | 1.9                 | 1.9            | 2.9            | 2.2          | 7.6       | 5.8       | 3.3       | 3.0       | 2.5       | 2.3      |
| R Aql  | 1612          | 1.7            | 2.0            | 2.7                 | 2.7            | 2.6            | 2.5          | 1.7       | 1.7       | 1.7       | 1.6       | 1.5       | 1.6      |
| R Aql  | 1667          | 3.0            | <2.0           |                     |                |                | 4.0          |           |           |           |           |           |          |
| -20540 | 1612          | 2.0            | 1.8            | 2.2                 | 2.2            | 2.2            | 2.0          | 7.6       | 5.8       | 3.3       | 2.3       | >1.7      | 2.7      |
| RR Aql | 1612          | 2.5            | 2.0            | 2.0                 | 2.0            | 2.5            | 2.0          | 3.6       | 3.3       | 2.8       | 2.3       | 2.3       | 2.7      |
| -10529 | 1612          | 4.5            | †              | 2.5                 | 2.5            | †              | 2.5          | †         | 6.3       | 4.8       | 3.3       | >2.8      | >2.3     |

TABLE 6 (continued)

| Star    | v-OH<br>(MHz) | MICROWAVE      |                |                     |                |              | INFRARED |      |      |      |      |     |
|---------|---------------|----------------|----------------|---------------------|----------------|--------------|----------|------|------|------|------|-----|
|         |               | Peak<br>Lo Vel | Peak<br>Hi Vel | Peak<br>*<br>Lo Vel | Intg<br>Hi Vel | Intg<br>Flux | 1.2μ     | 1.6μ | 2.2μ | 3.5μ | 4.8μ | 10μ |
| NML Cyg | 1612          | <1.3           | <1.3           | 1.4                 | 1.5            | 1.4          | 1.6      | 1.6  | 1.6  | 1.5  | 1.5  | 1.6 |
| NML Cyg | 1665          |                | 1.7            |                     | <2.0           |              |          |      |      |      |      |     |
| NML Cyg | 1667          | <2.0           | 1.5            | 3.0                 | 3.0            | 2.5          |          |      |      |      |      |     |
| U Ori   | 1665          | <2.0           | <2.0           |                     |                | <2.0         | 2.3      | 2.3  | 2.3  | 1.9  | 1.9  | 1.7 |
| U Ori   | 1667          | <2.0           | <2.0           |                     |                | 2.5          |          |      |      |      |      |     |
| W Hya   | 1665          | <2.0           | <2.0           |                     |                | 2.0          | 1.6      | 1.6  | 1.6  | 1.3  | 1.4  | 1.3 |
| W Hya   | 1667          |                | 3.0            |                     |                | >2.5         |          |      |      |      |      |     |
| S CrB   | 1665          | <2.0           | <2.0           |                     |                | 2.5          | 2.3      | 2.3  | 2.1  | 1.9  | >1.6 | 1.7 |
| S CrB   | 1667          | <2.0           | <2.0           |                     |                | 2.5          |          |      |      |      |      |     |
| U Her   | 1665          | <2.0           | <2.0           |                     |                | 1.7          | 2.3      | 2.3  | 2.1  | 1.7  | >1.4 | 1.6 |
| U Her   | 1667          | <2.0           | <2.0           |                     |                | 1.8          |          |      |      |      |      |     |

\*Or both features

† Insufficient data

## APPENDIX B

## INSTRUMENTATION AND OBSERVING TECHNIQUES

## I. Photometer

Most of the observations reported in this study were made with an infrared photometer mounted at the Cassegrain focus of the 60-inch telescope of the Hale Observatories on Mt. Wilson. The photometer has been described previously by Becklin (1968) and Hilgeman (1970), and only the basic details will be described here.

The important elements of the photometer are: (1) a chopper, (2) an offset guiding eyepiece, and (3) a movable slide for interchanging two detector systems. The chopper is a device which alternately admits radiation to the detector from two adjacent fields on the sky at frequencies between 5 and 15 Hz. The two types of choppers used have been described by Becklin (1968) and Glass (1972) and are pictured schematically in Figure 1. The guide eyepiece is offset from the field being observed and allows one to guide on a visible star when optically invisible sources are observed. Since at least two different detectors are necessary to observe at all six wavelengths, the movable slide allows one to measure a source at all wavelengths on one night.

## II. Detector Systems

A typical detector system is shown schematically in Figure 2. Since the response of a detector generally varies over its area, a field lens is used to image the primary telescope mirror onto the detector. The field of view on the sky is defined by a circular

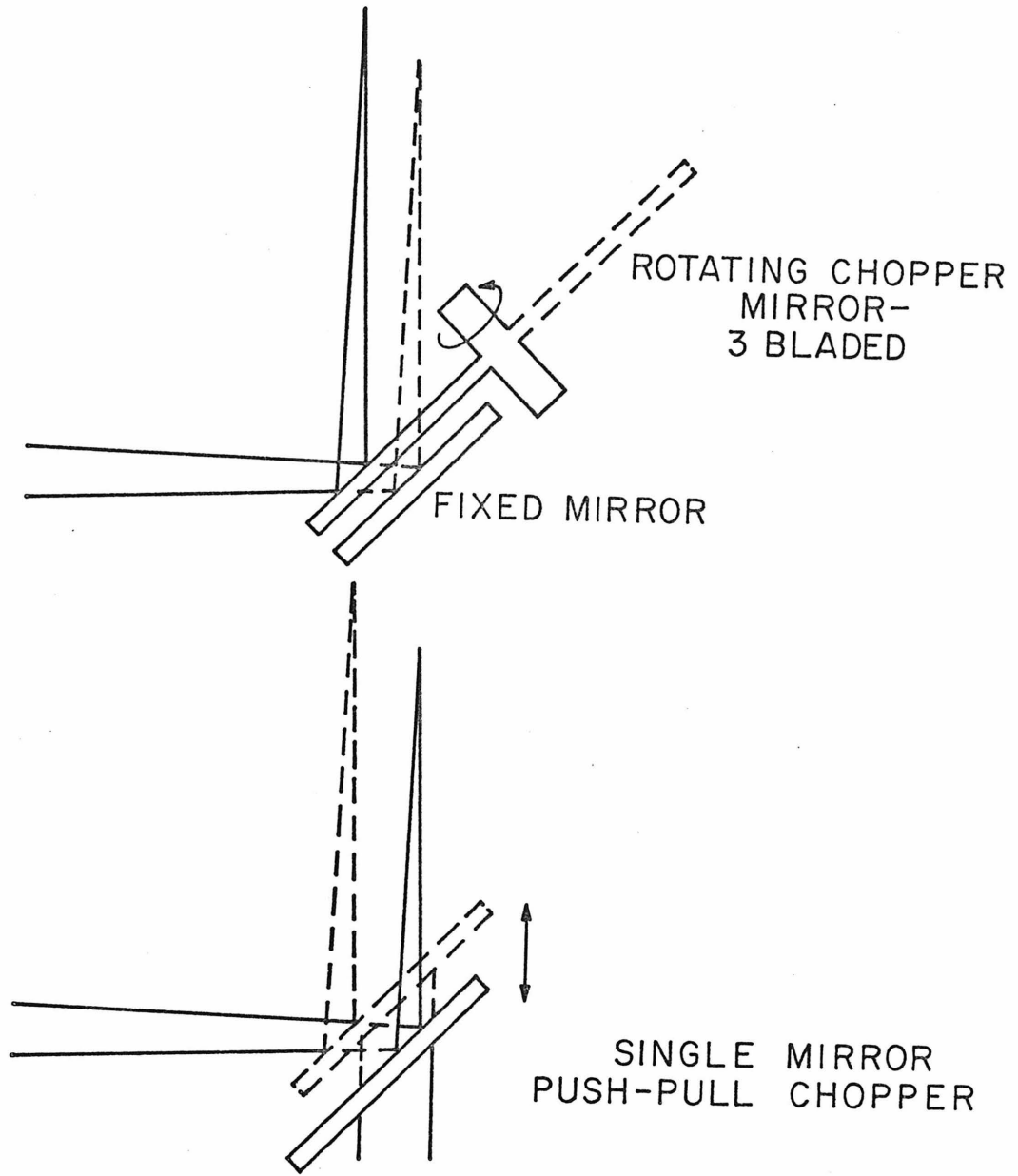


Fig. 1 (Appendix B) - The two types of choppers employed

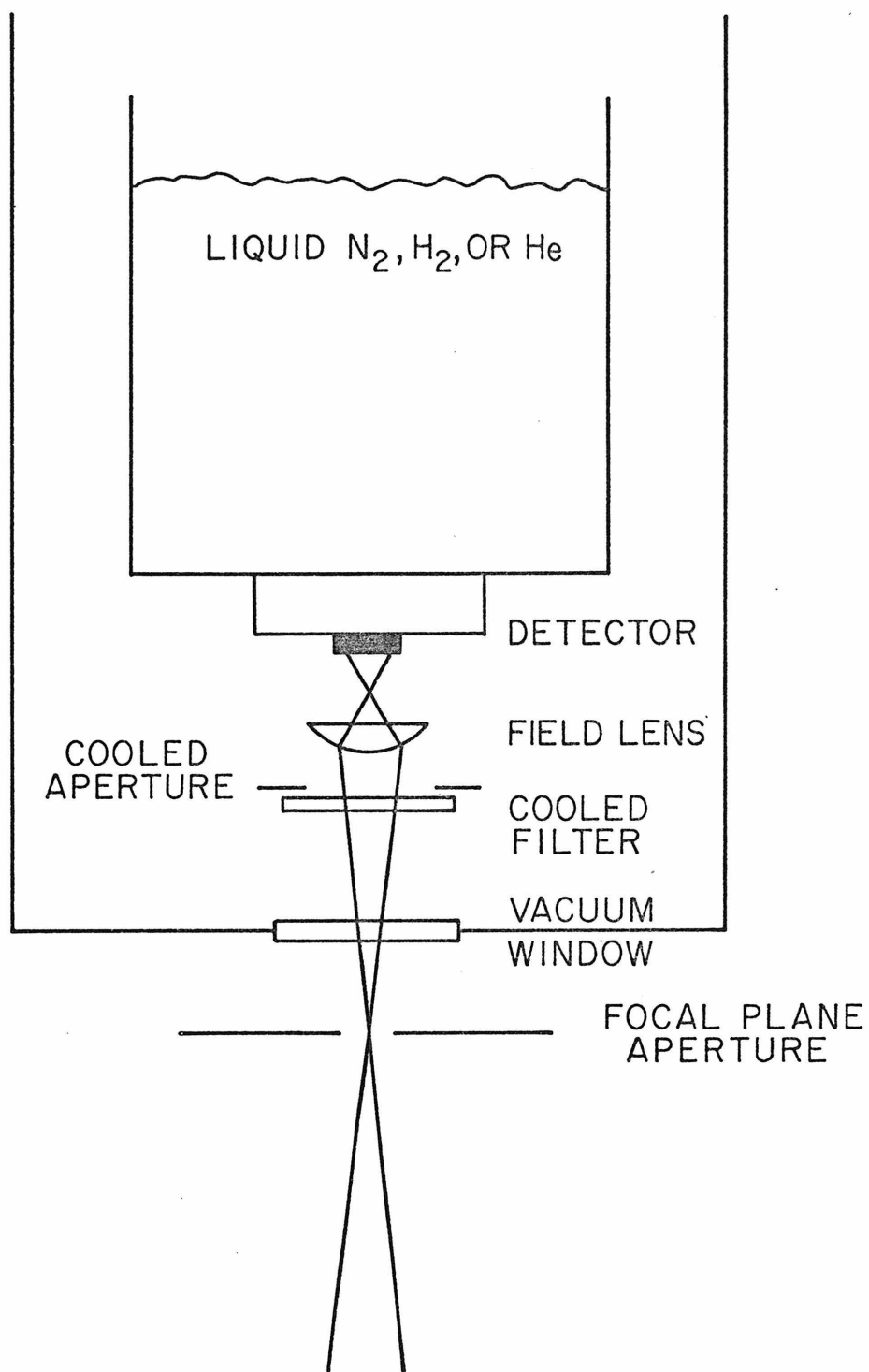


Fig. 2 (Appendix B) - A typical detector system

aperture in the focal plane of the telescope.

Ideally, for a program such as described in this thesis only one detecting system would have been used at each wavelength, but various reasons such as system failure or a desire for increased sensitivity to measure some special object have dictated the use of a variety of systems. The details of all the systems are summarized in Table 1, and after a short description of each, the differences between them will be discussed.

#### A. 1.25 $\mu$

At 1.25 $\mu$  only one lead sulfide photo-conductive detector has been used with a 1.25 $\mu$  bandpass interference filter at room temperature. Midway through the program it was found that the sensitivity could be significantly increased by preventing radiation longwards of about 2.8 $\mu$  from reaching the detector, and for some of the observations an appropriate filter was placed in the dewar. The measured transmission characteristics of this filter show it to be quite uniform in transmissivity across the bandpass of the 1.2 $\mu$  interference filter, and so it has no effect on the wavelength response of the system.

#### B. 1.65 and 2.2 $\mu$

At 1.65 and 2.2 $\mu$  lead sulfide photo-conductive systems similar to those of Becklin (1968) have been used. The only differences between each of the systems are the particular detector and which, if any, cooled filter were used.

TABLE 1 - DETECTOR SYSTEMS

| $\lambda(\mu)$ | Dewar | Detector, Mode, @ T | Cooled Filter @ T      | Warm Filter     | Lens, f.l.            | Window           |
|----------------|-------|---------------------|------------------------|-----------------|-----------------------|------------------|
| 1.25           | D-36  | PbS, P.C., 77°K     | None                   | 1.15-1.35 $\mu$ | Si 8mm                | Sapphire         |
| 1.25           | D-36  | PbS, P.C., 77°K     | <0.5-2.75 $\mu$ , 77°K | 1.15-1.35 $\mu$ | Si 8mm                | Sapphire         |
| 1.65           | D-36  | PbS, P.C., 77°K     | None                   | 1.50-1.75 $\mu$ | Si 8mm                | Sapphire         |
| 1.65           | D-36  | PbS, P.C., 77°K     | <0.5-2.75 $\mu$ , 77°K | 1.50-1.75 $\mu$ | Si 8mm                | Sapphire         |
| 1.65           | D-15  | PbS, P.C., 77°K     | 1.4-2.5 $\mu$ , 77°K   | 1.50-1.75 $\mu$ | Si 8mm                | Sapphire         |
| 2.2            | D-36  | PbS, P.C., 77°K     | None                   | 2.0-2.4 $\mu$   | Si 8mm                | Sapphire         |
| 2.2            | D-36  | PbS, P.C., 77°K     | <0.5-2.75 $\mu$ , 77°K | 2.0-2.4 $\mu$   | Si 8mm                | Sapphire         |
| 2.2            | D-15  | PbS, P.C., 77°K     | 1.4-2.5 $\mu$ , 77°K   | 2.0-2.4 $\mu$   | Si 8mm                | Sapphire         |
| 3.5            | D-36  | PbS, P.C., 77°K     | None                   | 3.2-4.1 $\mu$   | Si 8mm                | Sapphire         |
| 3.5            | D-20  | PbS, P.C., 77°K     | 3.25-4.05 $\mu$ , 77°K | None            | Si 8mm                | Sapphire         |
| 3.5            | D-41  | Ge, Bol., 2°K       | None                   | 3.2-4.1 $\mu$   | BaF <sub>2</sub> 16mm | BaF <sub>2</sub> |
| 4.8            | D-13  | PbSe, P.C., 77°K    | 4.55-5.30 $\mu$ , 77°K | None            | Si 8mm                | Sapphire         |
| 4.8            | D-41  | Ge, Bol., 2°K       | None                   | 4.65-5.10 $\mu$ | BaF <sub>2</sub> 16mm | BaF <sub>2</sub> |
| 10.1           | D-33  | Ge: Hg, P.C., 20°K  | 8.1 $\mu$ cut-on, 20°K | None            | KBr 12mm              | BaF <sub>2</sub> |
| 10.1           | D-41  | Ge, Bol., 2°K       | None                   | 8.2-13.3 $\mu$  | BaF <sub>2</sub> 16mm | BaF <sub>2</sub> |

C. 3.5 $\mu$ 

At 3.5 $\mu$  three fairly different systems have been used. The two lead sulfide systems are similar to Becklin's, differing in the particular interference filter used and whether it was cooled. The germanium bolometer uses the same interference filter as one of the lead sulfide systems. The wavelength response of the bolometer is relatively constant with wavelength, while the lead sulfide detectors have a long wavelength cut-off starting inside the passband of the interference filter.

D. 4.8 and 10 $\mu$ 

At each of the two longest wavelengths, 4.8 and 10 $\mu$ , two systems have been used, a photo-conductor and a germanium bolometer. The most important point to note about the 4.8 $\mu$  system is the narrow bandwidth of the filter. In the 10 $\mu$  systems the wavelength responses of the two detectors differ only slightly. The bolometer has a relatively flat response with wavelength, and the photo-conductor is slightly peaked near the center of the band.

## E. Comparison of Spectral Response

All the bandpasses, with the exception of those at 3.5 and 10 $\mu$ , have  $\Delta\lambda/\lambda$  less than 0.25 which minimizes the effect of differences in filter cut-off wavelength, detector response, and the shape of the filter transmission curve. At 1.2 $\mu$  no observational comparison was made of the difference in spectral response because of the negligible difference between the two systems used. At all other wavelengths, except 10 $\mu$ , comparisons have been made almost simultaneously between the relative signal from a "blue" star and a very "red" star with two

different systems mounted side by side on the photometer. At 1.65, 2.2, and 4.8 $\mu$ , no systematic differences greater than five percent were found between any of the systems used at a particular wavelength. No direct comparison was made at 10 $\mu$ , however, the relatively red star, VY CMa, has remained constant in brightness within the errors at all infrared wavelengths including 10 $\mu$ . The photo-conductive detector was used for all observations before 1971, and the germanium bolometer from 1971 onwards, and no jump is evident in the 10 $\mu$  magnitude determined relative to blue standard stars.

At 3.5 $\mu$  small systematic differences were found between the three detecting systems. These results are summarized in Figure 3 as graphs of the differences in the magnitude of a red star determined relative to blue standard stars versus the color of the red star. It is apparent that the major difference in color sensitivity is between the D-20 system and the other two systems, although there is probably also a small difference between the D-41 and D-36 systems. These differences can be understood qualitatively from the differing filter properties.

From the relationships determined from Figure 3, the small amount of 3.5 $\mu$  data taken with the D-20 system have been corrected to be consistent with the data taken with the D-41 system. Larger error limits were also assigned to the data taken with the D-20 system. The difference between the D-41 and D-36 systems is negligible compared to the typical errors of the measurements, and no corrections have been made to any of these data.

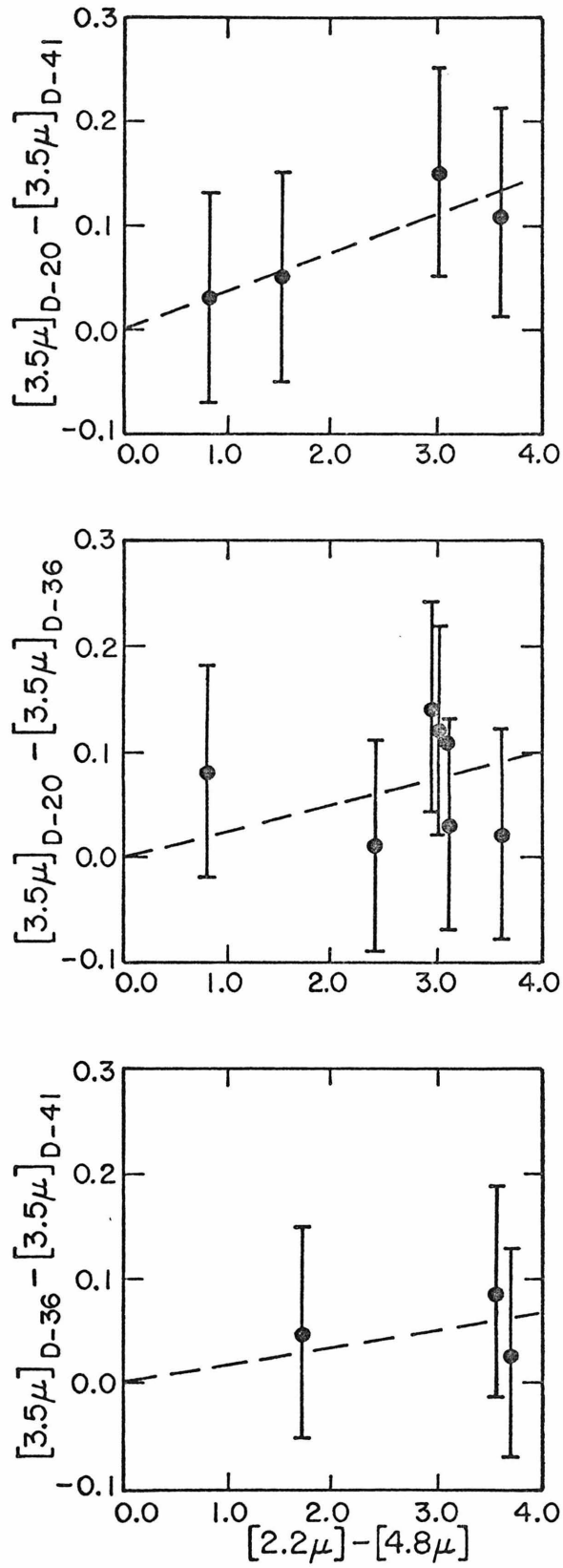


Fig. 3 (Appendix B) - The difference in  $3.5\mu$  magnitude obtained with two different detector systems on several stars is plotted against the  $[2.2\mu] - [4.8\mu]$  color index which measures the spectral slope near  $3.5\mu$ . Graphs are shown for comparison of all three systems used.

### III. Electronics

The electronics used to record the signal are standard in infrared observations. A bias voltage ranging from -8 to +45 volts, depending on the detector, is applied across the detector in series with a 1 or 5 megohm load resistor. The AC signal caused by the chopping is amplified by a preamp on the dewar with a gain of 10 or 1000 and by a variable gain amplifier located somewhat farther from the detector. The signal is then synchronously demodulated in phase with the chopper and recorded both as a DC voltage on a strip chart recorder and through a voltage-to-frequency converter as a 10-second integration of counts on a scaler and a digital paper tape printer.

### IV. Observing Techniques

The observing procedure for this program has been to measure about six standard calibration stars during each night of observing. These are chosen from a set of about 40 stars whose brightnesses are believed to be constant. These measurements establish the relative sensitivity for the night which may vary up to about 25 percent from night to night, though typically about 10 percent. This number of standards generally implies about one standard observed for every two OH/infrared stars, although the same standards are not observed every time a particular OH source is measured.

A typical observation at 1.2, 1.6, or 2.2 $\mu$  involves doing one, or at the most eight, 10-second integrations with the source in the "signal beam" (positive signal), twice as many 10-second integrations with both

beams on the sky or with the source in the "reference beam" (negative signal), and then a set of integrations back on the source again. The signal is computed as the difference between the sum of all the "positive" signals and the sum of the "negative" signals. At 3.5, 4.8, and 10 $\mu$ , observations are always made with alternating sets of two 10-second integrations on and then two integrations off or in the reference beam, always ending with two integrations on the source. The signal is then computed as the average of the individual differences between adjacent "positive" and "negative" integrations in order to minimize drifts in the background.

## APPENDIX C

## ANALYSIS OF THE DATA

## I. Description

The statistical data analysis described in this thesis is performed by a main computer program which sets up the data and several sub-programs which compute the various statistical parameters. The basic features of all these programs are outlined below.

## A. Main Program

- (1) For a particular star the first guess parameters for the sine wave fitting and all the radio and infrared data are read in.
- (2) The total integrated flux is computed as the sum of the integrated fluxes of the two velocity features for all measurements of the two features made on the same day or within three days of each other.
- (3) For each parameter of the microwave data:
  - (a) All dates are picked out on which a measurement of that parameter was made.
  - (b) The Least Squares Sine Wave Fitting Program is called.
  - (c) The Statistical Parameters Determination Program is called.
- (4) For each infrared wavelength:
  - (a) All dates are picked out on which a measurement at that wavelength was made.

(b) The Least Squares Sine Wave Fitting Program

is called.

(c) The Statistical Parameters Determination Program

is called.

(d) The Microwave-Infrared Correlation Program

is called.

#### B. Least Squares Sine Wave Fitting Program

This program is a slight revision by the author of a Caltech library subroutine called LSQENP. LSQENP is a slight revision by Caltech of IBM share program #3094 by D. Marquardt based on his algorithm (Marquardt 1963) for least squares fitting to a non-linear relationship. The Caltech revision did not alter the method of solution of the original program but only modified the options of the user to change the form of the output. The author's revisions to LSQENP were: (1) to change the form of the graphical output which illustrates the fitting as it progresses in order to be better able to visualize the goodness of fit, and (2) to weight the data according to the individual errors since the original program weighted all points equally. The confidence limits have been calculated with the option described as "Non-linear Confidence Limits Desired" in the Caltech write-up of LSQENP. An outline of the computational procedure for this calculation is given in Marquardt's description of IBM share program #3094 (Marquardt 1964).

#### C. Statistical Parameters Determination Program

This is a slight revision of Bevington's (1969) subroutine called XFIT. The original program computes the mean, standard deviation of

the mean, and standard deviation of a set of data. In addition to these operations a computation of the values of  $\chi^2$  and the reduced  $\chi^2$  was added.

D. Microwave - Infrared Correlation Program

- (1) For each date of a radio measurement the nearest infrared measurement is found.
- (2) If the infrared measurement was made within 0.1 period (for periodic variables) or 30 days (for NML Cyg and VY CMa) of the radio measurement, an interpolated value for the date of the radio measurement is found.
  - (a) For periodic variables, if three or more measurements were made within a time span of two-thirds of a period around the radio date, a sine wave is fit to those points. The period and average level are fixed to that determined by all the infrared data and the amplitude and phase are allowed to vary to fit the nearby data. The value of that sine wave on the date of the radio measurement is then computed.
  - (b) For NML Cyg and VY CMa, if there is an infrared observation within 30 days of the radio observation, the infrared flux on the date of the radio observation is interpolated between the two nearest infrared observations on either side of the radio date.

- (3) The correlation coefficient is then computed for the pairs of microwave -- infrared observations with the terms weighted by their relative errors.
- (4) The probability that such a correlation coefficient could arise from uncorrelated data is then computed with a subroutine of Bevington (1969) called PCORRE.

## II. Sample Output

The following pages contain a sample of the output of the data analysis program.

# OF # OF  
OBSER- PARAMETERS  
VATIONS VARIABLE

N = 26 K = 4 IP = 0 M = 1 IFF = 0 GAMMA CRIT = 0.450E 02 DEL = 0.100E-04  
 FF = 0.400E 01 I = 0.200E 01 E = 0.500E-04 TAU = 0.100E-02 XL = 0.100E-01 ZETA = 0.100E-70

AVERAGE FLUX 1/2 P-P AMPLITUDE PERIOD PHASE  
 PARAMETERS 0.1170000E 02 0.1000000E 02 0.6700000E 03 0.8000000E 03

PHI S E LENGTH GAMMA LAMBDA ANALYTIC PARTIALS USED  
 0.10012156E 03 0.21354322E 01 0.838E-01 0.231E 02 0.100E-01

PARAMETERS 0.11507947E 02 0.98522253E 01 0.65935425E 03 0.78389355E 03

PHI S E LENGTH GAMMA LAMBDA ANALYTIC PARTIALS USED  
 0.38442978E 02 0.13218956E 01 0.134E 02 0.135E 02 0.100E-01

PARAMETERS 0.11422729E 02 0.88496914E 01 0.65391968E 03 0.77551636E 03

PHI S E LENGTH GAMMA LAMBDA ANALYTIC PARTIALS USED  
 0.37054108E 02 0.12977972E 01 0.150E 01 0.184E 02 0.100E-01

PARAMETERS 0.11422468E 02 0.88894439E 01 0.65197290E 03 0.77261792E 03

PHI S E LENGTH GAMMA LAMBDA ANALYTIC PARTIALS USED  
 0.36863983E 07 0.12944632E 01 0.547E 00 0.203E 02 0.100E-01

PARAMETERS 0.11422998E 02 0.89021721E 01 0.65126392E 03 0.77155176E 03

PHI S E LENGTH GAMMA LAMBDA ANALYTIC PARTIALS USED  
 0.36838425E 02 0.12340149E 01 0.207E 00 0.210E 02 0.100E-01

PARAMETERS 0.11423325E 02 0.89367593E 01 0.65100659E 03 0.77116528E 03

PHI S E LENGTH GAMMA LAMBDA ANALYTIC PARTIALS USED  
 0.36835236E 02 0.12939587E 01 0.782E-01 0.208E 02 0.100E-01

PARAMETERS 0.11423052E 02 0.89056811E 01 0.65099976E 03 0.77117798E 03

PHI S E LENGTH GAMMA LAMBDA ANALYTIC PARTIALS USED  
 0.36815068E 02 0.27919558E 01 0.449E-02 0.124E 02 0.100E 01

EPSILON TEST

BEST FIT

N = 76 K = 4 IP = 0 M = 1  
 FF = 0.400E 01 T = 0.200F 01 E = 0.500E-04 TAU = 0.100E-02

PARAMETERS 0.11423J52F 02 0.89066811E 01 0.65099976E 03 0.77117798E 03

| OBS   | ORED  | DIFF  | WT DIFF | ERROR | FLUX/MAG | DATE    |
|-------|-------|-------|---------|-------|----------|---------|
| 4.32  | 4.99  | -0.67 | -1.05   | .10   | 5.89     | 19AUG68 |
| 19.92 | 19.29 | 0.63  | 0.21    | .10   | 4.23     | 8AUG69  |
| 22.04 | 20.02 | 2.02  | 0.48    | .13   | 4.12     | 31AUG69 |
| 19.55 | 20.19 | -0.63 | -0.22   | .10   | 4.25     | 9SEP69  |
| 21.24 | 20.31 | 0.94  | 0.30    | .10   | 4.16     | 5OCT69  |
| 21.05 | 20.08 | 0.97  | 0.31    | .10   | 4.17     | 22OCT69 |
| 17.19 | 19.04 | -1.85 | -0.73   | .10   | 4.39     | 23NOV69 |
| 10.95 | 13.24 | -2.30 | -1.42   | .10   | 4.88     | 16FEB70 |
| 2.35  | 2.52  | -0.17 | -0.31   | .16   | 6.55     | 15AUG70 |
| 2.22  | 2.73  | -0.51 | -1.19   | .13   | 6.61     | 11SEP70 |
| 3.49  | 5.04  | -1.54 | -2.99   | .10   | 6.12     | 7NOV70  |
| 7.78  | 7.30  | 0.48  | 0.42    | .10   | 5.25     | 10DEC70 |
| 13.53 | 11.01 | 2.52  | 1.76    | .10   | 4.65     | 24JAN71 |
| 22.45 | 20.33 | 2.12  | 0.64    | .10   | 4.10     | 11JUL71 |
| 22.24 | 20.00 | 2.25  | 0.68    | .10   | 4.11     | 8AUG71  |
| 19.72 | 19.04 | 0.69  | 0.24    | .10   | 4.24     | 5SEP71  |
| 18.50 | 17.53 | 0.97  | 0.35    | .10   | 4.31     | 3OCT71  |
| 16.72 | 15.81 | 0.91  | 0.37    | .10   | 4.42     | 28OCT71 |
| 12.57 | 12.48 | 0.09  | 0.05    | .10   | 4.73     | 8OEC71  |
| 8.69  | 10.08 | -1.39 | -1.08   | .10   | 5.13     | 5JAN72  |
| 7.78  | 8.17  | -0.39 | -0.17   | .20   | 5.25     | 28JAN72 |
| 8.86  | 6.29  | 2.57  | 1.96    | .10   | 5.11     | 22FEB72 |
| 4.16  | 2.52  | 1.64  | 2.67    | .10   | 5.93     | 29MAY72 |
| 4.09  | 2.86  | 1.22  | 2.03    | .10   | 5.95     | 30JUN72 |
| 6.53  | 5.86  | 0.67  | 0.67    | .10   | 5.44     | 25SEP72 |
| 12.45 | 9.56  | 2.89  | 1.57    | .10   | 4.74     | 20OCT72 |



PHI 0.36835068E 02 S E 0.12939558E 01 LAMBDA 0.100E 01 ANALYTIC PARTIALS USED CHINUSQ 3.65

PTP INVERSE

|   |                |                 |                 |                 |
|---|----------------|-----------------|-----------------|-----------------|
| 1 | 0.14279461E 00 | 0.14428240E 00  | 0.18697608E 00  | 0.53189658E 00  |
| 2 | 0.14428240E 00 | 0.20828694E 00  | -0.23368919E 00 | 0.21703545E -01 |
| 3 | 0.18697560E 00 | -0.23369007E 00 | 0.39057144E 02  | 0.74568008E 02  |
| 4 | 0.53188539E 00 | 0.21701731E -01 | 0.74567993E 02  | 0.16237010E 03  |

PARAMETER CORRELATION MATRIX

|   |        |         |         |        |
|---|--------|---------|---------|--------|
| 1 | 1.0000 | 0.8366  | 0.0792  | 0.1105 |
| 2 | 0.8366 | 1.0000  | -0.0819 | 0.0037 |
| 3 | 0.0792 | -0.0819 | 1.0000  | 0.9364 |
| 4 | 0.1105 | 0.0037  | 0.9364  | 1.0000 |

STD ERROR ONE - PARAMETER SUPPORT PLANE

| B | LOWER          | UPPER          | LOWER          | UPPER          |
|---|----------------|----------------|----------------|----------------|
| 1 | 0.48896229E 00 | 0.10445127E 02 | 0.12400976E 02 | 0.94672031E 01 |
| 2 | 0.59054154E 00 | 0.77255983E 01 | 0.10087764E 02 | 0.65445150E 01 |
| 3 | 0.80866690E 01 | 0.63482642E 03 | 0.66717285E 03 | 0.61865308E 03 |
| 4 | 0.16488159E 02 | 0.73820166E 03 | 0.80415430E 03 | 0.70522534E 03 |

NONLINEAR CONFIDENCE LIMITS

PHI CRITICAL = 0.63624176E 02

SINE WAVE FIT FOR 1.6μ

| PARAMETER | LOWER B        | LOWER PHI      | UPPER B        | UPPER PHI      |
|-----------|----------------|----------------|----------------|----------------|
| 1         | 0.10407433E 02 | 0.63634338E 02 | 0.12437738E 02 | 0.63624069E 02 |
| 2         | 0.77083502E 01 | 0.63609512E 02 | 0.10106588E 02 | 0.63624039E 02 |
| 3         | 0.64051685E 03 | 0.64229986E 02 | 0.66391357E 03 | 0.63985199E 02 |
| 4         | 0.74821948E 03 | 0.63304016E 02 | 0.79219946E 03 | 0.63269714E 02 |

SINE WAVE FIT PARAMETERS ARE

MEAN= 11.4  
 AMP= 8.9  
 PERIOD= 651.0  
 PHASE= 120.2  
 AVERAGE 1.6  
 FLUX OF +10011 = 13.15  
 SIGMA MEAN= 3.27  
 SIGMA= 7.15  
 CHISQ= 4731.92  
 CHINUSQ= 189.28

## INFRARED AND MICROWAVE VALUES USED FOR CORRELATIONS

CORRELATIONS OF 1612 FLUXES WITH 1.6 FLUX OF +10011

| RADIO DATE | NEAREST IR | NEAR FLUX | INTERP FLUX | NEAR MAG | INTERP MAG | RADIO FLUXES |       |       |       |       |    |
|------------|------------|-----------|-------------|----------|------------|--------------|-------|-------|-------|-------|----|
| 22AUG69    | 31AUG69    | 22.04     | 22.04       | 4.12     | 4.12       | 37.20        | 36.00 | 23.00 | 22.00 | 45.00 | 6  |
| 23OCT69    | 22OCT69    | 21.05     | 21.05       | 4.17     | 4.17       | 24.00        | 24.90 | 15.60 | 18.20 | 33.80 | 6  |
| 30DEC69    | 23NOV69    | 17.19     | 15.86       | 4.39     | 4.48       | 34.00        | 31.50 | 20.80 | 23.80 | 41.60 | 7  |
| 3FEB70     | 16FEB70    | 10.95     | 10.95       | 4.88     | 4.88       | 31.80        | 34.20 | 19.00 | 19.00 | 38.00 | 7  |
| 4MART0     | 16FEB70    | 10.95     | 10.95       | 4.88     | 4.88       | 26.40        | 23.70 | 17.50 | 13.00 | 30.50 | 7  |
| 9JUL70     | 15AUG70    | 2.35      | 2.60        | 6.55     | 6.44       | 19.40        | 17.20 | 18.80 | 13.00 | 31.80 | 6  |
| 10JUL70    | 15AUG70    | 2.35      | 2.57        | 6.55     | 6.45       | 19.20        | 21.30 | 13.00 | 17.50 | 30.50 | 6  |
| 15JUL70    | 15AUG70    | 2.35      | 2.45        | 6.55     | 6.50       | 17.60        | 17.50 | 13.00 | 11.70 | 24.70 | 6  |
| 5AUG70     | 15AUG70    | 2.35      | 2.35        | 6.55     | 6.55       | 0.0          | 18.30 | 0.0   | 12.30 | 0.0   | 6  |
| 10SEP70    | 11SEP70    | 2.22      | 2.22        | 6.61     | 6.61       | 15.70        | 0.0   | 7.80  | 0.0   | 17.50 | 6  |
| 11SEP70    | 11SEP70    | 2.22      | 2.22        | 6.61     | 6.61       | 0.0          | 14.30 | 0.0   | 9.70  | 0.0   | 6  |
| 25SEP70    | 11SEP70    | 2.22      | 2.22        | 6.61     | 6.61       | 17.50        | 20.00 | 11.00 | 8.00  | 19.00 | 6  |
| 6OCT70     | 11SEP70    | 2.22      | 2.48        | 6.61     | 6.49       | 16.00        | 14.40 | 11.00 | 6.50  | 17.50 | 5  |
| 7NOV70     | 7NOV70     | 3.49      | 3.49        | 6.12     | 6.12       | 18.30        | 15.20 | 13.00 | 10.40 | 23.40 | 5  |
| 21DEC70    | 10DEC70    | 7.78      | 7.78        | 5.25     | 5.25       | 35.60        | 22.80 | 27.20 | 16.90 | 44.10 | 5  |
| 26JAN71    | 24JAN71    | 13.53     | 13.53       | 4.65     | 4.65       | 39.40        | 30.20 | 25.30 | 22.70 | 48.00 | 5  |
| 19FEB71    | 24JAN71    | 13.53     | 14.42       | 4.65     | 4.58       | 39.20        | 32.90 | 25.30 | 23.40 | 48.70 | 8  |
| 7MAY71     | 11JUL71    | 22.45     | 22.60       | 4.10     | 4.09       | 33.00        | 31.00 | 24.00 | 22.00 | 46.00 | 9  |
| 3JUN71     | 11JUL71    | 22.45     | 23.42       | 4.10     | 4.05       | 33.00        | 32.00 | 25.00 | 23.00 | 48.00 | 10 |
| 30JUN71    | 11JUL71    | 22.45     | 22.45       | 4.10     | 4.10       | 32.00        | 30.00 | 23.00 | 21.00 | 46.00 | 10 |
| 6AUG71     | 8AUG71     | 22.24     | 22.24       | 4.11     | 4.11       | 30.00        | 28.00 | 21.00 | 24.00 | 45.00 | 10 |
| 10SEP71    | 5SEP71     | 19.73     | 19.73       | 4.24     | 4.24       | 40.00        | 0.0   | 26.00 | 0.0   | 0.0   | 10 |
| 13SEP71    | 5SEP71     | 19.73     | 19.73       | 4.24     | 4.24       | 0.0          | 30.00 | 0.0   | 0.0   | 0.0   | 10 |
| 10OCT71    | 30OCT71    | 18.50     | 18.50       | 4.31     | 4.31       | 46.50        | 46.50 | 34.00 | 38.00 | 72.00 | 10 |
| 1NOV71     | 28OCT71    | 16.72     | 16.72       | 4.42     | 4.42       | 32.30        | 35.70 | 28.30 | 30.30 | 58.60 | 10 |
| 4NOV71     | 28OCT71    | 16.72     | 16.72       | 4.42     | 4.42       | 38.80        | 40.50 | 22.00 | 32.00 | 54.00 | 10 |
| 5JAN72     | 5JAN72     | 8.69      | 8.69        | 5.13     | 5.13       | 30.00        | 33.00 | 21.40 | 30.00 | 51.40 | 10 |
| 17FEB72    | 22FEB72    | 8.86      | 8.86        | 5.11     | 5.11       | 23.00        | 31.30 | 16.60 | 26.20 | 42.80 | 10 |
| 12APR72    | 29MAY72    | 4.16      | 5.53        | 5.93     | 5.62       | 22.70        | 22.30 | 15.00 | 15.50 | 30.50 | 11 |
| 23MAY72    | 29MAY72    | 4.16      | 4.16        | 5.93     | 5.93       | 23.10        | 18.10 | 10.40 | 12.50 | 22.90 | 11 |
| 18JUL72    | 30JUN72    | 4.09      | 4.55        | 5.95     | 5.83       | 26.40        | 10.50 | 18.80 | 6.70  | 25.50 | 11 |
| 3AUG72     | 25SEP72    | 6.53      | 6.53        | 5.44     | 5.44       | 26.20        | 19.80 | 19.80 | 6.20  | 26.00 | 11 |



CORRELATION COEFFICIENT FOR LVPK FLUX= 0.702 FOR 29 OBSERVATIONS  
PROBABILITY FROM UNCORRELATED DATA= 0.00002

CORRELATION COEFFICIENT FOR HVPK FLUX= 0.709 FOR 30 OBSERVATIONS  
PROBABILITY FROM UNCORRELATED DATA= 0.00001

CORRELATION COEFFICIENT FOR INLV FLUX= 0.649 FOR 29 OBSERVATIONS  
PROBABILITY FROM UNCORRELATED DATA= 0.00014

CORRELATION COEFFICIENT FOR INHV FLUX= 0.634 FOR 30 OBSERVATIONS  
PROBABILITY FROM UNCORRELATED DATA= 0.00016

CORRELATION COEFFICIENT FOR INTG FLUX= 0.716 FOR 29 OBSERVATIONS  
PROBABILITY FROM UNCORRELATED DATA= 0.00001

## REFERENCES - PART I

- Allen, R. J. 1967, Ph.D. Thesis, Massachusetts Institute of Technology.
- Becklin, E. E. 1968, Ph.D. Thesis, California Institute of Technology.
- Becklin, E. E. and Neugebauer, G. 1968, Ap. J., 151, 145.
- Bevington, Phillip R. 1969 Data Reduction and Error Analysis for the Physical Sciences, (New York: McGraw-Hill).
- Davies, R. D., Mashedier, M. R. W., and Booth, R. S. 1972, Nature Phys. Sci., 237, 21.
- Deutsch, Armin J. 1960, in Stellar Atmospheres, ed. J. L. Greenstein, (Chicago: University of Chicago Press), p. 543.
- Doherty, Lowell R. 1972, in The Scientific Results From the Orbiting Astronomical Observatory, ed. Arthur D. Code, (Washington, D.C.: NASA), p. 411.
- Eliasson, B. and Bartlett, J. F. 1969, Ap. J. (Letters), 155, L79.
- Frogel, J. A. 1971, Ph.D. Thesis, California Institute of Technology.
- Fujita, Yoshio 1970, Interpretation of Spectra and Atmospheric Structure in Cool Stars, (Tokyo: University of Tokyo Press), p. 92.
- Gehrz, R. D. and Woolf, N. J. 1971, Ap. J., 165, 285.
- Gilman, Robert C. 1972, Ap. J., 178, 423.
- Glass, I. S. 1972, Observatory, 92, 140.
- Gunderman, E. 1965, Ph.D. Thesis, Harvard University.
- Hilgeman, T. W. 1970, Ph.D. Thesis, California Institute of Technology.
- Hyland, A. R., Becklin, E. E., Frogel, J. A., and Neugebauer, G. 1972, Astr. and Ap., 16, 204.
- Johnson, H. L. 1968, Ap. J. (Letters), 154, L125.
- Kellermann, K. I., Pauliny-Toth, I. I. K., and Williams, P. J. S. 1969, Ap. J., 157, 1.

- Kukarkin, B. V., Kholopov, P. N., Efremov, Yu. N., Kukarkina, N. P., Kurochkin, N. E., Medvedeva, G. I., Perova, N. B., Fedorovich, V. P., and Frolov, M. S. 1969, General Catalog of Variable Stars (3d ed.; Moscow: Astronomical Council of the Academy of Sciences in the USSR).
- Litvak, M. M. 1969, Ap. J., 156, 471.
- Litvak, M. M. 1970, Phys. Rev. A, 2, 2107.
- Litvak, M. M. and Dickinson, Dale F. 1972, Ap. Lett., 12, 113.
- Lockwood, G. W. and Wing, Robert F. 1971, Ap. J., 169, 63.
- Marquardt, D. W. 1963, J. Soc. Ind. and Ap. Math., 11, 431.
- Marquardt, Donald W. 1964, IBM Share Program #3094 Description.
- Mendoza, V., E. E. 1967, Bol. Obs. Ton. y Tac., 4, 114.
- Merrill, P. W. 1960, in Stellar Atmospheres, ed. J. L. Greenstein, (Chicago: University of Chicago Press), p. 525.
- Merrill, Paul W. and Deutsch, Armin J. 1959, Ap. J., 130, 570.
- Neugebauer, G. and Leighton, R. B. 1969, Two-Micron Sky Survey, A Preliminary Catalogue, (Washington, D.C.: NASA).
- Pettit, E. and Nicholson, S. B. 1933, Ap. J., 78, 320.
- Robinson, B. J., Caswell, J. L., and Goss, W. M. 1970, Ap. Lett., 7, 79.
- Robinson, B. J., Caswell, J. L., and Dickel, Helene R. 1971, Ap. Lett., 8, 171.
- Rogers, A. E. E., Moran, J. M., Crowther, P. P., Burke, B. F., Meeks, M. L., Ball, J. A., and Hyde, G. M. 1967, Ap. J., 147, 369.
- Wallerstein, George 1971, Ap. Lett., 7, 199.
- Weaver, H., Williams, D. R. W., and Dieter, W. T. 1965, Nature, 208, 29.
- Wilson, W. J. 1970, Ph.D. Thesis, Massachusetts Institute of Technology.
- Wilson, W. J. and Barrett, A. H. 1972, Astr. and Ap., 17, 385.
- Wilson, W. J., Barrett, A. H., and Moran, J. M. 1970, Ap. J., 160, 545.
- Wilson, W. J., Schwartz, P. R., Neugebauer, G., Harvey, P. M., and Becklin, E. E. 1972, Ap. J., 177, 523.

Woolf, N. J. 1972, Mem. Soc. Royal Sci. Liege, 6e serie, t. III, p. 209.

Zuckerman, B., Yen, J. L., Gottlieb, C. A., and Palmer, Patrick 1972,  
Ap. J., 177, 59.

PART II

A ONE MILLIMETER WAVELENGTH DETECTING SYSTEM  
FOR THE 200-INCH TELESCOPE

## I. INTRODUCTION

Observations of astronomical objects at wavelengths near 1 mm are relatively scarce because of the small source strengths relative to the sensitivity of existing detectors. Microwave type receivers are not yet practical for wavelengths shorter than several millimeters; therefore, the only detectors presently available are broad-band infrared bolometers. Observations of some of the planets between 1.2 and 1.4 mm with such bolometers were made by Low and Davidson (1965) and Kostenko et al. (1971). Only four objects outside of the solar system have been observed in this wavelength region: the quasar 3C273 (Low 1965), the infrared source in the Orion Nebula (Low and Aumann 1970; Park et al. 1970; Zabolotny et al. 1971; and Baluteau et al. 1972), the Crab Nebula (Beckman et al. 1969; and Zabolotny et al. 1971), and the center of the Galaxy (Low and Aumann 1970).

Because of the growing number of astrophysical sources which appear to emit most of their energy in the far infrared between 10 and 1000 $\mu$  (Low and Aumann 1970; Harper and Low 1971; Hoffmann et al. 1971) and the daytime availability of the 200-inch Hale telescope, it was decided to develop a millimeter and sub-millimeter wave detecting system for use on the 200-inch telescope. This is the subject of Part II of this thesis. The instrumentation is described in Chapter 2, and in Chapters 3 and 4 the observing techniques and calibration procedures are discussed. Chapter 5 discusses several measurements of astrophysical sources to illustrate the calibration procedures, but the interpretation of the measurements is not considered in this thesis.

## II. INSTRUMENTATION

A. Detector

Three types of detectors were considered for use in this system: a semi-conducting bolometer of doped silicon<sup>1</sup>, a semi-conducting bolometer of doped germanium<sup>2</sup>, and an indium-antimonide electron bolometer<sup>3</sup>. Of the three, the germanium bolometer in use now has the greatest sensitivity in this system and has been used for the measurements described here. This fact does not imply that it is inherently the best type of detector, because no attempt was made to select the best of each kind of detector or to optimize the optical configurations for each.

The theory of bolometers has been discussed by Jones (1953). Low (1961) has described germanium bolometers similar to the one used here. Therefore, only the important details of this detector will be mentioned. Some measure of the detector sensitivity can be obtained from its voltage vs. current (V-I) characteristics because electrical power dissipated in the bolometer element is roughly equivalent to radiation power absorbed by the element. The usual bolometer circuit is shown in Figure 1, and the V-I characteristics for the detector used in this work are shown in Figure 2. The electrical parameters at the operating point as well as the physical parameters of the detector are given in Table 1. Also given in Table 1 is an estimate of the efficiency of absorption of 1 mm radiation. It is impossible to measure this quantity directly in the

---

<sup>1</sup>Molelectron Corporation

<sup>2</sup>Constructed by H. Aumann

<sup>3</sup>Constructed by J. Pipher

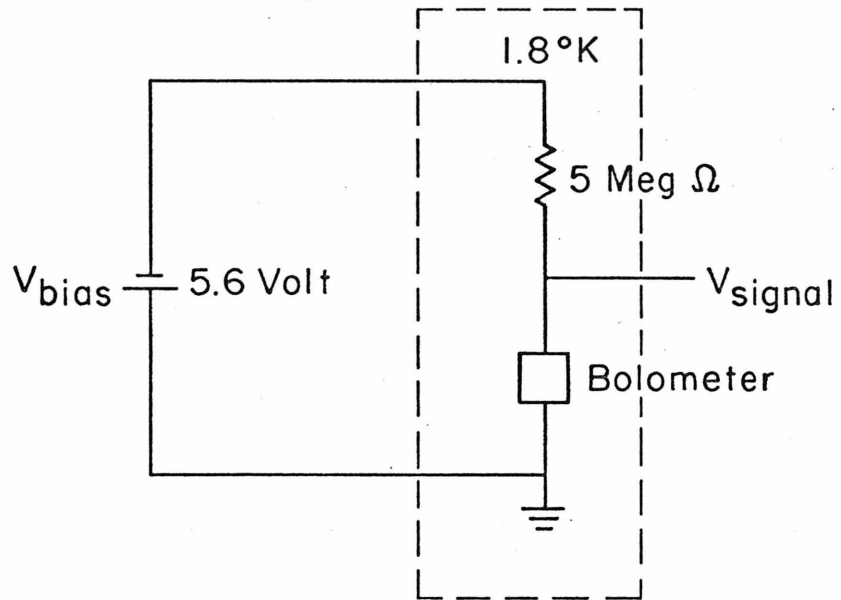


Fig. 1 - The bolometer electrical circuit

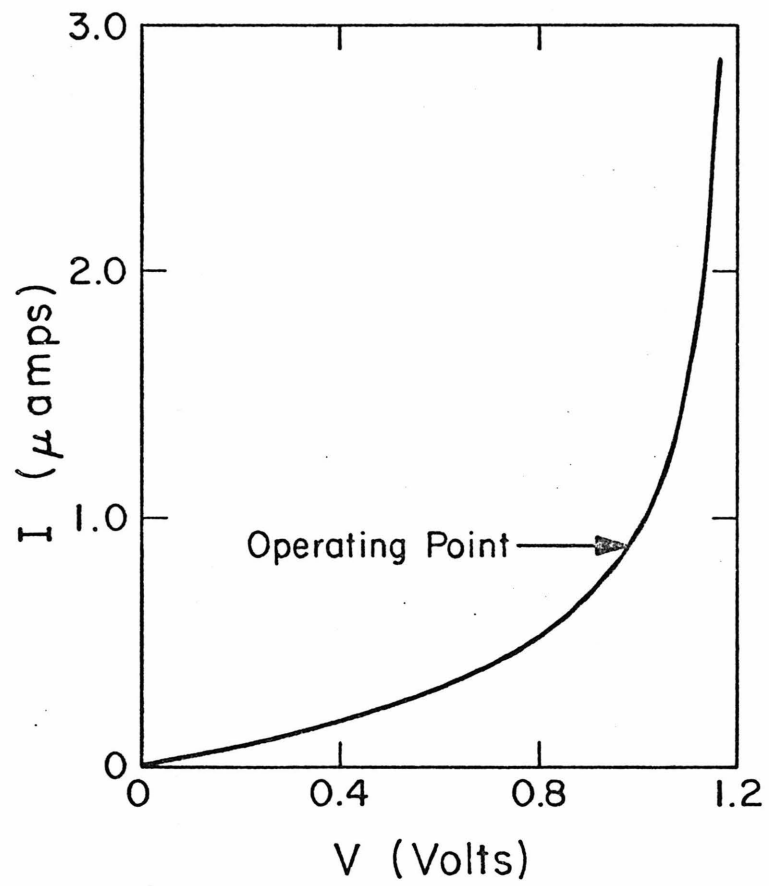


Fig. 2 - Voltage-Current characteristics of the germanium bolometer

TABLE 1

## Parameters of the Detector

|                                 |  |
|---------------------------------|--|
| Size                            | 3 x 3 x 0.2 mm   |
| Temperature                     | $\approx 1.8^{\circ}\text{K}$                                |
| Operating Resistance (Static)   | $\approx 1.1 \text{ Meg } \Omega$                            |
| Operating Resistance (Dynamic)  | $\approx 260 \text{ Kilo } \Omega$                           |
| Bias Voltage                    | 5.6 Volts  |
| Cooled Load Resistor            | 5.0 Meg $\Omega$   |
| Time Constant                   | $\approx 15 \text{ msec}$                                    |
| Electrical Responsivity         | $\approx 3.9 \times 10^5 \text{ Volt Watt}^{-1}$             |
| Thermal Conductivity - G        | $\approx 4.5 \text{ } \mu\text{Watt } ^{\circ}\text{K}^{-1}$ |
| Radiation Absorption Efficiency | $\approx 25\%$   |
| Electrical NEP                  | $\approx 8 \times 10^{-14} \text{ Watt Hz}^{-1/2}$           |
| System NEP                      | $\approx 2 \times 10^{-12} \text{ Watt Hz}^{-1/2}$           |

laboratory because of the difficulty of obtaining a calibrated, spectrally pure radiation source at 1 mm. An estimate can be made, however, from the efficiencies of the various optical components in the system and from the observed signal at the telescope from an object whose flux is known. This value of the efficiency,  $\sim 25\%$ , is very uncertain, but it is consistent with measurements of the far infrared absorptivity of germanium bolometers by Zwerdling and Theriault(1972).

The electrical noise-equivalent-power (NEP) given in Table 1 basically represents the limiting sensitivity of this system; the difference between this and the system NEP is due to the various system inefficiencies. The detector noise will, in fact, remain the limiting factor in this system until it can be made comparable to or smaller than the noise limit set by the background radiation fluctuations. Following the equations of Putley (1963), this limit is roughly  $2 \times 10^{-14}$  Watt Hz<sup>-1/2</sup> for the present system, but can be reduced to about  $5 \times 10^{-15}$  Watt Hz<sup>-1/2</sup> with improved baffling and narrower bandpass filters with  $\Delta\lambda/\lambda \sim 0.3$ . Therefore, significant detector improvements are desirable to reach the background limit for even fairly broad-band systems at 1 mm.

#### B. Optics and Photometer

A drawing of the entire optical system is shown in Figure 3. The simplest possible configuration has been chosen for coupling the incoming radiation to the detector in order to minimize diffraction and reflection losses. A "condensing" cone is located directly in front of the detector with the large diameter of the cone at the prime focus of the telescope. This cone can be viewed either as an optical condenser

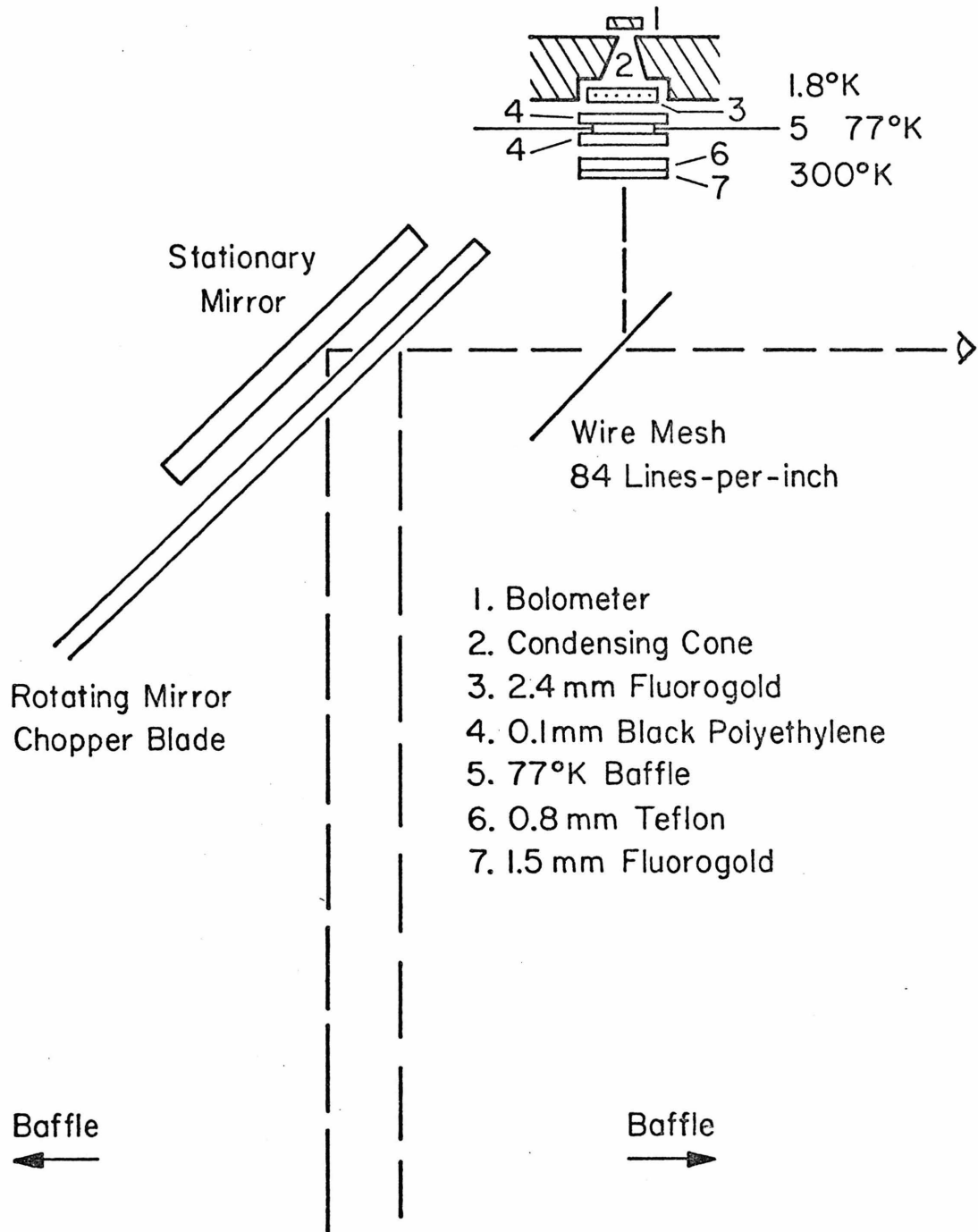


Fig. 3 - The 1 mm photometer and dewar optical components

(Witte 1965; Loewenstein and Newell 1969) or as an oversize conical microwave feed horn. The prime focus was chosen for mechanical reasons because it has the smallest diffraction-limited image size. The small diameter of the cone is located close to the detector so that radiation leaving the cone even at fairly large angles will be incident on the detector. The cone provides some rejection of radiation outside the  $f/3.3$  beam of the telescope but most of the baffling is accomplished with the aperture in the photometer.

The photometer is a device which chops the incoming radiation between two adjacent areas of sky. This cancels the background signal which would be seen if the sky radiation were compared to a fixed temperature source and also cancels fluctuations in the background when they are correlated over the spacing and time scale of the chopping. The chopper consists of a rotating two-bladed mirror and a fixed mirror offset from the plane of the rotating mirror. The separation between the two beams on the sky is about 1 cm or 2.2 arcminutes at the prime focus of the 200-inch telescope. The other important component of the photometer is the metal mesh "beamsplitter." This reflects millimeter wavelength radiation toward the detector and transmits wavelengths shorter than the spacing of the wires to an eyepiece for viewing.

### C. Filters

Each of the filters will be discussed individually, after which the spectral response of the whole system will be considered.

#### 1. Teflon dewar window

Teflon is used in this system only as a vacuum seal at the dewar

window. Its filtering properties are incidental because of other materials with much sharper cut-offs and more opaque stop-bands. The near infrared spectrum of teflon is composed of many absorption bands with a transmission between the bands of typically 10 to 50 percent (Liang and Krimm 1956), and teflon is virtually transparent in the far infrared longward of  $55\mu$  (Brandli and Sievers 1972).

## 2. Black Polyethylene

Black polyethylene is polyethylene in which carbon powder is suspended. The general shape of the transmission measured by Moller et al. (1966) shows a gradually increasing transparency with wavelength starting from less than 1 percent at  $3\mu$  to a peak of about 85 percent longward of  $200\mu$ . Measurements of the transmission of the black polyethylene used in this system are shown in Figure 4a for seven infrared bands between 1 and  $20\mu$ . The black polyethylene prevents heating of the filter and detector at  $1.8^{\circ}\text{K}$  by absorbing most of the radiation between 5 and  $20\mu$  and, in addition, absorbs all 1 to  $3\mu$  radiation from astronomical sources.

## 3. Fluorogold<sup>1</sup>

This is glass fiber impregnated teflon whose excellent low-frequency pass characteristics have been noted by Muehlner and Weiss (1972). Measurements of its transmission in seven infrared bands between 1 and  $20\mu$  are shown in Figure 4a. A scan of its transmission<sup>2</sup> on an infrared spectrometer is also shown in Figures 4a and b. The result of this scan is an upper limit between 2.5 and  $250\mu$  and an observed rapidly increasing

---

<sup>1</sup>Fluorocarbon Corporation, Anaheim, California

<sup>2</sup>By G. Rossman, C.I.T.

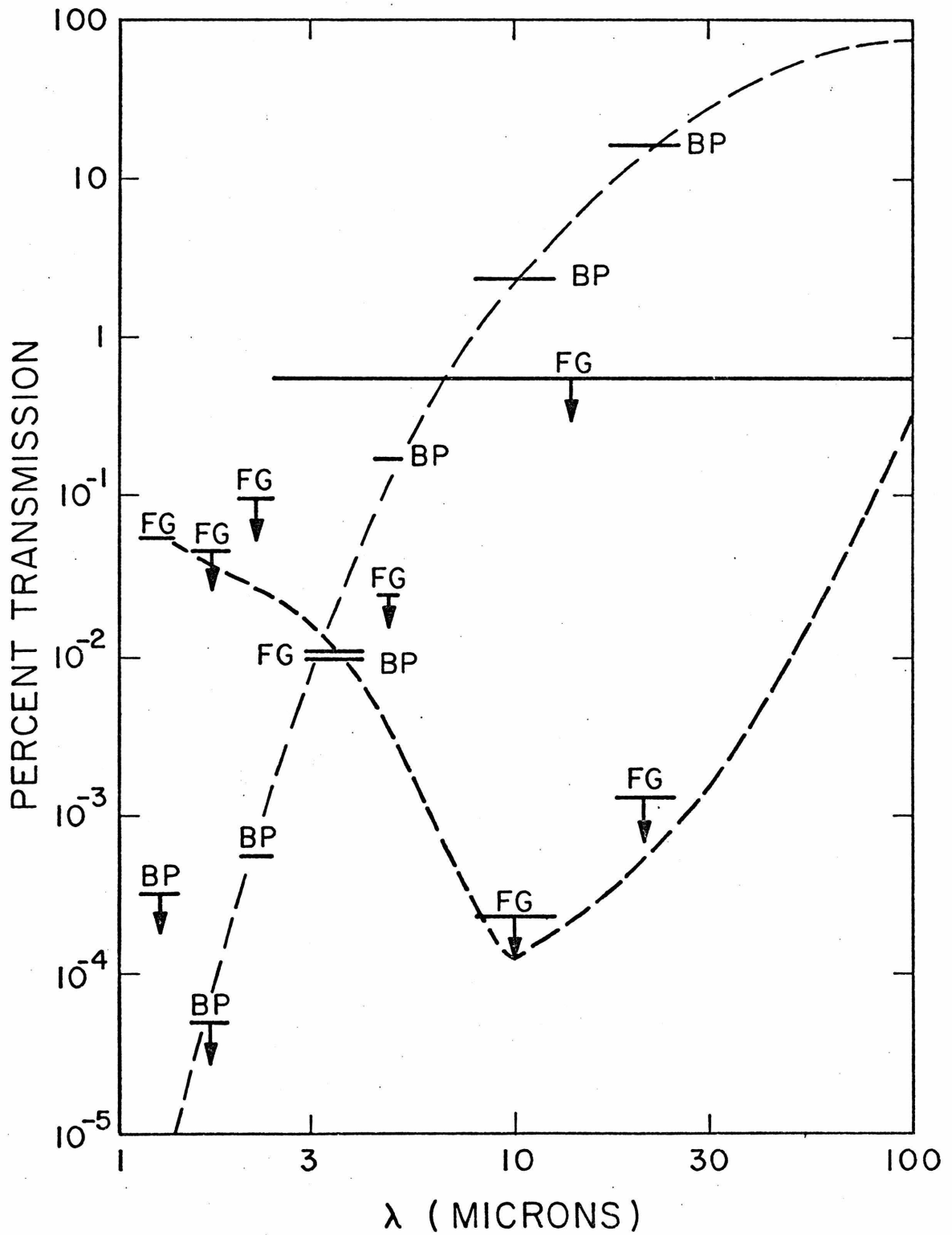


Fig. 4a - The properties of the individual filters used for near infrared blocking

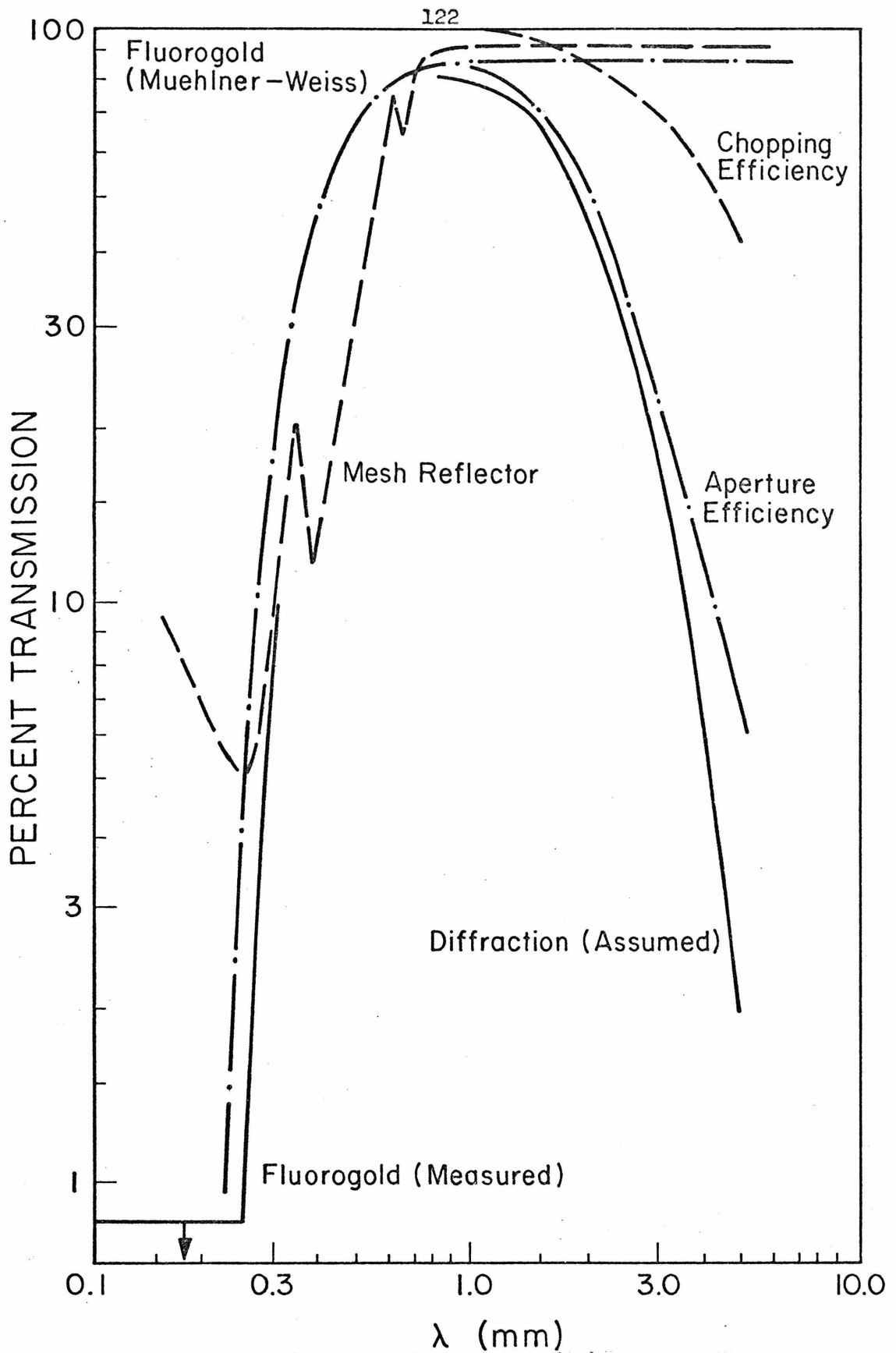


Fig. 4b - The properties of the individual 1 mm pass-band filters

transmission between 250 and 300 $\mu$ . The transmission between 200 and 1000 $\mu$  observed by Muehlner and Weiss (1972) is in reasonable agreement with the above measured spectrum where there is overlap. Therefore, the Muehlner and Weiss spectrum has been used in calculating the system response longward of 300 $\mu$ .

#### 4. Reflection Wire Mesh

The reflection properties of woven wire mesh have been investigated by Mitsubishi et al. (1963) and Ressler and Moller (1967); the results of both groups are in reasonable agreement. Therefore, the properties of the 84 lines-per-inch mesh used here were calculated by scaling from the data of Mitsubishi et al. for a 145 lines-per-inch mesh at an angle of incidence of 54°. The resulting reflection spectrum is shown in Figure 4b.

#### 5. Diffraction Effects

The long wavelength cut-off of the system is established by diffraction effects. A number of these effects contribute to the characteristics and each will be discussed individually.

Chopping Efficiency - The size of the diffraction limited image increases with wavelength, and near 3 mm the image size equals the chopping spacing causing a considerable reduction in signal. This decrease is readily analyzed for a point source. Consider a point source centered in one beam; the observed signal will be the difference of the signal from the main beam and that from the reference beam. If the signal in the main beam is 1.0, then the signal from the overlap with the reference beam is  $-\exp[-(S/R)^2]$  where S is the chopping spacing, and R is the effective beamwidth discussed in Section D. The total observed signal is then

$1 - \exp[-(S/R)^2]$ . The observed effective beamwidth of about 2 arcminutes at 1 mm is consistent with the convolution of: (1) the diffraction image size, (2) the focal plane aperture diameter, and (3) the de-focussed image size. Therefore, it is reasonable to use calculated beamwidths at longer wavelengths to compute the decrease in chopping efficiency with wavelength. This calculated response is shown in Figure 4b. Although it is only exact for point sources, this curve should also be a reasonable approximation for spatially extended sources.

Aperture Efficiency - The increase in image size with wavelength also causes a decrease in response because the image eventually becomes larger than the 6 mm entrance aperture of the detector feed cone. This effect depends more strongly on the spatial extent of the object than does the previous effect; the effect is negligible for a source that is large compared to the beam size. Many of the astrophysical objects for which it is important to know the long wavelength cut-off of the system, however, are point sources. Therefore, this effect is included in the assumed response of the system. The percentage of total flux in the image which is incident on the 6 mm aperture for various wavelengths is shown in Figure 4b as the aperture efficiency.

Component Size Relative to Wavelength - A third reason for the decrease in response with wavelength is the diffraction caused by the fact that the wavelengths are comparable in size to the 6 mm and 2.5 mm cone apertures. King and Wu (1959) have calculated this effect exactly for a circular aperture in an infinite conducting plane and find that the transmission coefficient does not decrease substantially until  $\lambda \approx \pi \times$  aperture diameter. At wavelengths on the order of the aperture size,

however, the diffracted waves leave the apertures at large scattering angles (Jackson 1962), and some power will, therefore, be reflected back out of the feed cone before reaching the detector. No spectrum of this effect is shown because it is difficult to calculate, but clearly it must provide an additional long wavelength cut-off.

#### 6. Sum of All Contributions

Because the quantitative details of several of the diffraction effects are unknown, a long wavelength cut-off for this system was assumed in considering the system calibration. This assumed transmission is shown in Figure 4b. The minimum long wavelength cut-off for spatially extended sources is equal to the chopping efficiency; for point sources this cut-off is equal to the product of the chopping and aperture efficiencies. The uncertainties in the calibration caused by this uncertainty in the long wavelength cut-off are discussed in Chapter 4. They are relatively small because the integrated power of most astrophysical sources,  $\nu F_\nu$  or  $\lambda F_\lambda$ , decreases with increasing wavelength at least as rapidly as  $1/\lambda$ .

The total relative system sensitivity has been estimated as the product of all the filter transmissions and is shown in Figures 5a and b. Several checks have been made on the gross characteristics of this estimated spectral response. The ratio of brightness of the bright to dark side of the Moon has been found to be about 2.5 every time it was measured. If there were any significant system sensitivity shortward of  $30\mu$ , this value of the ratio would not be observed. Furthermore, the transmission of a Flurogold filter and of a 10 lines-per-centimeter wire mesh have also been measured while observing astronomical sources. The transmis-

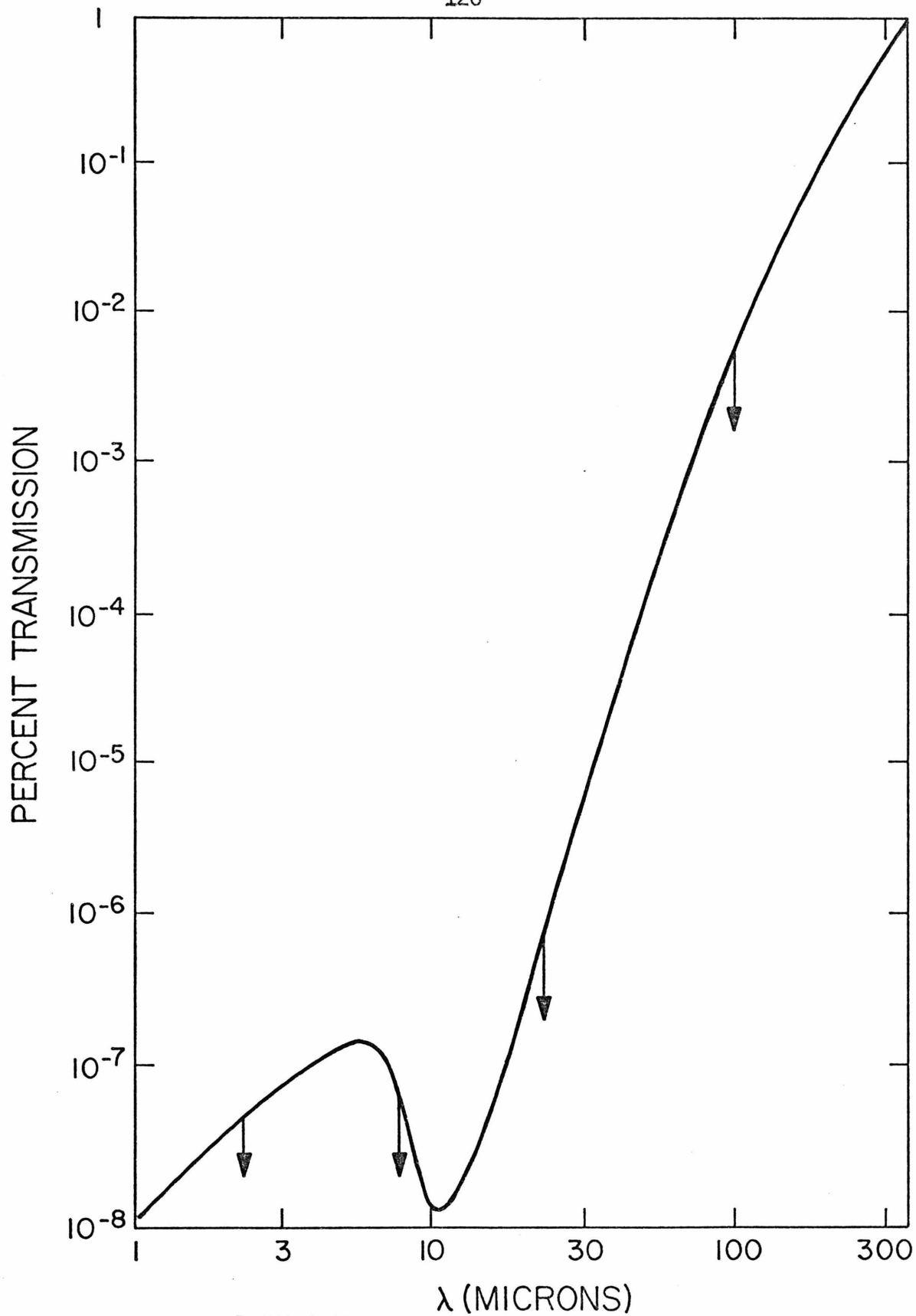


Fig. 5a - Upper limit to the near infrared transmission of the 1 mm system

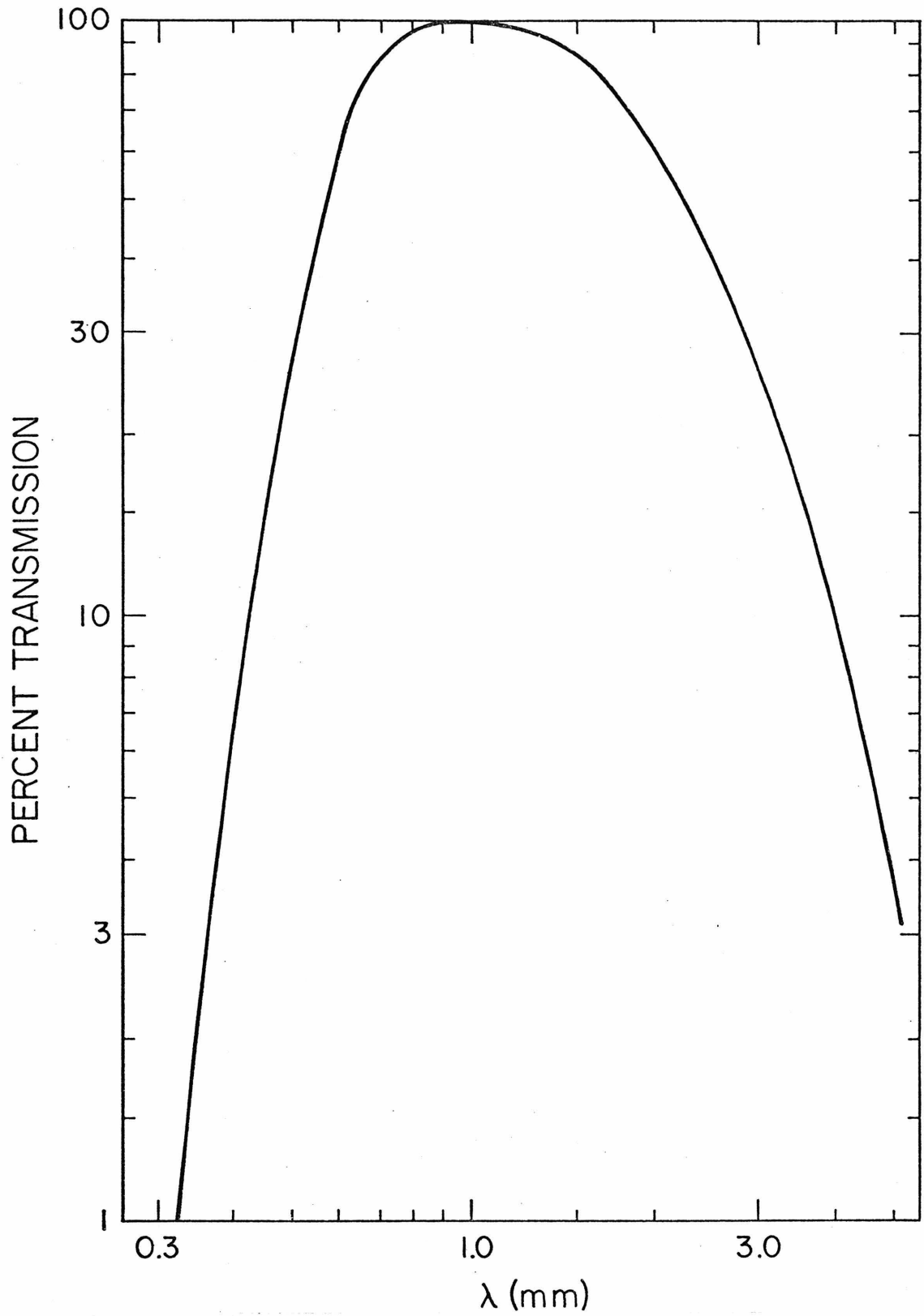


Fig. 5b - The estimated 1 mm pass-band of the entire system

sions of both are about 0.85. If there were either a significant response shortward of  $500\mu$ , or no response shortward of 2 mm, these ratios would also not be observed.

#### D. Beamwidth

The beamwidth is determined by diffraction effects and by the size, 6 mm, of the large diameter of the condensing cone. Figure 6 shows the response of the system as the telescope is slowly scanned across Jupiter, roughly a uniformly bright disc 30 arcseconds in diameter. This curve is fit quite well by the Gaussian,  $\exp -(r/R)^2$ , where  $R = 64$  arcseconds. For computational purposes this approximation is used.

Two quantities related to the beamwidth are important for the calibrations. The first is the decrease in signal from a source of finite angular extent because of the decrease in response off axis. The size of the actual signal relative to that of an equally strong point source is

$$\epsilon = \left[ \int_0^a \exp-(r/R)^2 2\pi r dr \right] / \pi a^2 = (R/a)^2 [1 - \exp-(a/R)^2]$$

where  $R = 64$  arcseconds and  $a$  is the source radius. The quantity,  $\epsilon$ , is graphed in Figure 7 as a function of the radius of the source. The second quantity is the effective beam size for sources large compared to the beam,  $R_e$ . This is the size of a circular beam with flat response over its area equal to the peak response of the real beam and with an integrated response equal to that of the real beam. This is given by

$$\pi R_e^2 = \int_0^\infty \exp-(r/R)^2 2\pi r dr, \text{ implying } R_e = R = 64 \text{ arcseconds.}$$

#### E. Electronics

The first stage of signal amplification is provided by a preamp (Aumann 1970) mounted on the detector dewar. The remaining electronics

## SCAN OF JUPITER

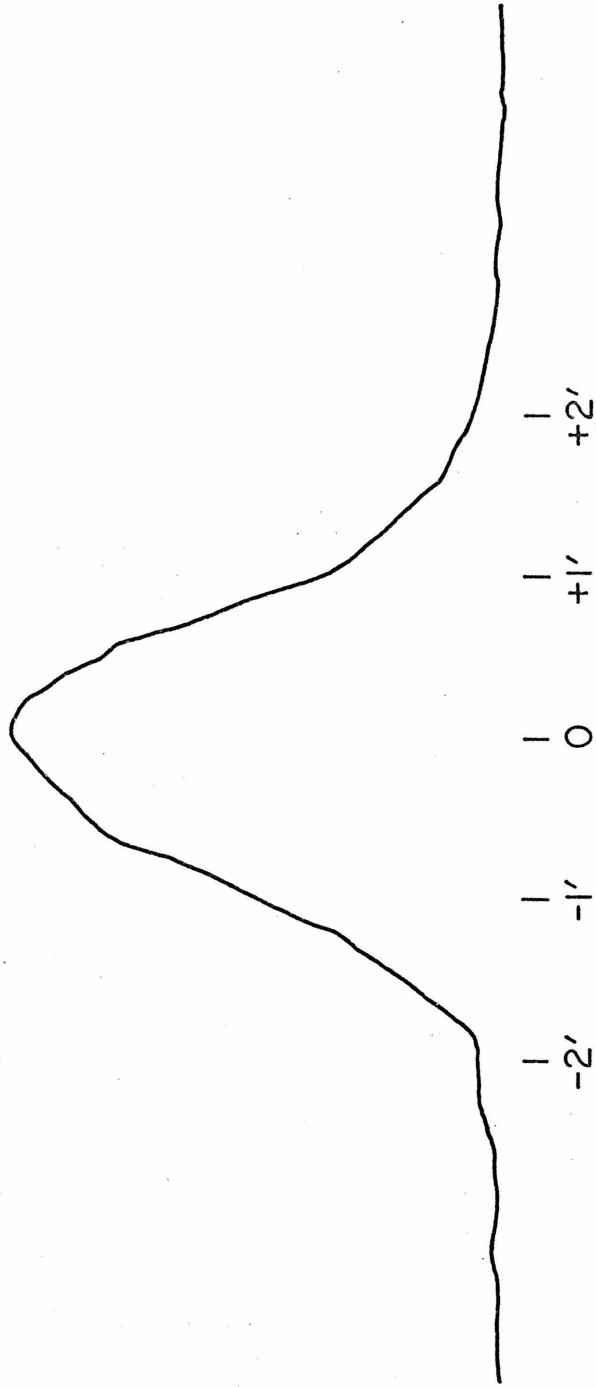


Fig. 6 - A scan of Jupiter with the 1 mm system on the 200-inch telescope

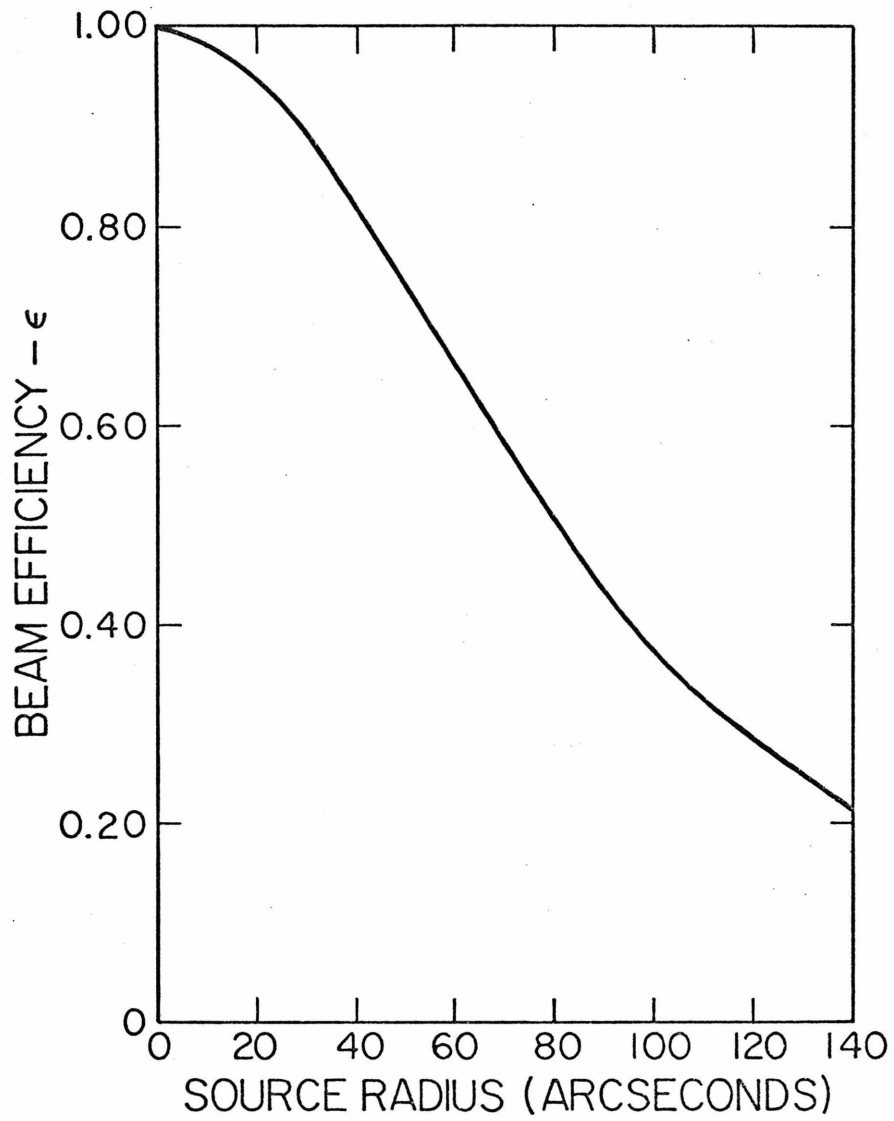


Fig. 7 - The decrease in signal from a source of finite radius,  $R$ , is shown relative to the signal from an equally strong point source.

are similar to those used for the near infrared observations in Part I of this thesis.

## III. OBSERVING TECHNIQUES

The observations described here have all been made during "twilight" time on the 200-inch telescope. This time extends from about three hours before sunset to one half hour after sunset in the evening and similarly in the morning. This daylight observing is practical because millimeter observations are not affected by scattered sunlight, and because in daylight the telescope can be pointed to an accuracy of about  $\pm 7$  arcseconds by off-setting from nearby visible stars brighter than 3.5 to 4.0 magnitude. Generally there are at least two such stars within a  $10^\circ$  radius of most sources observed.

In addition to observing the program sources, the typical observing procedure consists of measuring calibration sources at the beginning and end of each observing session and occasionally in the middle. These calibration measurements provide an estimate of the relative sensitivity of the system and of the change in atmospheric absorption with zenith angle. On both calibration and program sources the integration pattern is usually a sequence of two 10-second integrations in one beam of the chopper, four in the other beam, and then two in the first beam with as many repetitions as necessary to obtain the desired signal-to-noise ratio. On the planets Venus, Jupiter, and Saturn, the signal-to-noise ratio is greater than 20/1 in less than a minute of integration.

The above mode of integration was chosen to provide a large ratio of integration time to beam-switching time and is practical because there is little or no long-term drifting which would require more rapid beam switching and shorter integration times. This has been checked by

dividing a typical sample of data into two distinct halves and comparing the noise in each. One half was comprised of the differences between adjacent 10-second integrations in each beam. The other half was comprised of the differences of the remaining pairs of 10-second integrations. In this second half the members of a pair were separated in time by about 40 seconds as opposed to the 20-second separation in the first half. The rms values of the noise in each case were almost equal.

## IV. CALIBRATION PROCEDURES

A. Basis

A wide-bandwidth detecting system measures the total flux in its bandwidth; the flux density at some average frequency is uniquely determined only by a knowledge of the source spectrum. The spectrum cannot be determined from the wide-band data alone, but some limits may be obtained by making use of measurements at nearby wavelengths and by assuming moderately slow variations with frequency. This is the basis of the calibration procedure for this 1 mm system.

The absolute and relative calibrations of the responsivity are based on the assumption that the planets radiate like blackbodies in this spectral region. With this assumption, the total amount and spectral shape of their emitted fluxes are characterized by their brightness temperatures. The power incident on the detector is then the integral of a Planck function times the filter and atmospheric transmissions.

B. Planets

The assumption that the planets radiate like blackbodies will first be examined. In Tables 2 - 4 are listed measurements of the brightness temperatures at a variety of wavelengths for the three principal calibration sources, Venus, Jupiter, and Saturn, along with the adopted 1 mm brightness temperatures. There is a clear trend in all three planets for a decrease in brightness temperature with wavelength, generally attributed to a decrease in opacity with increasing wavelength and an increase in temperature with depth in the atmosphere (see e.g. Sagan 1971; Trafton 1967). The range of variation of brightness temperature between 10 $\mu$

TABLE 2

## Brightness Temperatures of Venus

 $T_b$  adopted at 1 mm = 285°K

| $\lambda$ (mm) | $T_b$ (°K) | Reference               |
|----------------|------------|-------------------------|
| 0.01           | 200-225    | Westphal et al. (1965)  |
| 0.02           | 248±10     | Low (1966b)             |
| 0.03-0.045     | 260±4      | Armstrong et al. (1972) |
| 0.045-0.080    | 274±3      | Armstrong et al. (1972) |
| 0.065-0.110    | 289±20     | Armstrong et al. (1972) |
| 0.125-0.300    | 280±45     | Armstrong et al. (1972) |
| 0.35           | 274±30     | Harper et al. (1972)    |
| 1.2            | 319±32     | Low and Davidson (1965) |
| 1.4            | 265±30     | Kostenko et al. (1971)  |
| 2.1            | 251±19     | Ulich (1973)            |
| 3.1            | 379±33     | Ulich (1973)            |
| 3.4            | 331±33     | Epstein et al. (1968)   |
| 8.0            | 416±67     | Efanov et al. (1969)    |
| 13.5           | 472±30     | Low and Staelin (1968)  |
| 27.0           | 612±37     | McCullough (1972)       |
| 45.2           | 654±35     | Dickel et al. (1968)    |

TABLE 3

## Brightness Temperatures of Jupiter

 $T_b$  adopted at 1 mm = 145°K

| $\lambda$ (mm) | $T_b$ (°K)                        | Reference                          |
|----------------|-----------------------------------|------------------------------------|
| 0.01           | 129±2                             | Willey et al. (1965)               |
| 0.02           | 127±6                             | Low (1965)                         |
| 0.03-0.045     | 136±1                             | Armstrong et al. (1972)            |
| 0.045-0.080    | 150±5                             | Armstrong et al. (1972)            |
| 0.065-0.110    | 153±7                             | Armstrong et al. (1972)            |
| 1.2            | 155±15                            | Low and Davidson (1965)            |
| 2.1            | 141±11                            | Ulich (1973)                       |
| 3.1            | 181±13                            | Ulich (1973)                       |
| 3.3            | 153±15                            | Epstein et al. (1970)              |
| 3.9            | 150 <sup>+45</sup> <sub>-35</sub> | Kislyakov and Lebskii (1968)       |
| 8.5            | 157±8                             | Wrixon et al. (1971)               |
| 9.9            | 130±7                             | Wrixon et al. (1971)               |
| 12.8           | 120±11                            | Kellermann (1970)                  |
| 20             | 145±15                            | Kellermann and Pauliny-Toth (1966) |
| 32             | 177±22                            | Giordimaine et al. (1959)          |
| 60             | 224±30                            | Dickel (1967)                      |
| 210            | 250±40                            | Branson (1968)                     |

TABLE 4

Brightness Temperatures of Saturn<sup>†</sup> $T_b$  observed at 1 mm = 170°K

| $\lambda$ (mm) | $T_b$ (°K)         | Reference               |
|----------------|--------------------|-------------------------|
| 0.01           | 94±5 <sup>x</sup>  | Becklin (private comm.) |
| 0.02           | 84±5 <sup>**</sup> | Becklin (private comm.) |
| 0.030-0.045    | 89±4 <sup>*</sup>  | Armstrong et al. (1972) |
| 0.045-0.080    | 94±2 <sup>*</sup>  | Armstrong et al. (1972) |
| 0.065-0.110    | 97±5 <sup>*</sup>  | Armstrong et al. (1972) |
| 0.125-0.300    | 93±4 <sup>*</sup>  | Armstrong et al. (1972) |
| 0.350          | 150                | Harper et al. (1972)    |
| 1.2            | 140±15             | Low and Davidson (1965) |
| 1.4            | 120±30             | Kostenko et al. (1971)  |
| 2.1            | 145±11             | Ulich (1973)            |
| 3.1            | 148±11             | Ulich (1973)            |
| 3.3            | 125±13             | Epstein (1970)          |
| 8.0            | 132±9              | Salomanovich (1965)     |
| 8.5            | 151±7              | Wrixon and Welch (1970) |
| 8.6            | 102±24             | Ulich (1973)            |
| 11.8           | 131±5              | Wrixon and Welch (1970) |
| 14.6           | 133±8              | Wrixon and Welch (1970) |
| 31.2           | 137±12             | Berge (1968)            |
| 60             | 179±19             | Kellermann (1966)       |
| 90             | 165±25             | Berge and Read (1968)   |

<sup>†</sup>Referred to area of disc unless otherwise noted<sup>\*</sup>Referred to area of disc and rings<sup>x</sup>Disc resolved -  $T_b$  rings  $\approx$  94°K<sup>\*\*</sup>Disc resolved -  $T_b$  rings  $\approx$  84°K

and several centimeters wavelength is considerable for all three planets, but there is no significant variation at wavelengths near 1 mm. Consequently, brightness temperatures at 1 mm for Venus and Jupiter have been adopted close to the 350 $\mu$ , 1.2 mm, and 1.4 mm relative measurements, and the 3 mm absolute measurements. The brightness temperature of Saturn is subject to possible variation due to varying contributions from the rings as their geocentric angle of inclination varies. Therefore, five independent measurements of the flux ratios of Saturn and Venus were made to determine the brightness temperature at the present time. Assuming a brightness temperature for Venus of 285°K, these measurements imply a brightness temperature for Saturn of 170°K  $\pm$  20°K.

### C. Atmospheric Transmission

The short wavelength cut-off of the system response is largely determined by the transmission of the atmosphere. No spectrometer has been available to measure directly the atmospheric transmission as a function of frequency while observing. In fact, this would probably not be practical because of the large amount of observing time required. Therefore, in order to estimate the effects of atmospheric variations and the problems of comparing sources with different spectra, a computer program has been written which calculates the transmission of the atmosphere as a function of the meteorological conditions, principally the amount of precipitable water vapor. This program and the reliability of its predictions are described in the Appendix. In addition to the transmission as a function of frequency, the program also calculates: (1) a weighted average frequency,  $\bar{\nu}$ , and (2) the integral of the product of

the atmospheric transmission with the filter transmission and spectra of any desired power law, which is the quantity actually measured by the detector.

In Table 5 are shown the values of the weighted average frequency

$$\bar{\nu} = [\int_0^{\infty} \nu F_{\nu} T(\nu) d\nu] / [\int_0^{\infty} F_{\nu} T(\nu) d\nu]$$

for several different power law spectra,  $F_{\nu} \propto \nu^{\alpha}$ , and for various amounts of water vapor. In Table 6 are shown the ratios of the integrated flux from a spectrum,  $F_{\nu} \propto \nu^{\alpha}$ , relative to the integrated flux from a black-body spectrum in the Rayleigh-Jeans approximation,  $F_{\nu} \propto \nu^2$ . The spectra were normalized to equal  $F_{\nu}$  at the appropriate  $\bar{\nu}$  from Table 5. The uncertainties given in Tables 5 and 6 are the estimated variations due to insufficient knowledge of the filter transmission and diffraction characteristics. These uncertainties were determined by performing the integrals with various filter transmission curves believed to represent the maximum range of possible characteristics. Clearly sources with equal  $F_{\nu}$  at their respective  $\bar{\nu}$  but with different spectral indices will not in general produce the same signal at the detector. The necessary correction factor, however, appears to be a function only of the spectral index and not of the atmospheric water vapor.

It is apparent from the preceding discussions that to calibrate any measurement two quantities must be known roughly -- the precipitable water vapor in the atmosphere, and the frequency dependence of the flux density from the sources under observation. The amount of water vapor can be estimated in two ways. The decrease in signal strength with increasing zenith angle of the calibration sources gives some indication of the atmospheric opacity. The opacity can be used to estimate the

TABLE 5

Computed Effective Frequency ( $\text{cm}^{-1}$ ) as a Function  
of Precipitable Water Vapor and Spectral Index

| mm H <sub>2</sub> O | Spectral Index, $\alpha$ , for $F_v \propto \nu^\alpha$ |                                      |                                       |                                       |
|---------------------|---|--------------------------------------|---------------------------------------|---------------------------------------|
|                     | 0   | 1                                    | 2                                     | 3                                     |
| 1.5                 | 8.53 <sup>+.20</sup> <sub>-.80</sub>                    | 9.42 <sup>+.30</sup> <sub>-.80</sub> | 10.33 <sup>+.40</sup> <sub>-.80</sub> | 11.36 <sup>+.65</sup> <sub>-.90</sub> |
| 3.0                 | 8.07 <sup>+.15</sup> <sub>-.75</sub>                    | 8.77 <sup>+.15</sup> <sub>-.65</sub> | 9.39 <sup>+.20</sup> <sub>-.50</sub>  | 9.95 <sup>+.20</sup> <sub>-.45</sub>  |
| 6.0                 | 7.61 <sup>+.10</sup> <sub>-.75</sub>                    | 8.25 <sup>+.15</sup> <sub>-.60</sub> | 8.79 <sup>+.15</sup> <sub>-.45</sub>  | 9.23 <sup>+.10</sup> <sub>-.35</sub>  |
| 12.0                | 7.01 <sup>+.10</sup> <sub>-.80</sub>                    | 7.64 <sup>+.10</sup> <sub>-.65</sub> | 8.16 <sup>+.10</sup> <sub>-.45</sub>  | 8.58 <sup>+.10</sup> <sub>-.35</sub>  |

TABLE 6

Ratio of Signal Produced at Detector By Source Spectra of Different Slope With Equal  $F_\nu$  @  $\bar{\nu}$  - Relative to a  $F_\nu \propto \nu^2$  Spectrum -

$$\equiv [\int F_\nu \alpha T(\nu) d\nu][F_{\nu 2}(\bar{\nu}_{\nu 2})] / [\int F_{\nu 2} T(\nu) d\nu][F_{\nu \alpha}(\bar{\nu}_{\nu \alpha})]$$

| mm H <sub>2</sub> O | Spectral Index, $\alpha$ , for $F_\nu \propto \nu^\alpha$ |           |      |           |
|---------------------|---|-----------|------|-----------|
|                     | 0   | 1         | 2    | 3         |
| 1.5                 | 0.75±0.02   | 0.83±0.01 | 1.00 | 1.33±0.06 |
| 3.0                 | 0.80±0.05   | 0.87±0.03 | 1.00 | 1.19±0.03 |
| 6.0                 | 0.81±0.05   | 0.88±0.04 | 1.00 | 1.16±0.05 |
| 12.0                | 0.81±0.06   | 0.88±0.05 | 1.00 | 1.15±0.07 |

water vapor content from the theoretical extinction coefficients calculated by the computer program in the Appendix and shown in Figure 8<sup>1</sup>. In addition, a device is available<sup>2</sup> which compares the flux from the sun at two nearby wavelengths in the near infrared. One wavelength is situated in the center of a water absorption line and the other in the nearby continuum. This provides a rough independent measure of the total precipitable water vapor in the line of sight to the sun. The frequency dependence of the flux density, as noted before, must be estimated on the basis of data at other wavelengths.

---

<sup>1</sup>These calculated opacities vs. water vapor are in reasonable agreement with the values measured by Low (1966a)

<sup>2</sup>Constructed by J. Westphal.

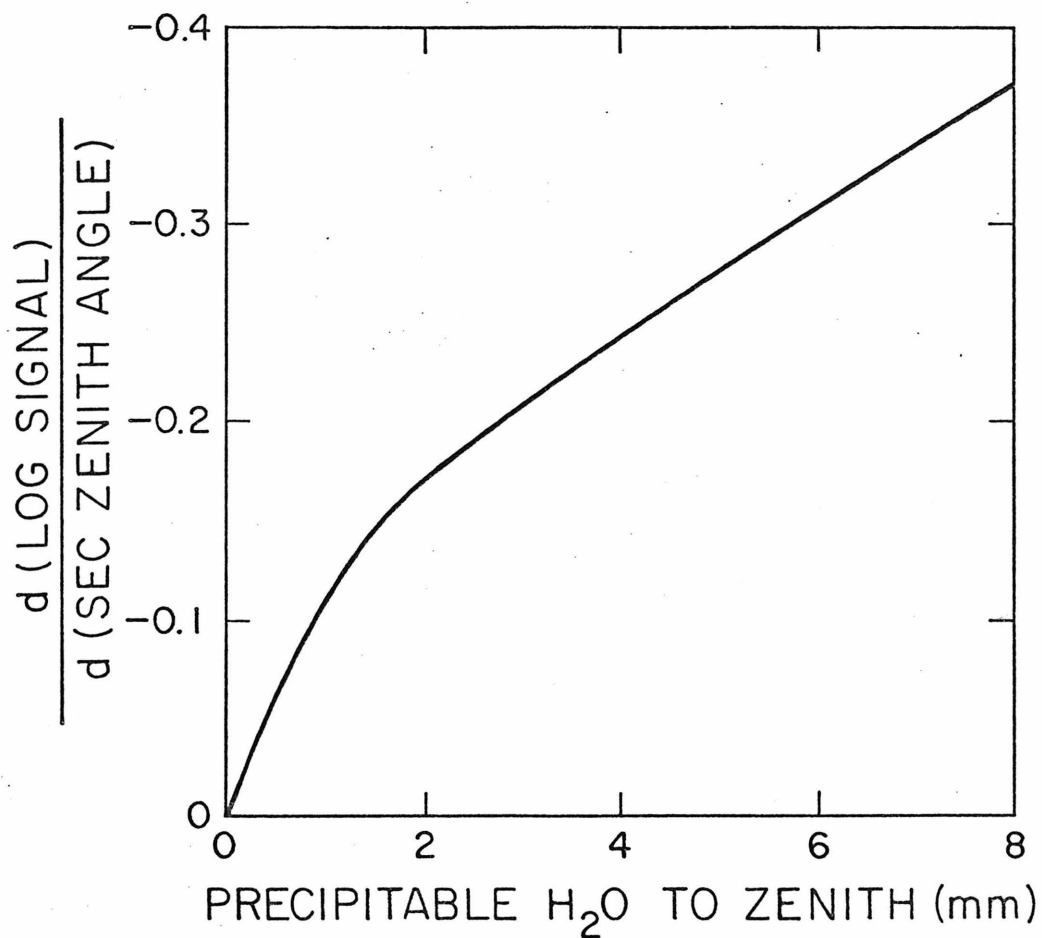


Fig. 8 - The predicted logarithmic decrease in signal from zenith angle =  $0^\circ$  to zenith angle =  $60^\circ$  is shown as a function of the precipitable water vapor in a line of sight to the zenith.

## V. SAMPLE OBSERVATIONS

As an example of the calibration procedure, measurements of two sources will be discussed, the H II region W 51 and the quasar 3C273. The observations of each and their calibration sources are summarized in Table 7.

A. W 51 -- Component G49.5-0.4

This H II region has been observed at a variety of radio frequencies and with a variety of spatial resolutions. It is composed of a diffuse component several arcminutes in extent and several compact regions less than one arcminute in size (Martin 1972, and references therein). On November 13, 1972, six regions of the component G49.5-0.4 of W 51 were measured at 1 mm along with Jupiter at two elevation angles; on March 30, 1973, several more regions were observed along with the Moon and Jupiter. Only the peak brightness measurements will be discussed here. The relative sizes of the signals from the observed regions of W 51 indicate that the emission arises from an area several arcminutes in extent. Therefore, at the peak position the source fills the 1.7 arcminute beam of the system. For this reason and because of possible cancellation of part of the signal due to the finite extent of the chopping, the observed signal represents a lower limit to the total flux from this area of W 51.

In Table 8 the calibration of the W 51 observations is summarized. The atmospheric extinction coefficients were determined from the observations of the calibration sources and were used to determine the ratios of the fluxes at equal zenith angles. The spectrum of this component

TABLE 7 - OBSERVATIONS

| Object  | Date         | Sidereal Time | Sec Z | Relative Signal* |
|---------|--------------|---------------|-------|------------------|
| Jupiter | Nov 13, 1972 | 1840          | 1.82  | 161              |
| W 51    | "            | 1930          | 1.05  | 4.6±.45          |
| Jupiter | "            | 2125          | 2.94  | 118              |
| Jupiter | Mar 30, 1973 | 1730          | 2.78  | 124              |
| Moon    | "            | 1750          | 2.76  | 1288             |
| Jupiter | "            | 1840          | 1.96  | 192              |
| Moon    | "            | 1845          | 2.03  | 1787             |
| Jupiter | "            | 2010          | 1.65  | 210              |
| Moon    | "            | 2015          | 1.50  | 2181             |
| W 51    | "            | 2030          | 1.10  | 7.16±.26         |
| Jupiter | "            | 2120          | 1.68  | 237              |
| Moon    | "            | 2125          | 1.42  | 2611             |
| Venus   | Nov 15, 1972 | 0955          | 2.03  | 43.0             |
| Saturn  | "            | 1005          | 2.30  | 40.9             |
| 3C273   | "            | 1155          | 1.21  | 0.84±.16         |
| Venus   | "            | 1225          | 1.32  | 50.5             |
| 3C273   | Feb 9, 1973  | 1620          | 2.30  | 2.07±.23         |
| Jupiter | "            | 1730          | 2.21  | 71.2             |
| Jupiter | "            | 1840          | 1.84  | 96.1             |

\*Equal units on all dates

TABLE 8

## Calibration of W 51 Observations

|  | <u>Nov 13, 1972</u>  | <u>Mar 30, 1973</u>   |
|--|--|---|
| Log extinction per<br>air mass                                   | -0.12±.04  | -0.23±.03   |
| Sig(W 51)/Sig(Jupiter)<br>@ equal zenith angle                   | 2.29 x 10 <sup>-2</sup>  | 2.37 x 10 <sup>-2</sup>   |
| ∫ H <sub>2</sub> O from near IR<br>calibration                   | 3.0±1.5 mm   | 4.2±1.5 mm  |
| ∫ H <sub>2</sub> O from change in<br>signal with zenith<br>angle | 2.0±1.0 mm   | 4.4±1.0 mm  |
| ∫ H <sub>2</sub> O at zenith angle<br>of W 51 (assumed)          | 3.0 mm   | 4.7 mm  |
| $\bar{\nu}$ - W 51   | 9.4±0.5 cm <sup>-1</sup>   | 9.1±0.5 cm <sup>-1</sup>  |
| F <sub>ν</sub> ( $\bar{\nu}$ ) - Jupiter                         | 6190 x 10 <sup>-26</sup> Wm <sup>-2</sup> Hz <sup>-1</sup>             | 6480 x 10 <sup>-26</sup> Wm <sup>-2</sup> Hz <sup>-1</sup>            |
| Beam efficiency<br>(Figure 7)                                    | 0.97   | 0.97  |
| Spectral Shape Correc-<br>tion (Table 6)                         | 1.00   | 1.00  |
| F <sub>ν</sub> - W 51 @ $\bar{\lambda}$                          | 137 x 10 <sup>-26</sup> Wm <sup>-2</sup> Hz <sup>-1</sup><br>@ 1.06 mm | 150 x 10 <sup>-26</sup> Wm <sup>-2</sup> Hz <sup>-1</sup><br>@ 1.1 mm |
|  | ±14 (statistics)<br>±35 (calibration)                                  | ±6 (statistics)<br>±35 (calibration)                                  |

of W 51 follows roughly a  $\nu^{-0.1}$  dependence between 9.5 and 60 mm wavelength, but between 9 mm and 100 $\mu$  the flux rises by several orders of magnitude (Hoffmann et al. 1971). Therefore, a spectrum proportional to  $\nu^2$  was adopted. From Table 5 and the estimated precipitable water vapor, this spectral shape implies the effective frequencies given in Table 8. The assumed brightness temperature of Jupiter and its calculated flux density on each date lead to the derived fluxes for W 51 also given in Table 8. These determinations are reasonably consistent with a  $\nu^2$  dependence of the flux between 1mm and 100 $\mu$ . The errors quoted are: (1) a statistical error, and (2) an absolute calibration error which has been taken as  $\sigma = (\sigma_1^2 + \sigma_2^2 + \sigma_3^2)^{1/2}$  where

$\sigma_1 = \pm 10$  percent error in assumed temperature for Jupiter

$\sigma_2 = \pm 15$  percent error from insufficient knowledge of filter properties

$\sigma_3 = \pm 15$  percent error from insufficient knowledge of water vapor and spectral dependence of flux

### B. 3C273

This is the brightest optical and millimeter wavelength quasar and is effectively a point source. It was observed with the 1 mm system on November 15, 1972, and on February 9, 1973, with derived fluxes which differ by a factor of three. Both measurements will be discussed here, but a detailed discussion of possible reasons for the difference between the two measurements will not be given. In Table 9 the calibration of the 3C273 observations is summarized. The spectrum of 3C273 at millimeter wavelengths follows roughly a  $\nu^0$  dependence (Kellermann 1972)

TABLE 9  
Calibration of 3C273 Observations

|  | <u>Nov 15, 1972</u>  | <u>Feb 9, 1973</u>   |
|--|--|--|
| Log extinction per air mass                                | -0.10±.04  | -0.35±.10  |
| Sig(3C273)/Sig(Planet) @ equal zenith angle                | 1.64 x 10 <sup>-2</sup> for Venus                                    | 2.90 x 10 <sup>-2</sup> for Jupiter                                    |
| ∫ H <sub>2</sub> O from near IR calibration                | 3.0±1.5 mm   | no measurement   |
| ∫ H <sub>2</sub> O from change in signal with zenith angle | 1.8±1.0 mm   | 7.5±4 mm   |
| ∫ H <sub>2</sub> O at zenith angle of 3C273 (assumed)      | 2.5 mm   | 17 mm  |
| $\bar{\nu}$ - 3C273  | 8.2±0.3 cm <sup>-1</sup>   | 6.7±0.6 cm <sup>-1</sup>   |
| $\bar{\nu}$ - Planets                                      | 9.5±0.5 cm <sup>-1</sup>   | 7.9±0.4 cm <sup>-1</sup>   |
| F <sub>ν</sub> ( $\bar{\nu}$ ) - Planet                    | 2267 x 10 <sup>-26</sup> Wm <sup>-2</sup> Hz <sup>-1</sup> for Venus | 4061 x 10 <sup>-26</sup> Wm <sup>-2</sup> Hz <sup>-1</sup> for Jupiter |
| Beam Efficiency (Figure 7)                                 | 1.00   | 0.97   |
| Spectral Shape Correction (Table 6)                        | 0.80   | 0.81   |
| F <sub>ν</sub> ( $\bar{\nu}$ ) - 3C273 @ $\bar{\lambda}$   | 30 x 10 <sup>-26</sup> Wm <sup>-2</sup> Hz <sup>-1</sup> @ 1.2 mm    | 93 x 10 <sup>-26</sup> Wm <sup>-2</sup> Hz <sup>-1</sup> @ 1.5 mm      |
|  | ±6 (statistics)<br>±8 (calibration)                                  | ±10 (statistics)<br>±23 (calibration)                                  |

with  $F_{\nu} \approx 30$  to  $50 \times 10^{-26} \text{ Wm}^{-2}\text{Hz}^{-1}$ , and this dependence has been assumed at 1 mm. The appropriate weighted average frequencies and derived fluxes are given in Table 9 with errors determined as for W 51. The assumed spectral dependence of  $\nu^0$  is roughly consistent with the derived 1 mm fluxes. Barring gross mistakes in the measurements, the derived fluxes on the two dates differ by considerably more than the possible uncertainties in the calibration and are very tentative evidence for 1 mm variability of 3C273.

## APPENDIX

## CALCULATION OF THE ATMOSPHERIC TRANSMISSION

Three assumptions are made in calculating the atmospheric transmission: (1) that the only significant contribution to the opacity is from water vapor, (2) that Burch's (1957) empirically determined expressions for water vapor opacity are valid, and (3) that the atmosphere can be reasonably well represented by a plane-parallel homogeneous layer, one scale height in thickness.

The first assumption is justified from many published spectra of the sun (Harries and Ade 1972, and references therein), although there is some debate about the presence of the water dimer,  $(\text{H}_2\text{O})_2$  (Harries and Ade 1972). The next most conspicuous molecule in far infrared atmospheric spectra is  $\text{O}_2$ . Although its effects are quantitatively insignificant, several of the  $\text{O}_2$  lines have been included in the computer program described here since they appear in published spectra. Atmospheric homogeneity is assumed for simplicity; it is the only reasonable first order approximation.

According to Burch (1957) the major problem in calculating the water vapor absorption between  $300\mu$  and several millimeters wavelength is that of determining the absorption coefficient in the wings of strong lines since that part of the absorption coefficient determines the absorption in the atmospheric windows. The measured absorption coefficient as a function of frequency,  $K(\nu)$ , in the windows cannot be fit by any simple expression for the line shapes. Therefore, Burch has developed an expression for  $K(\nu)$  that includes a slowly varying continuous absorp-

tion coefficient, empirically determined, which is added to the analytic expression for the line contributions. The agreement between this empirical formula and his own and other published measurements of  $K(\nu)$  at various frequencies is quite good. Additionally, the author has compared the predicted  $K(\nu)$  of the program described here to the more recent published atmospheric spectra of Harries and Ade (1972), Mather et al. (1972) and Nolt et al. (1971) and has found good agreement between the predicted and observed spectra. Therefore, it seems reasonable to use Burch's expressions as a basis for a computer program which calculates the atmospheric transmission.

In addition to computing the atmospheric transmission as a function of frequency,  $T_a(\nu)$ ; the product of the atmospheric and filter transmissions,  $T_a(\nu)T_f(\nu) = T(\nu)$ ; and the product of these with a power law spectrum,  $T_a(\nu)T_f(\nu)F_0\nu^\alpha$ , normalized to  $F_\nu(\lambda=1 \text{ mm}) = 10^{-24} \text{ Wm}^{-2}\text{Hz}^{-1}$ ; the program also computes several integral quantities related to the observed power received by the detecting system. These are:

- (1)  $[\int_0^\infty \nu T(\nu)\nu^\alpha d\nu]/[\int_0^\infty T(\nu)\nu^\alpha d\nu] \quad \equiv \text{weighted average frequency}$
- (2)  $[\int_0^\infty F_0 \nu^\alpha T(\nu) d\nu]/[\int_0^\infty T(\nu) d\nu] \quad \equiv \text{weighted average flux}$
- (3)  $\int_0^\infty F_0 \nu^\alpha T(\nu) d\nu \quad \equiv \text{integrated flux}$
- (4)  $[\int_0^\infty T^2(\nu)\nu^\alpha d\nu]/[\int_0^\infty T(\nu)\nu^\alpha d\nu] \quad \equiv \text{weighted average transmission}$
- (5)  $[\int_0^\infty T(\nu)\nu^\alpha d\nu]/[\int_0^\infty \nu^\alpha d\nu] \quad \equiv \text{straight average transmission}$
- (6)  $[\int_0^\infty T(\nu)T_a(\nu)\nu^\alpha d\nu]/[\int_0^\infty T(\nu)\nu^\alpha d\nu] \quad \equiv \text{weighted average atmospheric transmission}$
- (7)  $\int_{\nu_1}^{\nu_2} F_0 \nu^\alpha T(\nu) d\nu \quad \equiv \text{integrated flux in six atmospheric windows.}$

A copy of the program and a sample of its output are shown on the following pages.

## ATMOSPHERIC TRANSMISSION PROGRAM

```

REAL NU1,NU2,NUKCC,INCR,NU,INDEX,KCINT,KC,KCC
DIMENSION KCC(21),NUKCC(21),TL(6),SI(65),SIC(65),FR(65),S(65,6),
INEXP(6),ALFA(65,6),A(65),AC(65),FL(65),TRANS(900),TFLUX(900),
2X(900),IDATX(900),IDATY(900),SC(4),ALF(65,6),NS(900),AR(900),
3FM(6),FP(6),CXNU(9),OXS(9),FFILT(50),TFILT(50),SF(6)
DATA FM/C.0,6.0,12.0,15.0,19.0,25.0/,FP/6.0,12.0,15.0,19.0,25.0/,
1 33.0/
C   FREQUENCY OF OXYGEN LINES
DATA CXNL/3.8,12.29,14.17,16.25,23.8,25.81,27.82,35.39,37.38/
C   STRENGTH OF OXYGEN LINES
DATA CXS/.7,.62,5.7,2.1,1.5,8.7,2.9,1.8,9.5/
C   STRENGTH AND FREQUENCY OF FAKE CONTINUOUS ABSORPTION COEFFICIENTS
DATA KCC/.008,.029,.076,.18,.31,.43,.60,.79,1.1,1.5,2.7,3.5,4.4,
1 5.2,5.8,6.6,7.6,8.6,9.6,10.8/, NUKCC/1.,2.,3.,4.,5.,6.,8.,10.,
2 12.,14.,16.,18.,20.,22.,24.,26.,28.,30.,32.,34.,36./
DATA TL/20.,300.,280.,260.,240.,220./, PI/3.14159/
NFILT=C
N LINES=34
C   READ PARAMETERS OF WATER LINES
DO 20 I=1,N LINES
100  READ (5,100) FL(I),((S(I,JT),NEXP(JT)),JT=1,6)
    FORMAT (F5.2,9X,6(F4.2,12,4X))
    DC 10 JT=1,6
10  S(I,JT)=S(I,JT)*10.**(NEXP(JT))
101  FORMAT (14X,6(F5.3,5X))
20  READ (5,101) (ALFA(I,JT),JT=1,6)
102  FORMAT (F4.0,2X,F4.2,1X,F4.1,1X,F4.2,1X,F4.1,1X,F4.1,1X,F4.1,1X,
1 F4.2,1X,F4.2,3X,12)
C   READ ATMOSPHERIC CONDITIONS FOR DESIRED SPECTRUM
24  READ (5,102) TAIR,PAIR,PRWTR,HUM,INDEX,NU1,NU2,INCR,SCALE,IFILT
    IF (TAIR.EQ.0.) STOP
    IF (IFILT.NE.0) GO TO 25
103  FORMAT (F5.2,F5.3)
C   READ TRANSMISSION OF SYSTEM FILTERS
    READ (5,103) ((FFILT(I),TFILT(I)),I=1,IFILT)
    NFILT=IFILT
C   FINDS WHICH TEMP TO INTERPOLATE BETWEEN
25  DO 26 I=1,6
    IF (TAIR.GE.TL(I)) GO TO 28
26  CONTINUE
26  NF=I-1
    NI=I
C   FINDS VAPOR PRESSURE OF WATER IN UNITS OF ATMOSPHERES FROM
    APPROXIMATE ANALYTIC RELATIONS FROM "ASTROPHYS QUANT"
C   IF (HUM.LE.0.5) DEWPT=TAIR-3.5-20.*(0.8-HUM)
    IF (HUM.LE.0.5) DEWPT=TAIR-9.5-2.**((0.5-HUM)*12.)
    VAPRS=10./2.**((285.-DEWPT)/9.)
    PSWTR=VAPRS/(PAIR*760.)
C   CPAIR=EFFECTIVE LINE-BROADENING PRESSURE BY AIR
    CPAIR=C.02*PAIR
C   PCONT=EFFECTIVE LINE BROADENING PRESSURE FOR FAKE CONTINUUM ABS
    PCONT=13.*PSWTR+CPAIR
C   PLINE=EFFECTIVE LINE-BROADENING PRESSURE FOR LINES
    PLINE=5.0*PSWTR+CPAIR
    DO 32 I=1,N LINES
    DO 30 JT=1,6

```

```

30 ALF(I,JT)=ALFA(I,JT)*PLINE
32 CONTINUE
DEL=(TAIR-TL(NI))/20.
DELC=C.8
DC 34 I=1,6
34 SF(I)=C.C
C INTERPOLATES LINE STRENGTHS AND BROADENINGS FOR TEMP DESIRED, AND
C FOR 296K FOR COMPUTATION OF TEMP DEPENDENCE OF CONTINUUM ABS
DC 36 I=1,NLINES
SI(I)=S(I,NI)+DEL*(S(I,NF)-S(I,NI))
A(I)=ALF(I,NI)+DEL*(ALF(I,NF)-ALF(I,NI))
SIC(I)=S(I,3)+DELC*(S(I,2)-S(I,3))
36 AC(I)=ALF(I,3)+DELC*(ALF(I,2)-ALF(I,3))
PRINT 110, TAIR, PAIR, HUM, PRWTR, NU1, NU2, INCR, INDEX
110 FORMAT ('ATMOSPHERIC TRANSMISSION FOR // TEMPERATURE= ',F4.0,
1 ' K // PRESSURE= ',4X,F4.2// ' REL HUMIDITY= ',F4.2// ' PRC WATER=
2 ',F4.1// ' FREQUENCY RANGE= ',F5.2, ' CM**-1 TO ',F5.2, ' CM**-1 //
3 ' FREQUENCY INCREMENT= ',F3.2, ' CM**-1 // // ' NU**',F4.1, ' SPECTRAL
4 INDEX OF INCIDENT RADIATION')
PRINT 105
105 FORMAT ('TRANSMISSION OF FILTERS--NU/T //')
IF(NFILT.EQ.C) GO TO 38
106 FORMAT ( 8(F6.2,1X,F5.3,4X))
PRINT 106, ((FFILT(I),TFILT(I)), I=1,NFILT)
GO TO 40
38 PRINT 107
107 FORMAT ('100 PERCENT TRANSMISSION AT ALL NU')
40 SUMF=C.
SUMTF=C.
SUMTTF=C.
SUMNTF=C.
SUMATF=C.
F=NU1
PRWTR=PRWTR/10.
J=1
120 FORMAT ('HI, 'NU(CM-1) K CONTINUUM',7X,'K LINE',6X,'FM FLUX',3X,
1 'TR FLUX',3X,'LOG TR',5X,'TRANS',4X,'LAMDA',6X,'ATM TRANS')
PRINT 120
42 SUMK=C.
SUMKC=C.
C SUM OF CONTRIBUTIONS OF LINES AT FREQUENCY-F-
DO 46 I=1,NLINES
D1=(F-FL(I))**2
D2=(F+FL(I))**2
SUMK=SUMK+SI(I)*A(I)*(1./(D1+A(I)**2)+1./(D2+A(I)**2))/FL(I)**2
46 SUMKC=SUMKC+SIC(I)*AC(I)*(1./(D1+AC(I)**2)+1./(D2+AC(I)**2))/FL(I)
I**2
C INTERPOLATES CONTINUOUS ABSORPTION FOR FREQUENCY-F-
DO 50 I=1,21
IF (F.LE.NUKCC(I)) GO TO 52
50 CONTINUE
52 L=I-1
KCINT=KCC(L)+(F-NUKCC(L))*(KCC(I)-KCC(L))/(NUKCC(I)-NUKCC(L))
C CONTINUOUS ABSORPTION AT DESIRED TEMPERATURE
KC=KCINT*SUMK/SUMKC
X(J)=F

```

```

NS(J)=20
NR(J)=6
-----
AL=10000./F
T1=KC*PCNT
T2=(F**2)*SUMK/PI
T5=0.
C OXYGEN LINES
DO 54 I=1,9
54 T5=T5+CXS(I)/((F-0XNU(I))**2+.048**2)
T5=T5*.048*.8*PAIR/PI
T4=1.
-----
IF (NFILT.EQ.0) GO TO 64
INTERPOLATES FILTER TRANSMISSION AT FREQUENCY-F-
DO 60 I=1,NFILT
IF (F.LE.FFILT(I)) GO TO 62
60 CONTINUE
62 L=L-1
-----
T4=TFILT(L)+(F-FFILT(L))*(TFILT(L)-TFILT(L))/(FFILT(L)-FFILT(L))
64 T6=PRWTR*(T1+T2)*(-0.434)-T5
IF (T4.LE.0.) T4=0.0000001
TRANS(J)=T6+ALOG10(T4)
IF (T6.LT.-20.) T6=-20.
T6=10.**T6
IF (TRANS(J).LT.-20.) TRANS(J)=-20.
FLUX=100.*((F/10.)**INDEX)
T3=TRANS(J)
-----
TRANS(J)=10.**TRANS(J)
TFLUX(J)=FLUX*TRANS(J)
121 FORMAT (2H ,F5.2,3X,1PE12.3,3X,E12.3,3X,0PF7.1,3X,F7.1,3X,F7.2,3X
1 ,F7.5,3X,F5.0,8X,F7.5)
PRINT 121, F,T1,T2,FLUX,TFLUX(J),T3,TRANS(J),AL,T6
SUMF=SUMF+FLUX
SUMTF=SUMTF+TFLUX(J)
SUMTTF=SUMTTF+TFLUX(J)*TRANS(J)
SUMNTF=SUMNTF+F*TFLUX(J)
SUMATF=SUMATF+T6*TFLUX(J)
DO 66 I=1,6
66 IF (F.GT.FM(I).AND.F.LE.FP(I)) SF(I)=SF(I)+TFLUX(J)
F=F+INCR
IF (F.GT.NU2) GO TO 70
J=J+1
GO TO 42
70 AJ=J
AVTRNS=SUMTTF/SUMTF
AVTRS=SUMTF/SUMF
AVNU=SUMATF/SUMTF
AVATR=SUMATF/SUMTF
SUMF1=SUMTF/AJ
SUMF2=SUMTF*INCR*3./100.
PRWTR=PRWTR*10.
FDVIF=100.*((AVNU/10.)**INDEX)/SUMF2
PRINT 114, AVNU,SUMF1,SUMF2,AVTRNS,AVTRS,AVATR,FDVIF
114 FORMAT (10WEIGHTED AVERAGE FREQUENCY= ',F5.2,' CM**-'// ' AVERAGE
IFNU= ',F6.2,' F.U.'// ' INTEGRATED FLUX= ',F8.2,' IN UNITS OF 10**-'
214 W/M**2'// ' WEIGHTED AVERAGE TRANS= ',F5.3, '// ' STRAIGHT AVERAGE
3 TRANS= ',F5.3// ' WEIGHTED AVERAGE ATMOSPHERIC TRANS= ',F5.3//

```

```

4 * FNU(NUBAR)/INTEGRAL OF FNU= ',F6.2//' ')
DC 74 I=1,6
74 SF(I)=SF(I)*INCR*3./100.
PRINT 115,((FM(I),FP(I),SF(I)), I=1,6)
115 FORMAT ('INTEGRATED FLUXES IN ATMOSPHERIC WINDOWS IN UNITS OF 10*
1*-14 W/M**2',//,6(1H ,F4.1,' TO ',F4.1,' CM**-1',5X,F8.2,/)
PRINT 111
111 FORMAT ('PLOT OF TRANSMISSION VS FREQ (CM**-1)')
SC(2)=1.C/12.C
SC(4)=C.C
SC(1)=SCALE
I=NU1
YI=I
SC(2)=YI
I=NU2+1.
Y2=I
PX=(Y2-YI)/SCALE
CALL DGPLT (X,TRANS,J,NS,PX,10.0,1,SC,1DATX,1DATY,FR)
112 FORMAT (' DGPLT ERROR MESSAGE = ',F3.0)
IF (ER.LE.0.) PRINT 112,FR
PRINT 112
113 FORMAT ('PLOT OF TRANSMITTED FNU VS FREQ (CM**-1)')
SC(3)=0.C
SC(4)=C.C
CALL DGPLT (X,TFLUX,J,NR,PX,10.0,1,SC,1DATX,1DATY,FR)
IF (ER.LE.0.) PRINT 112,FR
GC TO 24
END

```

SAMPLE OUTPUT

ATMOSPHERIC TRANSMISSION FOR

TEMPERATURE= 275. K  
PRESSURE= 0.85  
REL HUMIDITY= 0.50

PREC WATER= 5.0

FREQUENCY RANGE= 3.00 CM\*\*1 TO 34.00 CM\*\*1  
FREQUENCY INCREMENT= .40 CM\*\*1

NUM\* 2.0 SPECTRAL INDEX OF INCIDENT RADIATION

TRANSMISSION OF FILTERS--NU/T

|             |             |             |            |            |            |             |             |
|-------------|-------------|-------------|------------|------------|------------|-------------|-------------|
| 2.00 0.020  | 3.00 0.170  | 4.00 0.350  | 5.00 0.520 | 6.00 0.780 | 8.00 0.950 | 10.00 1.000 | 15.00 0.780 |
| 20.00 0.282 | 25.00 0.628 | 30.00 0.005 | 35.00 0.0  | 40.00 0.0  |            |             |             |

CONTRIBUTION CONTRIBUTION  
FROM "FAKE" FROM  
CONTINUUM LINES (microns) T OF  
ATMOSPHERE

| $\nu$ | NU(CH-1) K CONTINUUM | K LINE    | EM FLUX | IR FLUX | LOG T  | T       | $\lambda$ | AIM IRANS |
|-------|----------------------|-----------|---------|---------|--------|---------|-----------|-----------|
| 3.00  | 7.598E-02            | 2.149E-02 | 9.0     | 1.4     | -0.80  | C.15738 | 3333.     | C.92575   |
| 3.40  | 1.179E-01            | 2.828E-02 | 11.6    | 2.3     | -0.69  | C.20239 | 2941.     | 0.83633   |
| 3.80  | 1.597E-01            | 3.704E-02 | 14.4    | 0.0     | -3.70  | C.00020 | 2632.     | 0.00063   |
| 4.20  | 2.067E-01            | 4.899E-02 | 17.6    | 5.4     | -0.52  | C.30396 | 2381.     | C.79156   |
| 4.60  | 2.586E-01            | 6.665E-02 | 21.2    | 7.9     | -0.43  | C.37318 | 2174.     | 0.82562   |
| 5.00  | 3.098E-01            | 9.511E-02 | 25.0    | 10.4    | -0.38  | C.41765 | 2000.     | 0.80218   |
| 5.40  | 3.557E-01            | 1.865E-01 | 29.2    | 13.7    | -0.33  | C.47114 | 1852.     | C.75503   |
| 5.80  | 3.991E-01            | 7.561E-01 | 33.6    | 13.6    | -0.39  | C.40548 | 1724.     | 0.55698   |
| 6.20  | 4.239E-01            | 5.493E 00 | 38.4    | 1.6     | -1.39  | C.04115 | 1613.     | 0.05163   |
| 6.60  | 4.760E-01            | 4.782E-01 | 43.6    | 22.3    | -0.29  | C.51245 | 1515.     | 0.61667   |
| 7.00  | 5.140E-01            | 2.616E-01 | 49.0    | 28.6    | -0.23  | C.58325 | 1429.     | 0.67428   |
| 7.40  | 5.526E-01            | 2.266E-01 | 54.8    | 33.2    | -0.22  | C.60560 | 1351.     | 0.67364   |
| 7.80  | 5.861E-01            | 2.308E-01 | 60.8    | 37.5    | -0.21  | C.61592 | 1282.     | C.66015   |
| 8.20  | 6.228E-01            | 2.519E-01 | 67.2    | 41.2    | -0.21  | C.61213 | 1220.     | 0.64098   |
| 8.60  | 6.610E-01            | 2.850E-01 | 74.0    | 46.1    | -0.22  | C.59646 | 1163.     | 0.61809   |
| 9.00  | 6.983E-01            | 3.205E-01 | 81.0    | 46.8    | -0.24  | C.57760 | 1111.     | 0.59241   |
| 9.40  | 7.345E-01            | 3.591E-01 | 88.4    | 49.0    | -0.26  | C.55466 | 1064.     | C.56311   |
| 9.80  | 7.681E-01            | 4.875E-01 | 96.0    | 50.4    | -0.28  | C.52457 | 1020.     | C.52721   |
| 10.20 | 8.065E-01            | 6.775E-01 | 104.0   | 48.4    | -0.33  | C.46485 | 980.      | 0.46898   |
| 10.60 | 8.250E-01            | 1.775E 00 | 112.4   | 29.3    | -0.58  | C.26047 | 943.      | 0.26753   |
| 11.00 | 8.724E-01            | 3.659E 00 | 121.0   | 11.7    | -1.01  | C.09677 | 909.      | 0.10122   |
| 11.40 | 9.839E-01            | 1.249E 00 | 130.0   | 36.5    | -0.55  | C.28084 | 877.      | 0.29927   |
| 11.80 | 1.048E 00            | 1.771E 00 | 139.2   | 28.6    | -0.69  | C.25571 | 847.      | 0.22340   |
| 12.20 | 1.103E 00            | 4.069E 00 | 148.8   | 2.3     | -1.80  | C.31576 | 820.      | 0.01745   |
| 12.60 | 1.119E 00            | 6.143E 01 | 158.8   | 0.0     | -13.72 | C.00060 | 794.      | 0.00000   |
| 13.00 | 1.248E 00            | 8.554E 00 | 169.0   | 0.8     | -2.34  | C.00454 | 769.      | 0.00523   |
| 13.40 | 1.354E 00            | 3.454E 00 | 179.6   | 10.8    | -1.22  | C.05993 | 746.      | 0.07047   |
| 13.80 | 1.442E 01            | 3.104E 00 | 190.4   | 6.0     | -1.50  | C.03170 | 725.      | C.03806   |
| 14.20 | 1.577E 00            | 4.073E 00 | 201.6   | 0.0     | -19.81 | C.00000 | 704.      | 0.00000   |
| 14.60 | 1.574E 00            | 1.654E 01 | 213.2   | 0.0     | -4.36  | C.00004 | 685.      | 0.00000   |
| 15.00 | 1.856E 00            | 6.568E 01 | 225.0   | 0.0     | -14.87 | C.00000 | 667.      | 0.00000   |
| 15.40 | 2.277E 00            | 8.409E 00 | 237.2   | 0.7     | -2.54  | C.00288 | 649.      | 0.00389   |
| 15.80 | 2.331E 00            | 1.023E 01 | 246.6   | 0.0     | -4.31  | C.00005 | 633.      | 0.00007   |
| 16.20 | 2.739E 00            | 1.146E 01 | 262.4   | 0.0     | -7.92  | C.00000 | 617.      | C.00000   |
| 16.60 | 3.005E 00            | 1.426E 01 | 275.6   | 0.0     | -4.14  | C.00007 | 602.      | C.00012   |
| 17.00 | 3.189E 00            | 2.237E 01 | 285.0   | 0.0     | -5.83  | C.00000 | 588.      | C.00000   |
| 17.40 | 3.362E 00            | 4.063E 01 | 302.8   | 0.0     | -9.90  | C.00000 | 575.      | 0.00000   |
| 17.80 | 3.528E 00            | 5.590E 01 | 316.8   | 0.0     | -20.00 | C.00000 | 562.      | 0.00000   |
| 18.20 | 3.690E 00            | 4.007E 02 | 331.2   | 0.0     | -20.00 | C.00000 | 549.      | 0.00000   |

|       |           |           |        |     |        |         |      |         |
|-------|-----------|-----------|--------|-----|--------|---------|------|---------|
| 18.60 | 3.555E 00 | 6.540E 03 | 346.0  | 0.0 | -20.00 | 0.00000 | 539. | 0.00000 |
| 19.00 | 4.064E 00 | 3.617E 02 | 361.0  | 0.0 | -20.00 | 0.00000 | 526. | 0.00000 |
| 19.40 | 4.265E 00 | 1.337E 02 | 376.4  | 0.0 | -20.00 | 0.00000 | 515. | 0.00000 |
| 19.80 | 4.440E 00 | 5.035E 01 | 392.0  | 0.0 | -12.42 | 0.00000 | 505. | 0.00000 |
| 20.20 | 4.581E 00 | 3.174E 01 | 408.0  | 0.0 | -8.46  | 0.00000 | 495. | 0.00000 |
| 20.60 | 4.287E 00 | 4.403E 01 | 424.4  | 0.0 | -11.09 | 0.00000 | 485. | 0.00000 |
| 21.00 | 4.737E 00 | 2.068E 01 | 441.0  | 0.0 | -6.16  | 0.00000 | 476. | 0.00000 |
| 21.40 | 5.024E 00 | 1.443E 01 | 458.0  | 0.0 | -4.91  | 0.00001 | 467. | 0.00006 |
| 21.80 | 5.031E 00 | 1.301E 01 | 475.2  | 0.0 | -4.65  | 0.00002 | 459. | 0.00012 |
| 22.20 | 5.255E 00 | 1.206E 01 | 492.8  | 0.0 | -4.54  | 0.00003 | 450. | 0.00017 |
| 22.60 | 5.465E 00 | 1.212E 01 | 510.8  | 0.0 | -4.66  | 0.00002 | 442. | 0.00014 |
| 23.00 | 5.598E 00 | 1.269E 01 | 529.0  | 0.0 | -5.11  | 0.00001 | 435. | 0.00006 |
| 23.40 | 5.717E 00 | 1.745E 01 | 547.6  | 0.0 | -6.10  | 0.00000 | 427. | 0.00001 |
| 23.80 | 5.834E 00 | 2.614E 01 | 566.4  | 0.0 | -14.78 | 0.00000 | 420. | 0.00000 |
| 24.20 | 5.971E 00 | 5.015E 01 | 585.6  | 0.0 | -13.48 | 0.00000 | 413. | 0.00000 |
| 24.60 | 6.119E 00 | 1.556E 02 | 605.2  | 0.0 | -20.00 | 0.00000 | 407. | 0.00000 |
| 25.00 | 6.001E 00 | 2.432E 03 | 625.0  | 0.0 | -20.00 | 0.00000 | 400. | 0.00000 |
| 25.40 | 6.416E 00 | 3.888E 02 | 645.2  | 0.0 | -20.00 | 0.00000 | 394. | 0.00000 |
| 25.80 | 6.615E 00 | 8.485E 01 | 665.6  | 0.0 | -20.00 | 0.00000 | 388. | 0.00000 |
| 26.20 | 6.800E 00 | 3.873E 01 | 686.4  | 0.0 | -12.13 | 0.00000 | 382. | 0.00000 |
| 26.60 | 7.000E 00 | 2.371E 01 | 707.6  | 0.0 | -8.52  | 0.00000 | 376. | 0.00000 |
| 27.00 | 7.197E 00 | 1.708E 01 | 729.0  | 0.0 | -7.11  | 0.00000 | 370. | 0.00000 |
| 27.40 | 7.389E 00 | 1.268E 01 | 750.7  | 0.0 | -6.55  | 0.00000 | 365. | 0.00002 |
| 27.80 | 7.572E 00 | 1.183E 01 | 772.8  | 0.0 | -17.17 | 0.00000 | 360. | 0.00000 |
| 28.20 | 7.726E 00 | 1.050E 01 | 795.2  | 0.0 | -6.14  | 0.00000 | 355. | 0.00005 |
| 28.60 | 7.449E 00 | 1.129E 01 | 817.9  | 0.0 | -6.07  | 0.00000 | 350. | 0.00007 |
| 29.00 | 8.067E 00 | 1.065E 01 | 841.0  | 0.0 | -6.11  | 0.00000 | 345. | 0.00008 |
| 29.40 | 8.285E 00 | 1.125E 01 | 864.3  | 0.0 | -5.37  | 0.00000 | 340. | 0.00005 |
| 29.80 | 8.365E 00 | 1.222E 01 | 888.0  | 0.0 | -6.93  | 0.00000 | 336. | 0.00002 |
| 30.20 | 7.929E 00 | 2.295E 01 | 912.0  | 0.0 | -9.25  | 0.00000 | 331. | 0.00000 |
| 30.60 | 7.755E 00 | 1.647E 02 | 936.3  | 0.0 | -20.00 | 0.00000 | 327. | 0.00000 |
| 31.00 | 8.963E 00 | 2.251E 01 | 961.0  | 0.0 | -9.46  | 0.00000 | 323. | 0.00000 |
| 31.40 | 8.285E 00 | 2.487E 01 | 985.9  | 0.0 | -8.86  | 0.00000 | 318. | 0.00000 |
| 31.80 | 9.483E 00 | 3.692E 01 | 1011.2 | 0.0 | -12.57 | 0.00000 | 314. | 0.00000 |
| 32.20 | 5.360E 00 | 5.875E 01 | 1036.8 | 0.0 | -20.00 | 0.00000 | 311. | 0.00000 |
| 32.60 | 1.000E 01 | 2.614E 02 | 1062.7 | 0.0 | -20.00 | 0.00000 | 307. | 0.00000 |
| 33.00 | 9.783E 00 | 2.541E 03 | 1089.0 | 0.0 | -20.00 | 0.00000 | 303. | 0.00000 |
| 33.40 | 1.060E 01 | 1.577E 02 | 1115.5 | 0.0 | -20.00 | 0.00000 | 299. | 0.00000 |
| 33.80 | 1.078E 01 | 7.146E 01 | 1142.4 | 0.0 | -20.00 | 0.00000 | 296. | 0.00000 |

WEIGHTED AVERAGE FREQUENCY= 6.94 CM\*\*2

---

AVERAGE FNU= 7.49 F.U.

---

INTEGRATED FLUX= 7.01 IN UNITS OF 10\*\*7-14 W/M\*\*2

---

WEIGHTED AVERAGE TRANS= 0.468

---

STRAIGHT AVERAGE TRANS= 0.018

---

WEIGHTED AVERAGE ATMOSPHERIC TRANS= 0.524

---

FNU(MUBAR)/INTEGRAL CF FNU= 11.40

---

INTEGRATED FLUXES IN ATMOSPHERIC WINDOWS IN UNITS OF 10\*\*7-14 W/M\*\*2

|                    |      |
|--------------------|------|
| 0.0 TO 6.0 CM**2   | 0.66 |
| 6.0 TO 12.0 CM**2  | 6.11 |
| 12.0 TO 15.0 CM**2 | 0.24 |
| 15.0 TO 19.0 CM**2 | 0.01 |
| 19.0 TO 25.0 CM**2 | 0.00 |
| 25.0 TO 33.0 CM**2 | 0.00 |





## References - Part II

- Armstrong, K. R., Harper, D. A., Jr., and Low, F. J. 1972, Ap.J. (Letters), 178, L89.
- Aumann, H. H. 1970, Ph.D. Thesis, Rice University.
- Baluteau, J. P., Epchtein, N., Gay, J., and Verdet, J. P. 1972, in Infrared Detection Techniques for Space Research, ed. Manno and Ring.
- Beckman, J. E., Bastin, J. E., and Clegg, P. E. 1969, Nature, 221, 944.
- Berge, G. L. 1968, Ap. Lett., 2, 127.
- Berge, G. L. and Read, R. B. 1968, Ap. J., 152, 755.
- Brandli, G. and Sievers, A. J. 1972, Phys. Rev. B, 5, 3550.
- Branson, N. J. B. A. 1968, M.N.R.A.S., 139, 155.
- Burch, D. E. 1957, J.O.S.A., 48, 1383.
- Dickel, J. R. 1967, Ap. J., 148, 535.
- Dickel, W., Warnock, W., and Medd, W. J. 1968, Nature, 220, 1183.
- Downes, D., Maxwell, A., and Rinehart, R. 1970, Ap. J. (Letters), 161, L123.
- Efanov, V. A., Kislyakov, A. G., Moissev, I. G., and Naumov, A. I. 1969, Sov. Astr.-AJ, 13, 110.
- Epstein, E. E., Dworetzky, M. M., Montgomery, J. W., and Fogarty, W. G. 1970, Icarus, 13, 276.
- Epstein, E. E., Oliver, J. P., Soter, S. L., Schorn, R. A., and Wilson, W. J. 1968, A. J., 73, 271.
- Gardner, F. F. and Morimoto, M. 1968, Aust. J. Phys., 21, 881.
- Giordimaine, J. A., Alsop, L. E., Townes, C. H., and Mayer, C. H. 1959, A. J., 64, 332.
- Harper, D. A. and Low, F. J. 1971, Ap. J. (Letters), 165, L9.
- Harper, D. A., Jr., Low, F. J., Rieke, G. H., and Armstrong, K. R. 1972, Ap. J. (Letters), 177, L21.
- Harries, J. E. and Ade, P. A. R. 1972, Infrared Phys., 12, 81.

- Jackson, John David 1962, Classical Electrodynamics, (John Wiley and Sons: New York), p. 294.
- Jones, R. C. 1953, J.O.S.A., 43, 1.
- Hoffmann, W. F., Frederick, C. L., and Emery, R. J. 1971, Ap. J. (Letters), 170, L89.
- Kellermann, K. I. 1966, Icarus, 5, 478.
- Kellermann, K. I. 1970, Rad. Sci., 5, 487.
- Kellermann, K. I. 1972, in External Galaxies and Quasi-Stellar Objects, ed. D. S. Evans, (D. R. Reidel: Holland), p. 190.
- Kellermann, K. I. and Pauliny-Toth, I. I. K. 1966, Ap. J., 145, 954.
- King, Ronold W. P. and Wu, Tai Tsun 1959, The Scattering and Diffraction of Waves, (Harvard University Press: Cambridge), p. 126.
- Kislyakov, A. G. and Lebskii, Yu. V. 1968, Sov. Astr.-AJ, 14, 561.
- Kostenko, V. I., Pavlov, A. V., Sholomitsky, G. B., Slysh, V. I., Soglasnova, V. A., Zabolotny, V. F. 1971, Ap. Lett., 8, 41.
- Law, S. E. and Staelin, D. H. 1968, Ap. J., 154, 1077.
- Liang, C. Y. and Krimm S. 1956, J. Chem. Phys., 25, 563.
- Loewenstein, E. V. and Newell, D. C. 1969, J.O.S.A., 59, 407.
- Low, F. J. 1961, J.O.S.A., 51, 1300.
- Low, F. J. 1965, Ap. J. (Letters), 142, 1287.
- Low, F. J. 1966a, Proc. I.E.E.E., 54, 477.
- Low, F. J. 1966b, A. J., 71, 391.
- Low, F. J. and Aumann, H. H. 1970, Ap. J. (Letters), 162, L79.
- Low, F. J. and Davidson, A. W. 1965, Ap. J. (Letters), 142, 1278.
- Martin, A. H. M. 1972, M.N.R.A.S., 157, 31.
- Mather, J. C., Werner, M. W., and Richards, P. L. 1972, Ap. J. (Letters), 170, L59.
- McCullough, T. P. 1972, Icarus, 16, 310.

- Mitsuishi, A., Otsuka, Y., Fujita, S., and Yoshinaga, H. 1963, Jap. J. App. Phys., 2, 574.
- Moller, K. D., McMahon, D. J., and Smith, D. R. 1966, Appl. Opt., 5, 403.
- Muehlner, D. and Weiss, R. 1972, Phys. Rev. D, 7, 326.
- Nolt, I. G., Martin, T. Z., Wood, C. W., and Sinton, W. M. 1971, J. Atm. Sci., 28, 238.
- Park, W. M., Vickers, D. G., and Clegg, P. E. 1970, Astr. and Ap., 5, 325.
- Putley, E. H. 1963, Proc. I.E.E.E., 51, 1412.
- Ressler, G. M. and Moller, K. D. 1967, Appl. Opt., 6, 893.
- Sagan, C. 1971, in Planetary Atmospheres, ed. Sagan, Owens, and Smith, (D. Reidel: Holland), p. 116.
- Salomanovich, A. E. 1965, Rad. Sci., 69 D, 1576.
- Trafton, L. M. 1967, Ap. J., 147, 765.
- Ulich, B. L. 1973, Ph.D. Thesis, University of Texas at Austin.
- Westphal, J. A., Wildey, R. L., and Murray, B. C. 1965, Ap. J., 142, 799.
- Wildey, R. L., Murray, B. C., and Westphal, J. A. 1965, J. Geophys. Res., 70, 3711.
- Witte, W. 1965, Infrared Phys., 5, 179.
- Wrixon, G. T. and Welch, W. J. 1970, Icarus, 13, 163.
- Wrixon, G. T., and Welch, W. J., and Thornton, D. D. 1971, Ap. J., 169, 171.
- Zabolotny, V. F., Sholomitsky, G. B., and Slysh, V. I. 1971, Ap. Lett., 8, 1.
- Zwerdling, S. and Theriault, J. P. 1972, Infrared Phys., 12, 165.